

Fifth International Conference

MMM 2010

Multiscale Materials Modeling

October 04 - 08, 2010, Freiburg, Germany

CONFERENCE PROCEEDINGS

Editors:
Peter Gumbsch
Erik van der Giessen

FRAUNHOFER VERLAG

Organized by Fraunhofer Institute
for Mechanics of Materials IWM.
Hosted by University of Freiburg.



Supported by



Mathematical Methods

A 3D Multiscale Modelling of Cortical Bone Structure, Using the Inverse Identification Method: Microfibril Scale Study

Abdelwahed Barkaoui, Ridha Hambli

**Institute PRISME, EA4229, University of Orleans
Polytech' Orléans, 8, Rue Léonard de Vinci 45072 Orléans, France**

Abdelwahed.barkaoui@etu.univ-orleans.fr

ABSTRACT

Complexity and heterogeneity of bone tissue require a multiscale modelling to understand their mechanical behaviour and their remodelling mechanism. Human cortical bone structure consists of six structural scale levels which are the (macroscopic) cortical bone, osteonal, lamellar, fibrous, fibril and microfibril. In this paper, a 3D model based on finite elements method was achieved to study the nanomechanical behaviour of collagen Microfibril. The mechanical properties and the geometry (gap, overlap and diameter) of both tropocollagen and mineral were taken into consideration as well as the effects of cross-links. An inverse identification method has been applied to determine equivalent averaged properties in order to link up these nanoscopic characteristics to the macroscopic mechanical behaviour of bone tissue. Results of nanostructure modelling of the nanomechanical properties of strain deformation under varying cross-links were investigated in this work.

Keywords: Cortical bone; Nanostructure; Multiscale modelling; Finite elements; Mechanical properties; Microfibril; Inverse identification method.

1. Introduction

A long bone like the femur consists of three parties from the center outward: the marrow, the spongy bone and cortical bone. In this study we are interested only in compact bone. A microscopic analysis reveals a complex architecture that can be described as follows. The bone is a composite material: it must imagine hollow cylinders juxtaposed next to each other and sealed by a matrix. The cylinders are called Osteon, the inner bore Haversian canal and the matrix pore system. Further analysis shows that osteons are in fact an assembly of cylindrical strips embedded in each other and each blade is composed of a network of fibers wound helically oriented collagen and inserted into hydroxyapatite crystals. The orientation of collagen fibers may be different between two consecutive slices. These fibers are one set of fibrils. Each fibril is in turn composed of micro fibrils. Finally, each micro fibril is a helical arrangement of five tropocollagen molecules. Fig1.provides a better understanding of this large complex architecture.

In the previous multiscale studies of cortical bone, it's used to be started by microfibril as compound mentioning only its geometry and its special arrangement of molecular rows, with neither regarding less its mechanical behaviours, on other word there are neither analytical studies nor numerical modeling at this level of scale. The most notable studies are those of Jager and Fratzl, 2000, Andreas Fritsch 2009, Markus 2008, [1, 2, 3, 4]. However, this work focuses on modeling of fibril scale, that is to say a larger scale than the one we want, our job is to fill this gap.

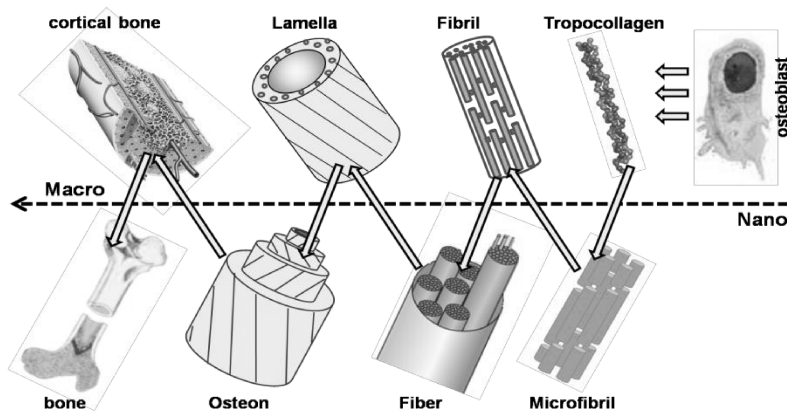


Figure 1.the hierarchical structure of cortical bone

2. Microfibril structure and composition

The microfibril is a helical assembly of five tropocollagen molecules (rotational symmetry of order 5), which are offset one another with an interval D (~ 67 nm) and creates a cylindrical formation with a diameter of about 4 nm. The orientation and axial arrangement of tropocollagen molecules in the microfibril have been deduced from an electron-microscopic observation showing transverse striations with a period D . The origin of this streaking was performed by a gradation in the arrangement of elements that are staggered tropocollagen with themselves at an interval D . [5, 6, 7, 8]. Fig2.

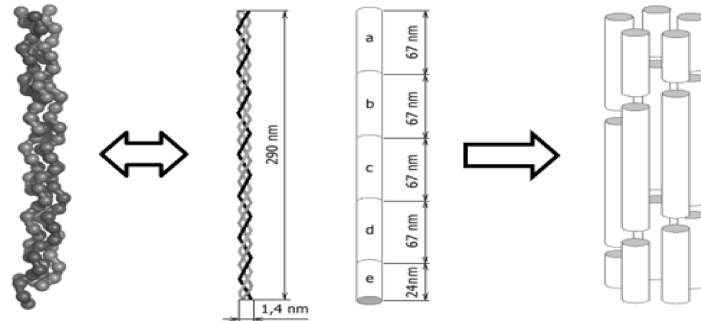


Figure 2.Schematic illustration of the three tropocollagen molecules and the formation of the microfibril

The mineral is almost entirely of crystalline hydroxyapatite $\text{Ca}_{10}(\text{PO}_4)_6(\text{OH})_2$ impure. This happens, a mature form of needles or leaves, included into the gap and between the tropocollagen molecular. The size of the sheets is several tens or several hundreds of nm in their plan, and a few nm in thickness.

In the biological sciences, crosslinking typically refers to a more specific reaction used to probe molecular interactions. For example, proteins can be cross-linked together using small-molecule crosslinkers. In biological tissue, crosslinks can be induced as disulfide bonds between tropocollagen molecules. Compromised collagen in the cornea, a condition known as keratoconus, can be treated with clinical crosslinking. In our finite element model the crosslinks are modeled as a spring with defined stiffness.

3. Methods

In this work we have used the method of finite elements in order to investigate the mechanical behavior of the microfibril, its damping capacity and its fracture resistance. The outputs of this simulation are used as inputs for the inverse identification method to identify equivalent properties, Young's modulus and Poisson's ratio of the microfibril.

A three- dimensional model of collagen microfibril with symmetric and periodic boundary conditions is considered here, with an array of 5 tropocollagen molecules cross-linked together using springs, the all is put into a mineral matrix. An entire plan of experience has been considered in order to investigate the influence of all geometric and mechanical parameters on the mechanical behaviour of the microfibril under the varying number of cross-links.

An inverse method was applied to identify the equivalent properties. A Newton Raphson algorithm written in python was coupled to Abaqus code, allows us to identify these properties.

4. Results

Below an example of the results of finite element simulation with E1 is the Young's modulus of collagen and E2 is the Young's modulus of the mineral. Fig4 illustrate the damping capacity of microfibril under different loading. Both graphs show the effect of number of cross links on the mechanical behaviour of the microfibril.

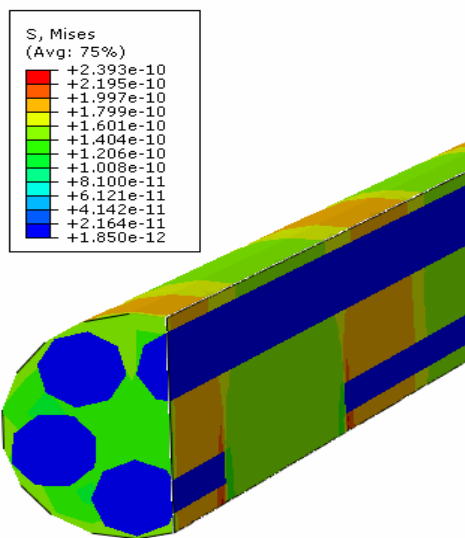


Figure3. FE Von Mises stress contour

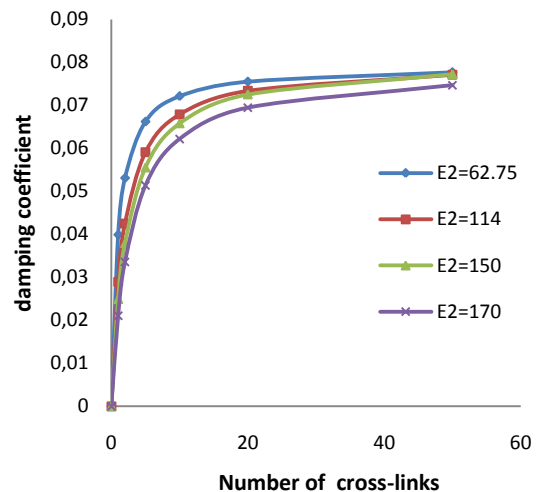


Figure 4.Relation between damping coefficient and number of cross-links with E1=2GPa

The maximum efforts determined by finite element numerical simulation are introduced in the program of inverse identification method in order to identify equivalent properties. The two graphs below illustrate some of the results.

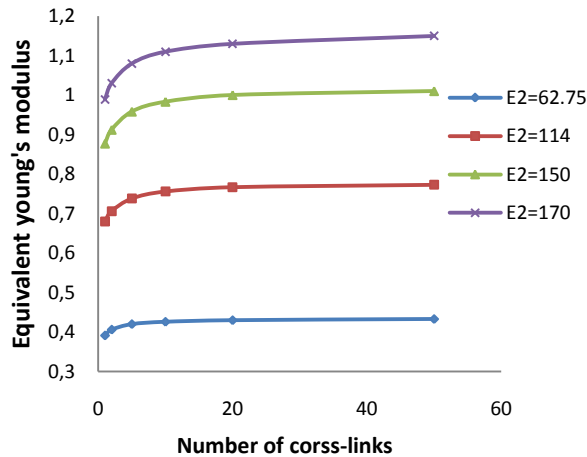


Figure 5.Relation between Young's modulus and number of cross-links with $E_1=2\text{GPa}$

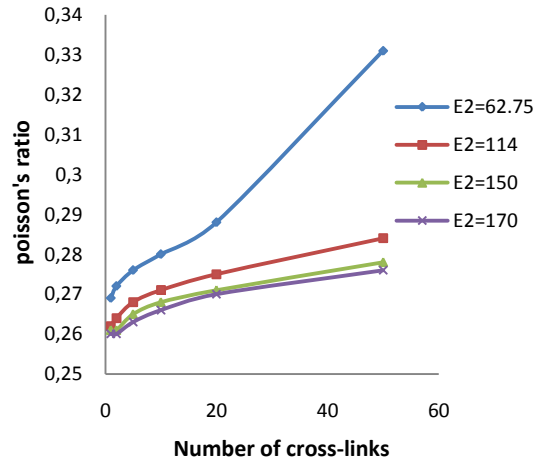


Figure 6.Relation between Poisson's ratios and number of cross-links with $E_1=2\text{GPa}$

5. Conclusion

In this paper we study for the first time the mechanical behaviour of the microfibril. This work also allows us to understand better this nanoscale and study the upper level scale which is the collagen fibril with the same methods by using the results found in this scale.

Acknowledgements

This work has been supported by French National Research Agency (ANR) through TecSan program (Project MoDos, n° ANR-09-TECS-018).

References

- [1] i. Jäger, P. Fratzl, Mineralized collagen fibrils: A mechanical model with a staggered arrangement of mineral particles, *Biophys. J.* 79 (2000) 1737–1746
- [2] A.Fritsch, C.Hellimich, L.Dormieux, Ductile sliding between mineral crystals followed by rupture of collagen crosslinks: Experimentally supported micromechanical explanation of bone strength, *J. Of theoretical biology* 260(2009) 230-252.
- [3] M.J.Buehler, Nanomechics of collagen fibrils under varying cross-links densities: Atomistic and continuum studies, *J.of the mechanical behaviour of biomedical materials* (2008) 59-67.
- [4] M.J.Buehler, Molecular architecture of collagen fibrils: A critical length scale for tough fibrils, *Current applied physics* 8 (2008) 440-442.
- [5] A. Blažej, A. Galatík, J. Galatík, M. Mládek, *Technologie kůže a kožešin*, SNTL Praha 1984
- [6] P.Bruckner, D. E Birk, *Collagen*, 2005
- [7] M. Stančíková, R. Stančík, Z. Gubzová, J. Rovenský, *Collagen in the Treatment of Rheumatic Diseases - Oral Tolerance*, Bratislavské listy 1999
- [8] Stephen C. Cowin, Do liquid crystal-like flow processes occur in the supramolecular assembly of biological tissues, *J. Non-Newtonion Fluid Mech.* 119 (2004) 155-162.

Multiscale modeling of MgO single crystal plasticity

J. Amodeo, Ph. Carrez and P. Cordier

Unité Matériaux et Transformations, UMR CNRS 8207, Université de Lille 1, 59655
Villeneuve d'Ascq Cedex, France

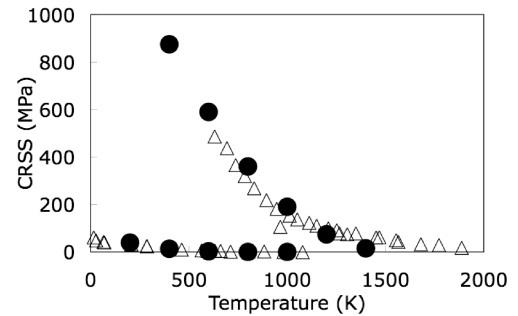
jonathan.amodeo@étudiant.univ-lille1.fr

In the 70', several experiments have been carried out in order to investigate MgO mechanical properties. Besides its importance in materials science, iron-bearing magnesium oxide is the second most abundant phase of the Earth's lower mantle. The internal heat of the Earth is dissipated through slow convection movements in the solid mantle (which extends down to 2900 km depth). This convection involves plastic flow of the constitutive minerals of mantle rocks. At these depths, minerals are submitted to extreme pressure and temperature conditions (up to 130 GPa and 3000K). Another theoretical and experimental challenge is associated with the extremely slow strain-rates of mantle flow: $\sim 10^{-16}$ s⁻¹. Despite recent progress in high-pressure deformation experiments, these conditions remain mostly out of reach. We propose here an alternative approach based on a multiscale modelling of MgO plasticity.

The first step of this numerical investigation consists in modelling dislocations core properties with the Peierls-Nabarro-Galerkin model, which incorporates gamma-surfaces calculated ab initio. We confirm that $\frac{1}{2}\langle 110 \rangle\{110\}$ is the dominant slip system of MgO at ambient pressure. The calculation of gamma-surfaces as a function of pressure allows to address the influence of this parameter on the dislocation core structure. We show here that $\frac{1}{2}\langle 110 \rangle\{100\}$ glide becomes easier at high pressure.

Then we model thermal activation of plastic glide based on the kink-pair theory. The critical kink-pair geometry and activation enthalpies are evaluated with the elastic interaction model. These parameters have been used to build up a thermally activated dislocation mobility law:

$$v = av_D \frac{b}{w^*} \frac{L}{w^*} \exp(-\Delta H_0/kT) \sinh\left(\frac{\Delta H_0(1 - (1 - (\tau/\tau_p)^p)^q)}{kT}\right)$$



Critical Resolved Shear Stress evolution against temperature. Triangles are experimental results (Copley and Pask, 1963, Sato and Sumino, 1980, Barthel, 1984); DD results are in full circles.

This mobility law has been incorporated in the Dislocation Dynamics code MicroMegs to describe the collective behaviour of dislocations and calculate the CRSS at various temperatures. The results are in fairly good description of experimental data at ambient pressure (figure above). This approach is used finally to study other aspects of MgO plasticity (pressure effects, strain hardening, etc.).

Hot Quasicontinuum Study of Nanovoids Evolution Under Tension

Ponga M.¹, Kulkarni Y², Romero I.³, Ariza M.P.¹ and Ortiz M.⁴

¹Universidad de Sevilla. C. de los Descubrimientos, s.n. 41092-Sevilla, Spain
(mponga@us.es)

²University of Houston, 4800 Calhoun Rd, Houston, TX 77204

³Universidad Politécnica de Madrid. J. G. Abascal, 2, 28006 Madrid, Spain

⁴California Institute of Technology, 1200 E. California Blvd. Pasadena, 91125

ABSTRACT

The mechanisms underlying the deformation near nanovoids in FCC materials when subjected to triaxial deformation is analysed using numerical simulations with the Quasicontinuum method. The complex structure of dislocations around the nanovoid and the evolution of stress, deformation and temperature of the sample is described in the present work.

1. Introduction

Atomistic simulations of materials have gained recent interest due to their applications in nano and micro mechanics. To understand the mechanical response of materials subject to dynamical loads the knowledge of the physical and thermodynamical properties of materials is required. In particular, we are interested in studying the response around nanovoids to understand deformation-dependent properties and their relation with the temperature field. In this paper we focus on the tri-axial strain response of FCC single crystal containing a nanovoid.

Molecular dynamics (MD) techniques have been used by many authors to study the mechanical response of materials with nano voids. However, a correct simulation of plastic phenomena requires the use of very large systems and appropriate boundary conditions, which may result in complex MD models. In this sense, multiscale (MS) modelling provides an alternative to MD simulation, especially for this type of problem. Particular MS technique, the Quasicontinuum method (QC) [1] has been successfully employed to many researches in the past. In the current work, QC method with extension to systems in thermodynamic equilibrium and non-equilibrium is used.

2. Methodology

2.1 The Quasicontinuum method

QC is a method for systematically coarse-graining lattice statics models. The method starts with a small and complete atomistic system around a core defect. Then the rest of the crystal is modelled in the geometry and reducing the configuration space of the crystal through a judicious application of a finite element-based kinematic constraints. To avoid full lattice sums, only atoms in small clusters, surrounding the representative atoms must be visited for computing the effective out-of-balance forces. Additionally, the selection of representative atoms is performed adaptively based on the local strain of the elements.

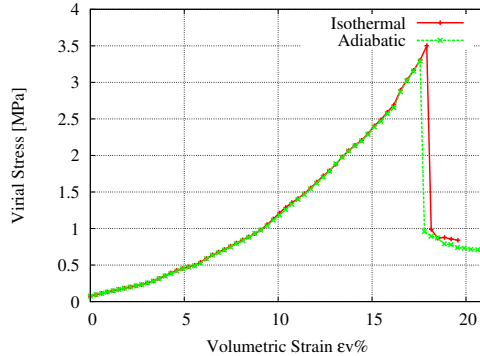


Figure 1: Virial Stress vs Volumetric Strain for adiabatic and isothermal case.

The tolerance governing the adaptation process is set so that the full atomistic resolution is attained only in the presence of dislocations.

The force among atoms is directly computed by empirical potentials. As in conventional continuum mechanics, QC permits the direct simulation of systems controlled through the application of remote boundary conditions. Details of the implementation of QC used in the present study and an analysis of convergence of the method may be found in [1]

2.2 Equilibrium and Non-Equilibrium QC

The QC extension to systems in thermodynamic equilibrium and non-equilibrium was developed in [2]. This extension is possible by the application of a variational mean-field theory and the maximum-entropy (*max-ent*) formalism. Using this formalism, we can directly approximate the probability density function to find the system in a certain state, not necessarily an equilibrium state. In this model, every representative atom has local state variables akin to temperature, entropy in addition to position, as parameters that determine the local statistics of the atom. Then, the *max-ent* variational principle provides the most likely probability density function within the assumed mean-field class and consistent with all constraints on the systems.

Attention to macroscopic processes that are quasi-static is performed. Under these conditions, the net result of the *max-ent* procedure is to define a non-equilibrium free energy depending on the positions and temperatures of all the atoms. The non-equilibrium free energy is computed explicitly by numerical quadratures and the result may be regarded as a temperature-dependent interatomic potential. The stable configuration of the system is found by minimization of the free energy for a given temperature field.

The next step in the development of the method therefore concerns the computations of the evolving temperature field. We accomplish this by coupling the free-energy minimization problem to a diffusion form of the energy-balance equation. The proper form of the coupling is suggested by the variational formulation of coupled thermo-mechanics problems proposed in [3].

3. Numerical test

Results are shown for numerical tests according to a non-equilibrium finite temperature problem using QC method. A nanovoid problem is considered to study the geometry and the temperature field of atoms around of a nanovoid. This problem has been studied by

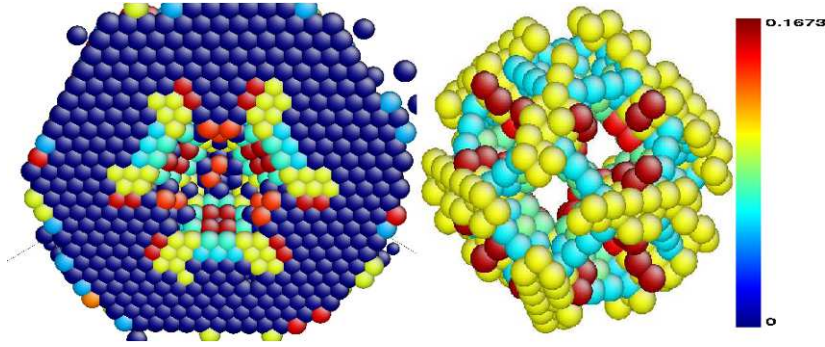


Figure 2: Core defect around nanovoid. Atoms are coloured with the **CSD** parameter. (Left) (1 1 1) cut plane. (Right) Core defect around nanovoid.

many authors, but none of them have included systems outside equilibrium. Also, the purpose of these tests is to understand the nucleation of particular arrangement of atoms around a nanovoid and the evolution of the temperature field in this process.

3.1 Test problem definition

The sample is a FCC nearest-neighbor LJ crystal with $72a_0 \times 72a_0 \times 72a_0$ cube, or 34.6 nm of length in size, and a total of 194,509 atoms. An equiaxed 3.35 nm void is initially created in the center of the cell with full atomistic resolution being provided *ab initio* within a $8a_0 \times 8a_0 \times 8a_0$ region surrounding the void. The initial mesh contains 681 nodes. Solid Argon is used as a test material since it can be modelled using LJ pair potential. The external load consist in a void expansion by prescribing pure dilatational displacements in the exterior boundary of the computational cell and the external deformation is increased by steps of 0.1% increments. At each loading step, a new stable equilibrium configuration is obtained by using the Polak-Ribière variant of the non-linear conjugate gradient algorithm. Before the loading process, the sample is allowed to equilibrate isothermally at uniform temperature of $T = 0.5T_m$, with $T_m = 83K$ being the melting temperature. Additionally, the test is performed with two time step equal to $\Delta t = 0$ which is adiabatic and $\Delta t = 30[k\sigma/k_B]$ with its intermediate between the adiabatic and isothermal case.

3.2 Results and discussion

Fig. 1 shows the evolution of the average virial stress vs. the volumetric deformation $\varepsilon_v = \Delta V/V_0$. In both cases, the curve shows three main stages. First a region with non-linear regime up to 6 % of deformation. This stages is followed by two linear steps, with change in the slope. This change in the slope is due to a boundary interaction of the sample. Finally, an interval with strong non-linearity indicates the fragile failure of the material. Before the fragile failure of the sample, the structure of the atoms around the nanovoid is show in Fig. 2 . Here, the spatial arrangement of the atoms is indicated using the adimensional centrosymmetry parameter [4]. Fig. 3-a shows the normal displacement field around nanovoid at $x = 0$ plane for a 18,5% volumetric strain. Note that the sample is split into four parts, and the atoms are displaced from the symmetry plane. In this step the atoms around the nanovoid have elevated energy, and present an increment in the temperature with respect to the atoms far away from the nanovoid. For the adiabatic case, this increment is approximately of 10,5 % for atoms near the nanovoid (Fig. 3-b).

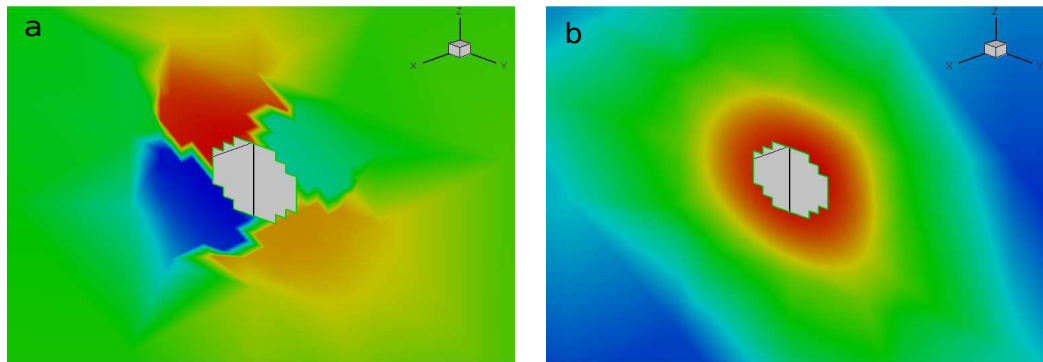


Figure 3: Displacement and Temperature map after the failure superposed around a nanovoid in arbitrary units.

4. Conclusions and Future Works

In this work we have studied the thermo-mechanical behavior of an argon crystal with a nano-void in the center. An extension of the Quasicontinuum method to non-equilibrium systems has provided a detailed solution of the forces, deformation, and temperature at every point of the sample, with atomistic resolution close to the defect. In this region, both adiabatic as well as isothermal simulations indicate that a fragile fracture occurs in the material shortly after dislocation structures appear. The multiscale resolution of the Quasicontinuum approach then serves to compute a macroscopic response of the whole crystal, where fracture is clearly identified. Future extensions of this work include larger samples and the study of materials other than argon, especially metals.

Acknowledgements

We gratefully acknowledge the support of the Ministerio de Educación y Ciencia of Spain (DPI2009-14305-C02-01/02), the support of the Consejería de Innovación of Junta de Andalucía (P09-TEP-4493) and the support of the Department of Energy National Nuclear Security Administration under Award Number DE-FC52-08NA28613 through Caltech's ASC/PSAAP Center for the Predictive Modeling and Simulation of High Energy Density Dynamic Response of Materials.

References

- [1] Tadmor, E.B., Ortiz, M., Phillips, R., Quasicontinuum analysis of defects in solids *Philos. Mag*, **73**, 1529-1563, 1996.
- [2] Kulkarni, Y., Knap, J., Ortiz, M. A variational approach to coarse graining of equilibrium and non-equilibrium atomistic description at finite temperature *J. Mechanics and Physics of Solids*, **56**, 1417-1449, 2008.
- [3] Yang, Q., Stainier, L., Ortiz, M., A variational formulation of the coupled thermo-mechanical boundary-value problem for general dissipative solids. *J. Mech. Phys. Solids* **54**, 401-424, 2006.
- [4] Kelchner, C.L., Plimpton, S.J., Hamilton, J.C. Dislocation nucleation and defect structure during surface nanoindentation. *Phys. Rev. B* **58**, 11085-11088, 1998.

Stability of discrete dislocations in graphene

Ariza MP.¹ and Ortiz M.²

¹Universidad de Sevilla. Camino de los descubrimientos, s.n. 41092-Sevilla, Spain (mpariza@us.es)

²California Institute of Technology, 1200 E. California Blvd. Pasadena, 91125, USA

We present an application of the theory of discrete dislocations to the analysis of dislocations in graphene. We discuss the specialization of the theory to graphene and its further specialization to the force-constant model of Aizawa et al. (1990). The ability of the discrete dislocation theory to predict dislocation core structures and energies is critically assessed for periodic arrangements of dipoles and quadrupoles. We show that, with the aid of the discrete Fourier transform, these problems are amenable to exact solution within the framework of discrete dislocation theory, which confers the theory a distinct advantage over conventional atomistic models. In particular, the discrete dislocation theory predicts 5-7 ring core structures that are consistent with observation and dislocation energies that fall within the range of prediction of other models.

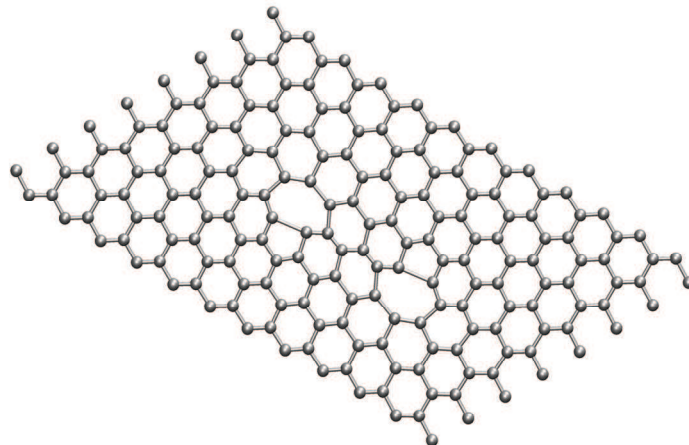


Figure 1. Discrete dipole core structure for the Aizawa et al. [1990] potential, exhibiting double pentagon-heptagon ring (5-7) structure.

We also present an assessment of the finite-temperature dynamical stability of discrete dislocations in graphene. In order to ascertain stability, we insert discrete dislocation quadrupole configurations into molecular dynamics calculations as initial conditions. In calculations we use Sandia National Laboratories Large-scale Atomic/Molecular Massively Parallel Simulator (LAMMPS) and the (AIREBO). The analysis shows that the core structures predicted by discrete dislocation theory are dynamically stable up to temperatures of 2,500K, though they tend to relax somewhat in the course of molecular dynamics.

Aizawa, T., Souda, R., Otani, S., Ishizawa, Y., Oshima, C., 1990. Bond softening in monolayer graphite formed on transition-metal carbide surfaces. *Physical Review B* 42 (18), 11469–11478.

Sampling point selection for energy estimation in the quasicontinuum method

L.A.A. Beex, R.H.J. Peerlings, M.G.D. Geers

Department of Mechanical Engineering, Eindhoven University of Technology
P.O.Box 513, 5600 MB, Eindhoven, the Netherlands
l.a.a.beex@tue.nl/r.h.j.peerlings@tue.nl/m.g.d.geers@tue.nl

ABSTRACT

The quasicontinuum (QC) method reduces computational costs of atomistic calculations by using interpolation between a small number of so-called repatoms to represent the displacements of the complete lattice and by selecting a small number of sampling atoms to estimate the total potential energy of the interpolated problem. In this contribution two new sampling point selections are introduced for the QC method. The first selection determines the total potential energy of the lattice exactly in correspondence with the interpolation. Since no error due to summation occurs, the fully resolved regions around lattice defects can remain small. However, in this case many sampling atoms must be used. Therefore a second sampling point selection is derived from the first selection that uses only one sampling atom to represent all atoms within interpolation together with the repatoms. This ensures that the exact lattice model is recovered in the fully resolved regions while a smooth transition is achieved towards coarse regions in which the method becomes very close to the local QC method [1].

1. Introduction

The quasicontinuum (QC) method [1] is a multiscale approach that allows efficient atomistic calculations. The QC method delivers full atomistic resolution where needed and a coarser description where a lower resolution suffices. Moreover, the QC method requires only the atomistic model; no equivalent continuum description (as used in combined continuum/atomistic approaches) is needed.

Large-scale atomistic models are computationally demanding because of two reasons. First they include many degrees of freedom (DOFs), since every atom represents three DOFs. Second, every atom must be visited to determine its potential energy. The QC method reduces the large number of DOFs by using interpolation to constrain the displacement of atoms to follow a set of representative atoms or repatoms. The triangulation used is adapted in such a way that in regions of interest the exact lattice model is captured while in far field regions the interpolation domains can be larger so that large number of atoms are interpolated and the number of DOFs is reduced (see Fig. 1).

An equally important ingredient of QC methods is the use of so-called summation rules to estimate the total potential energy of the system based on that of a limited number of atoms. The atoms used for this purpose are referred to here as sampling points, since they are used to sample the energies of the surrounding atoms. The selection of sampling atoms must be performed in correspondence with the triangulation to find a good estimate of the interpolated lattice's energy.

Two general classes of QC methodologies can be distinguished based on the sampling used. The local-nonlocal QC method [1] uses the Cauchy-Born rule to determine the potential energy of a sampling atom in the coarsened domain, which leads to an internal interface between the local domain and the nonlocal (fully resolved) domain. In the cluster QC method

[2], clusters of atoms centered at the reatoms are used. However, it is shown in [3] that even for large clusters of sampling atoms a poor approximation of the total potential energy is obtained. Since in the QC approaches the total potential energy is estimated, an error due to summation occurs in the coarsened domain. This is often compensated by using large fully resolved domains at the expense of the computational profit.

In this study the role of summation is examined in detail, leading to two new sampling point selections. The first sampling point selection determines the total potential energy exactly in correspondence with the triangulation so that no error due to summation occurs and the fully resolved regions can remain small. However, since in this case many sampling atoms are used the computational burden remains relatively large. For this reason, a second sampling point selection is introduced. Although an error due to summation is introduced in this second selection, much fewer sampling atoms are used which reduces the computational costs. Because the second sampling point selection is based on a clear comprehension of how the summation is related to the interpolation, the error due to summation remains small and the fully resolved regions only have to be slightly increased to obtain an acceptable error.

2. Sampling point selection

The starting point for our discussion is the idealized 2D lattice shown in Fig. 2 over which a triangulation is placed. In this idealized lattice only bonds between nearest neighbors are present which are modeled as linear springs. To determine the total potential energy of the lattice exactly all atoms in Fig. 2 must be visited to determine their site-energy. The site-energy of an atom is found by projecting half of the potential energies of its eight neighboring bonds onto the atom. The site-energy of atom p in Fig. 2 therefore depends on its own displacements and on the displacements of its eight neighbors.

Since linear interpolation is used, all similar bonds inside an interpolation triangle, e.g. all horizontal bonds, experience exactly the same relative displacement within one triangle. Only bonds between different interpolation triangles may be stretched differently. Therefore, the site-energy of atom p in Fig. 2, which has all its neighboring bonds and atoms within the same triangle equals the site-energy of its right neighbor $p+1$ which also has all its neighbors in the same triangle as atom p . On the other hand, atom q which has one neighboring atom in another triangle may have a different site-energy.

2.1 Exact energy computation

According to the above observation the total potential energy of the entire lattice remains exact if, instead of visiting all atoms of the lattice, only one atom with all its neighbors in the same triangle is used to represent all other atoms that have all their neighbors in that particular triangle. In this case still all atoms that have one or more neighbors in another triangle must be accounted for individually.

To illustrate this sampling point selection, it is used for the aforementioned idealized lattice of 250 by 250 unit cells. A zoom of the fully resolved region on the left in Fig. 3 shows that bands of discrete sampling atoms occur at the triangle edges while one sampling atom is used to represent all other atoms in every triangle. As can be seen in Fig. 3, a large number of sampling atoms must be used to determine the total potential energy exactly, which increases the computational burden. For a fully resolved region of four by four lattice spacings for instance, still 9,809 out of 63,001 atoms must be used for the sampling. If this QC variant is used for lattices in which also next-to-nearest neighbor interactions occur, as in atomistic lattices, the bands of discrete sampling points become wider and the computational efficiency of the sampling method is reduced even more.

2.2. Approximate energy computation

For this reason another sampling point selection is introduced that neglects inter-triangular interactions in the coarse domain. It uses only one sampling atom per triangle to sample all atoms within the triangle, whether or not they have one or more neighbors in another triangle. Only the reatoms remain discrete sampling points and they only represent their own site-energy. As a result also in this sampling point selection one single algorithm can be used to deal with coarse and fully resolved regions. In the right picture of Fig. 3 it is clearly visible that this sampling point selection leads to a considerable reduction of the number of sampling atoms (293 of 63,001).

This resulting sampling point selection combines the advantages of the local-nonlocal QC method [1] and the cluster QC method [2]. First it uses almost the same, small number of sampling points as the local-nonlocal QC method. In fact, in large triangles with many lattice points the local QC method is almost recovered since all neighboring atoms of the sampling point are located within the same triangle and the contributions of the discrete sampling points at triangle nodes are negligible. However, since only physical atoms are selected as in the cluster QC method (i.e. the Cauchy-Born rule is not used), no internal interface between the fully resolved domain and coarse domain occurs.

3. Results

To evaluate the accuracy of the two sampling point selections a multiscale example is considered based on the aforementioned idealized lattice of 250 by 250 unit cells as shown in Fig. 3. In this example one horizontal bond to the right of the center of the fully resolved region is removed. The model is loaded uniformly in horizontal direction; in vertical direction the model is free to contract.

The relative displacement field in Fig. 4 (relative to the case in which the bond is present) indicates two distinct peaks at the location of the atoms where the bond is removed. This fluctuation field matches the field of the full lattice calculation (without the use of the QC method) as shown in Fig. 5. Even for a small fully resolved region of four by four lattice spacings the maximum relative error is only 2.3%. This error is entirely due to interpolation as the summation is exact for the first sampling point selection. Therefore, the fully resolved regions can remain small in this QC approach although the computational burden is large due to the large number of sampling atoms.

The results of the second sampling point selection, indicated by the dashed line in Fig. 5, are clearly not as accurate as the results of the first sampling selection for small fully resolved regions. However, for fully resolved regions larger than six by six lattice spacings the maximum relative error is less than 1%, while the computational effort is significantly smaller compared to the first sampling point selection - as indicated in the previous section. Clearly only a marginal increase of the fully resolved region is necessary for the resulting second sampling point selection to obtain a small acceptable error. This originates from a clear understanding of the interaction between triangulation and the determination of the total potential energy.

4. Conclusion

Two new summation methods for QC methodologies have been presented. The first computes the total potential energy of an interpolated lattice exactly, but it is costly in terms of computing time. A second method uses only the reatoms plus one sampling point within each triangle. This method is less expensive and introduces little additional error.

5. Figures

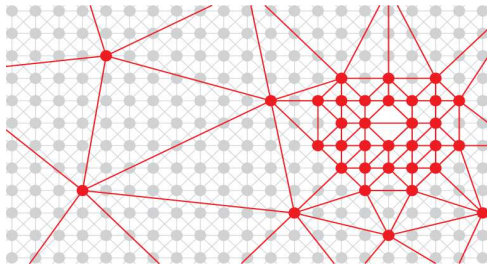


Fig. 1: Schematic representation of the two-dimensional lattice with triangulation. The size of the interpolation domains is decreased around the lattice defect so that the exact lattice model is captured there.

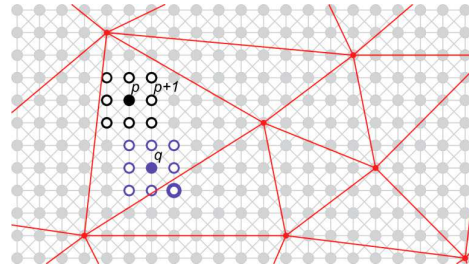


Fig. 2: The neighboring atoms of atom p and q are visible as open circles. The neighbors of p and $p+1$ are located in the same triangle and therefore p and $p+1$ have the same site-energy. Atom q has one neighbor in a different triangle and may thus have a different site-energy.

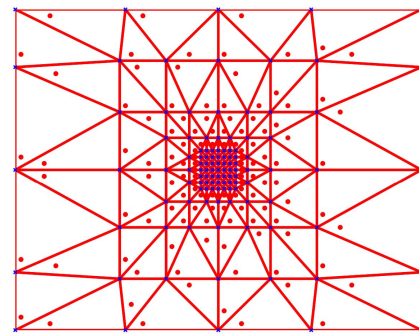
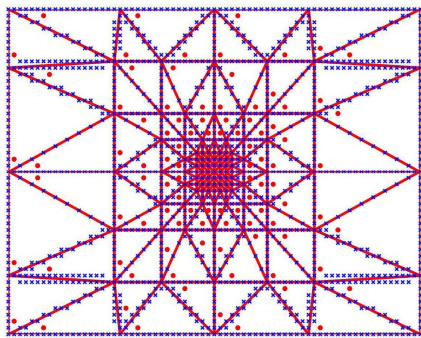


Fig. 3: Zoom of the fully resolved region. Discretely modeled sampling points are indicated by blue crosses and the sampling points used to represent the remaining atoms within every triangle are indicated by red circles. (Left) the result of the exact summation. (Right) the result of the approximate summation.

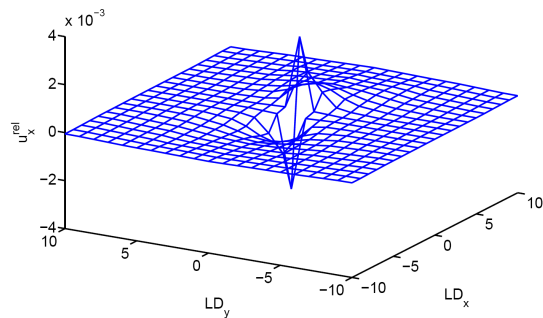


Fig. 4: Relative displacement in horizontal direction due to the missing bond for a fully resolved region of six by six lattice spacings and exact summation

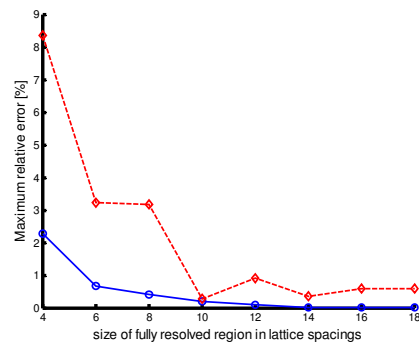


Fig. 5: Maximum relative error of the fluctuation at both peaks in Fig. 4. The blue solid line and circles are the errors for exact summation and the red dashed line and squares for the approximate summation.

6. References

- [1] E.B. Tadmor, M. Ortiz, R. Phillips, 'Quasicontinuum analysis of defects in solids', *Philosophical Magazine A*, 73, 1529-1563, 1996.
- [2] J. Knap, M. Ortiz, 'An analysis of the quasicontinuum method', *Journal of the Mechanics and Physics of Solids*, 49, 1899-1923, 2001.
- [3] M. Luskin, C. Ortner, 'An analysis of node-based cluster summation rules in the quasicontinuum method', *SIAM Journal on Numerical Analysis*, 47, 3070-3086, 2009.

Constitutive Equations and Multiscale Analysis of Graphene

Ted Belytschko¹, Mei Xu², Jeffrey Paci³

¹*Walter P. Murphy and McCormick Institute Distinguished Professor
Department of Mechanical Engineering, Northwestern University
2145 Sheridan Road, Evanston, IL, 60208, U.S.A.
e-mail: tedbelytschko@northwestern.edu*

²*Department of Mechanical Engineering, Northwestern University
2145 Sheridan Road, Evanston, IL, 60208, U.S.A.
e-mail: MeiXu2008@u.northwestern.edu*

³*Department of Chemistry, University of Victoria
PO Box 3065, Victoria, British Columbia, V8W 3V6, Canada.*

Single layer graphene sheets are becoming of increasing interest in nanotechnology. It has high mechanical strength, excellent thermal properties and unusual electric properties. However, a constitutive characterization of grapheme is lacking. Here we develop a constitutive equation for grapheme based density functional theory (DFT) calculations. The properties are unusual in that the grapheme is almost isotropic until strain of about 10% and then there is a significant deviation from isotropy. A hyperelastic constitutive equation that accounts for this transition is developed. This constitutive equation is particularly useful for coupled DFT/continuum calculations, since the continuum model then closely matches the DFT model, so that the disparities in basic properties that result in anomalous behavior at interfaces are eliminated. Comparisons are made the DFT/atomistic/continuum model presented in [1]. The disparities between strength of grapheme sheets and nanotubes in the armchair and zigzag directions are examined along with the effects of existing flaws and cracks. Comparisons will also be made with nanoindentation experiments.

References

[1] Khare, R., Mielke, S.L., Paci, J.T., Zhang, S.L., Ballarini, R., Schatz, G.C., and Belytschko, T., "Coupled quantum mechanical/molecular mechanical modeling of the fracture of defective carbon nanotubes and graphene sheets," *Physical Review*

B, 75(7): Art. No. 075412 (Feb 2007)

A parametric simulation method for discrete dislocation dynamics

Michal Benes¹, Vojtěch Minárik¹, Petr Pauš¹ and Jan Kratochvíl²

¹Department of Mathematics, Faculty of Nuclear Sciences and Physical Engineering, Czech Technical University in Prague, Trojanova 13, Prague, Czech Republic, {michal.benes, vojtech.minarik, petr.paus}@fjfi.cvut.cz;

²Department of Physics, Faculty of Civil Engineering, Czech Technical University in Prague, Thákurova 7, Prague, Czech Republic, kratochvil@fsv.cvut.cz

ABSTRACT

The contribution summarizes results obtained by a computer simulation method employed in discrete dislocation dynamics. The method has been applied to elementary interactions among glide dislocations and dipolar dislocation loops. The glide dislocations are represented by parametrically described curves moving in glide planes whereas the dipolar loops are treated as rigid objects. All mutual force interactions are considered in the models. As a consequence, the computational complexity rapidly increases with the number of objects considered. This difficulty is treated by advanced computational techniques such as suitable accurate numerical methods and parallel implementation of the algorithms. Therefore the method is able to simulate particular phenomena of dislocation dynamics which occur in crystalline solids deformed by single slip: generation of glide dislocations from the Frank-Read source, interaction of glide dislocations with obstacles, their encounters in channels of the bands, sweeping of dipolar loops by glide dislocations and a loop clustering.

1. Introduction

Discrete dislocation dynamics (DDD) became a highly efficient tool of exploration of plastic deformation mechanisms at micro-scale. DDD is used at the same scale as the electron microscopy. While nearly all electron microscopy observations are carried out on specimens after deformation, DDD can realistically simulate elementary deformation processes. However, despite a steady progress in DDD methods and ever increasing power of computational resources, DDD is still far from a possibility to simulate complexity documented by electron micrographs. Nevertheless, as demonstrated in this article, the current DDD is able to model some dislocation mechanisms and early stages of dislocation patterning.

Plastic deformation in crystalline solids is carried by dislocations. Theoretical description of dislocations is widely provided in literature such as^{1,2}. The approach of this article explores basic dynamic properties of dislocations and dipolar loops and nature of their mutual interactions.

Dislocation is a line defect of the crystalline lattice. Along the dislocation curve the regularity of the crystallographic arrangement of atoms is disturbed. The dislocation can be represented by a curve closed inside the crystal (resulting into dipolar loops) or by a curve ending on surface of the crystal. At low homologous temperatures the dislocations can move only along crystallographic planes (gliding planes) with the highest density of atoms. The motion results in mutual slipping of neighboring parts of the crystal along the gliding planes. The slip displacement carried by a single dislocation, called the Burgers vector, is equal to one of the vectors connecting the neighboring atoms.

A field given by displacement of atoms from their regular crystallographic positions in the

vicinity of a dislocation curve can be treated as the elastic stress and the strain fields. On the other hand, a stress field exerts a force on a dislocation. The combination of these two effects causes the elastic interaction between dislocations.

The discrete dislocation dynamics first treated dislocations as long parallel straight lines. Later more physical but considerably more complex three-dimensional situations of plastic deformation processes were investigated. Application of this approach addressed a variety of meso-scale plasticity problems. Details can be found e.g. in^{3,4,5}.

Methods treating dynamics of curved dislocations can be divided into the following groups. Some methods consider discrete segments of the curve moving over a discrete grid imitating crystalline lattice on a larger scale (see³). Other methods discretize the curve into piecewise linear (see^{5,6}) or piecewise polynomially represented segments (see⁴).

Due to the above mentioned complexity, formation of dislocation structures as a consequence of interactions between dislocations is still an open problem. The aim of this contribution is to summarize description of the parametric model treating several dislocation curves and a dipolar loops.

2. Parametric approach

Discrete dislocation dynamics is devoted to the study of interactions between one or more dislocation curves and several other defects such as dipolar loops. The mentioned objects are located in a 3D domain with finite volume. At low-temperature, glide dislocations can be represented as smooth planar curves. As described in earlier results such as^{3,7,4,6} and in references therein, motion of the dislocation curve Γ can be described by the evolution law

$$Bv_{\Gamma} = -T\kappa_{\Gamma} + F, \quad (1)$$

relating its normal velocity v_{Γ} to the curvature κ_{Γ} and sum F of forces acting on Γ in the normal direction. Here, B denotes the drag coefficient and T stands for the line tension.

In general, the law (1) can be treated by methods of the level-set type, of the phase-field type or by the parametric approach (see⁵). The last approach is suitable for dislocation dynamics as such material defects are represented by open curves. Self-intersections as well as other topological changes can be incorporated to this approach in an algorithmic way.

For this purpose, we introduce notation for quantities related to this representation. A planar curve $\Gamma(t)$ evolving during the time interval $\langle 0, T \rangle$ can be described parametrically by a smooth vector mapping $\vec{X} : \langle 0, T \rangle \times \langle 0, 1 \rangle \rightarrow \mathbb{R}^2$ depending on time and on parameter u from a fixed bounded interval $\langle 0, 1 \rangle$. Then, the curve is expressed as

$$\Gamma(t) = \{\vec{X}(t, u) = [X^1(t, u), X^2(t, u)] \mid u \in \langle 0, 1 \rangle\}.$$

The unit tangential vector to the curve \vec{T} is defined as $\vec{T} = \partial_u \vec{X} / |\partial_u \vec{X}|$. The unit normal vector the curve \vec{N} is perpendicular to the tangential vector in selected direction and is denoted as $\vec{N} = \partial_u \vec{X}^{\perp} / |\partial_u \vec{X}|$. Substituting corresponding quantities into the law (1) yields the equation for parametrization $\vec{X} = \vec{X}(t, u)$ in the form (in agreement with^{8,9})

$$\partial_t \vec{X} = T \frac{\partial_{uu}^2 \vec{X}}{|\partial_u \vec{X}|^2} + F \frac{\partial_u \vec{X}^{\perp}}{|\partial_u \vec{X}|}, \quad (2)$$

where the law (1) can be recovered by multiplying the vectorial equation (2) by the vector \vec{N} .

This equation is accompanied either by the periodic boundary conditions

$$\vec{X}(t, 0) = \vec{X}(t, 1),$$

for closed dislocation curves (e.g. appearing in the Frank-Read source), or with fixed ends

$$\vec{X}(t, 0) = \vec{X}_{\text{fixed},0}, \quad \vec{X}(t, 1) = \vec{X}_{\text{fixed},1},$$

for open dislocation curves. The initial condition for the curve position is prescribed as

$$\vec{X}(0, u) = \vec{X}_{\text{ini}}(u).$$

Remark. According to ¹⁰, the law (1) can be also treated by the *arc-length* parametrization which is a smooth vector mapping $\vec{X} = \vec{X}(t, s)$ depending on time $t \in (0, T)$ and the arc length $s \in (0, L(t))$ where $L(t)$ is the length of the dislocation curve at a given time t . The mapping satisfies the identity $|\partial_s \vec{X}(t, s)| = 1$. Values of $\vec{X}(t, s)$ are in the glide plane. The motion law (1) then has the form

$$B\partial_t \vec{X} = T\partial_{ss}^2 \vec{X} + F\partial_s \vec{X}^\perp, \quad (3)$$

where $\partial_s \vec{X}^\perp$ represents the normal vector to $\Gamma(t)$, accordingly.

The dislocation curves interact dynamically with other material defects such as dipolar loops through the elastic force field. The interaction dynamics is studied in the coordinate system xyz where the xz -plane represents the dislocation glide plane. The dipolar loops are considered in their stable configurations - having long rectangular fixed shapes (see ^{7,6} and references therein).

Therefore their motion can be fully described by motion of their barycenters, at the given level of approximation. They are assumed to have longer edges parallel with the z -axis whereas their shorter edges are parallel with either $[1, 1, 0]$ or $[1, -1, 0]$ vectors. This means that a dipolar loop can move along the x -axis only, keeping the y - and z -coordinates constant. The Burgers vector is set as $\vec{b} = [b, 0, 0]$.

As indicated above, each dipolar loop is assumed to have a rectangular shape and to have one of the two stable configurations in the atomic lattice depending of the defect type - vacancy and interstitial configurations. We also assume that dipolar loops have the same size which is described by the average half-width h , the average half-length l , and the average perimeter $P = 2(2h\sqrt{2} + 2l)$. The position of a dipolar loop Λ_j , $j = 1, \dots, N$ is given by the coordinates $[x^{(j)}, y^{(j)}, z^{(j)}]$ of its barycenter. According to the previous assumptions, $y^{(j)} = \text{const.} \neq 0$ and $z^{(j)} = \text{const.}$, whereas $x^{(j)} = x^{(j)}(t)$ is given by the motion law

$$\frac{dx^{(j)}}{dt} = \frac{1}{BP} F_{x,\text{total}}^{(j)}(\Gamma, x^{(1)}, \dots, x^{(N)}), \quad (4)$$

where the term $F_{x,\text{total}}^{(j)}$ is given by the force interaction with other dipolar loops and with the dislocation curve $\Gamma(t)$ described by the parametrization \vec{X} . This interaction is projected to the only possible direction of the loop motion - to the direction of the x -axis.

The interaction dynamics of dislocation curves $\Gamma_1, \dots, \Gamma_K$ parametrized by $\vec{X}^{(1)}, \dots, \vec{X}^{(K)}$ and dipolar loops $\Lambda_1, \dots, \Lambda_N$ discussed in this article is therefore described by the following set of

equations endowed by the boundary and initial conditions

$$\partial_t X^{\vec{l}} = T \frac{\partial_{uu}^2 X^{\vec{l}}}{|\partial_u X^{\vec{l}}|^2} + F(t, X^{\vec{1}}, \dots, X^{\vec{M}}, \Lambda_1, \dots, \Lambda_N) \frac{\partial_u X^{\vec{l}}^\perp}{|\partial_u X^{\vec{l}}|}, \quad l = 1, \dots, K, \quad (5)$$

$$X^{\vec{l}}(t, 0) = X^{\vec{l}}_{\text{fixed},0}, \quad X^{\vec{l}}(t, 1) = X^{\vec{l}}_{\text{fixed},1}, \quad l = 1, \dots, K, \quad (6)$$

$$X^{\vec{l}}(0, u) = X^{\vec{l}}_{\text{ini}}(u), \quad l = 1, \dots, K \quad (7)$$

$$\frac{dx^{(j)}}{dt} = \frac{1}{BP} F_{x,\text{total}}^{(j)} \left(X^{\vec{1}}, \dots, X^{\vec{K}}, x^{(1)}, \dots, x^{(N)} \right), \quad (8)$$

$$x^{(j)}(0) = x_{\text{ini}}^{(j)}, \quad j = 1, \dots, N. \quad (9)$$

Acknowledgements

The authors were partly supported by the project LC06052 of the Ministry of Education, Youth and Sports of the Czech Republic, the first, second and third author was partly supported by the project MSMT 6840770010 of the Ministry of Education of the Czech Republic. The research of the fourth author was supported by the project MSMT 6840770021 of the Ministry of Education of the Czech Republic.

References

- [1] J.P. Hirth and J. Lothe. *Theory of Dislocations*. John Wiley, New York, 1982.
- [2] T. Mura. *Micromechanics of Defects in Solids*. Kluwer Academic Publishers Group, Netherlands, 1987.
- [3] B. Devincre and L.P. Kubin. Mesoscopic simulations of dislocations and plasticity. *Mater. Sci. Eng. A*, 8–14:234–236, 1997.
- [4] N.M. Ghoniem, J. Huang, and Z. Wang. Affine covariant-contravariant vector forms for the elastic field of parametric dislocations in isotropic crystals. *Phil. Mag. Lett.*, 82:55–63, 2002.
- [5] M. Beneš, J. Kratochvíl, J. Křišťan, V. Minárik, and P. Pauš. A parametric simulation method for discrete dislocation dynamics. *European Phys. J. ST*, 177:177–192, 2009.
- [6] V. Minárik, M. Beneš, and J. Kratochvíl. Simulation of dynamical interaction between dislocations and dipolar loops. *J. Appl. Phys.*, 107:061802, 2010.
- [7] Š. Verecký, J. Kratochvíl, and F. Kroupa. The stress field of rectangular prismatic dislocation loops. *Phys. Stat. Sol. (a)*, 191:418–426, 2002.
- [8] K. Deckelnick, G. Dziuk, and C.M. Elliott. Computation of geometric partial differential equations and mean curvature flow. *Acta Numerica*, 14:139–232, 2005.
- [9] P. Pauš and M. Beneš. Direct approach to mean-curvature flow with topological changes. *Kybernetika*, 45(4):591–604, 2009.
- [10] G. Dziuk. Convergence of a semi discrete scheme for the curve shortening flow. *Mathematical Models and Methods in Applied Sciences*, 4:589–606, 1994.

Coherent hydrides in zirconium: role of long-range interactions

Ludovic Thuinet and Rémy Besson

Unité Matériaux et Transformations, CNRS UMR 8207,
Université de Lille 1, 59655 Villeneuve d'Ascq cedex, FRANCE

Ludovic.Thuinet@univ-lille1.fr, Remy.Besson@univ-lille1.fr

ABSTRACT

The thermodynamic properties of the coherent metastable compounds induced by hydrogen in zirconium may strongly influence the formation of stable hydrides, with critical consequences on the thermomechanical behaviour of Zircaloy materials used in nuclear industry. While they constitute an efficient way towards a better knowledge of these metastable phases, atomic-scale approaches using ab-initio-based cluster expansions have to take into account the long-ranged elastic contributions to the H-Zr energetics. This issue is explored here by investigating the relation between the so-called “k=0 singularity” of the atomic-scale modelling and the macroscopic elastic properties of long-period Zr//Zr₂H multilayers. The validity of the approach is assessed by direct comparison with ab initio calculations on similar structures. Finally, the influence of anharmonic effects, possibly requiring extensions beyond linear elasticity, is discussed.

1. Introduction

The mechanical behaviour of zirconium alloys used in nuclear industry strongly depends on the properties of metastable coherent phases appearing in the early stage of hydride precipitation. These properties can be conveniently investigated at the atomic scale using cluster expansions, namely configuration energy models of the form:

$$E = E_{\text{points}} + E_{\text{pairs}} + E_{\text{triplets}} + \dots \quad (1)$$

where « points », « pairs », ... label the different kinds of clusters. This methodology has already been successfully used in various cases: metallic alloys, oxides and semi-conductors, essentially binary, substitutional systems with cubic symmetry. A severe restriction to its use, possibly critical in H-Zr, is due to the existence of elastic interactions, induced by the long-range deformation and stress fields around interstitial H atoms and entailing a poor convergence of relation (1) with the cluster size. Assuming that these long-range effects are entirely included in pairs, a convenient way to account for them consists in reformulating the pair energy in Fourier space [1], leading to reciprocal-space energy coefficients $\tilde{J}(\vec{k})$, where the wave vector \vec{k} belongs to the first Brillouin zone (FBZ). This approach corresponds to analyzing an alloy in terms of modulations of composition, in a viewpoint quite similar to that of « concentration waves » [2]. The interest of the reciprocal-space formalism relies on its capability to take into account pair interactions with arbitrary range, the key-issue then being transferred to the achievement of a realistic description of the behaviour of \tilde{J} within the FBZ. Focusing on H-Zr, the context of the present work is thus the improvement of the description of $\tilde{J}(\vec{k})$, the origin of the reciprocal space being characterized by a discontinuity of \tilde{J} in the limit of infinite wavelengths ($\vec{k} \rightarrow 0$, the so-called « k=0 singularity»). For the case of binary AB cubic alloys with monatomic unit cells, it was shown [1] that the behaviour of \tilde{J} around $\vec{k} = 0$ is directly related to the energetic properties of A//B multilayered structures with period

$p \rightarrow \infty$, the latter being characterized by their « coherency strain » (also called « constituent strain ») energy E_{cs} . The present work aims at extending these considerations to the case of (i) multisite unit cells and (ii) lower hexagonal/trigonal symmetry, in order to enable application of cluster expansions to the hexagonal H-Zr system.

2. Coherency strain energy of H-Zr multilayers: methodology

In this context, our aim for H-Zr will be the determination of the energy E_{cs} of any coherent α/β multilayered structure of direction \vec{k} , period $p \rightarrow \infty$ and proportion x of α unit cells. It should be noted that the multisite unit cell of H-Zr implies the existence of several variants for the occupation of sites by H, an issue irrelevant and thus ignored for all AB alloys investigated hitherto. In the $p \rightarrow \infty$ limit, the relative contribution of the α/β interface becomes negligible, as well as the elastic inhomogeneities within each phase, which fully justifies the treatment by means of continuous elasticity. Moreover, although this assumption may be criticized in some cases [3], it seems reasonable to tackle the problem under the simplifying harmonic assumption of an elastic energy quadratic with respect to deformations. Due to the choice of α and β structures in this work and the crystalline systems they belong to, the relevant elastic energy density ω of each phase, in the ([2-1-10],[01-10],[0001]) referential, is expressed as:

$$\begin{aligned} \omega = & \frac{1}{2} C_{11} [(\epsilon_{11})^2 + (\epsilon_{22})^2 + 2(\epsilon_{12})^2] + C_{12} [\epsilon_{11}\epsilon_{22} - (\epsilon_{12})^2] + 2C_{44} [(\epsilon_{23})^2 + (\epsilon_{31})^2] \\ & + C_{13}\epsilon_{33}(\epsilon_{11} + \epsilon_{22}) + \frac{1}{2} C_{33}(\epsilon_{33})^2 + 2C_{14}[\epsilon_{13}(\epsilon_{11} - \epsilon_{22}) - 2\epsilon_{12}\epsilon_{23}] \end{aligned} \quad (2)$$

If α belongs to the hexagonal crystalline system, $C_{14} = 0$. In this work, ω thus involves at most 6 elastic constants.

The procedure to calculate E_{cs} consists in two steps similar to those exposed in [1]:

(i) For each phase α and β considered separately, a deformation field is imposed in the interface plane defined by its normal \vec{k} . The structure is then relaxed in the direction parallel to \vec{k} . Although the deformation resulting from this relaxation generally depends on the symmetry, it is reasonable to assume that it reduces to an elongation along the direction normal to the interface.

(ii) An epitaxy condition within the α/β interface plane is applied and an energy minimisation procedure allows calculating the deformations inside the interface plane. It should be noted that the isotropic approximation for in-plane deformation ($\epsilon_{11} = \epsilon_{22}$ and $\epsilon_{12} = 0$), acceptable in the cubic case and thus admitted throughout in the literature, proved to be invalid in trigonal/hexagonal symmetry, implying to handle a more general case, formally more complex ($\epsilon_{11} \neq \epsilon_{22}$ and $\epsilon_{12} \neq 0$).

Since the quantity E_{cs} depends on the elastic constants of both phases in the multilayer, a preliminary step consists in calculating these parameters. To this end, we employed ab initio calculations (density functional theory with plane waves and pseudopotentials, as implemented in the VASP software [4,5]), in conditions identical to those of a previous study of H-Zr [6]. These elastic constants can be determined only numerically, since the elastic properties of the metastable H-Zr phases considered cannot be experimentally measured. Fig. 1 displays the influence of the composition x_H on the elastic constants of various Zr-H structures. Although some constants (in particular C_{13}) are hardly sensitive to x_H , the trend is an increase with the H amount. With stronger variations for $x_H > 1/2$, the general shape recalls that of $T = 0$ K energy-composition curves (ground-state properties of H-Zr [6]): two composition domains are separated by the ZrH compound. Several values are reported on Fig.

1 for $x_H = 1/2$, corresponding to the three configurational variants of ZrH. Note that the dispersion between these variants may be significant (50 GPa).

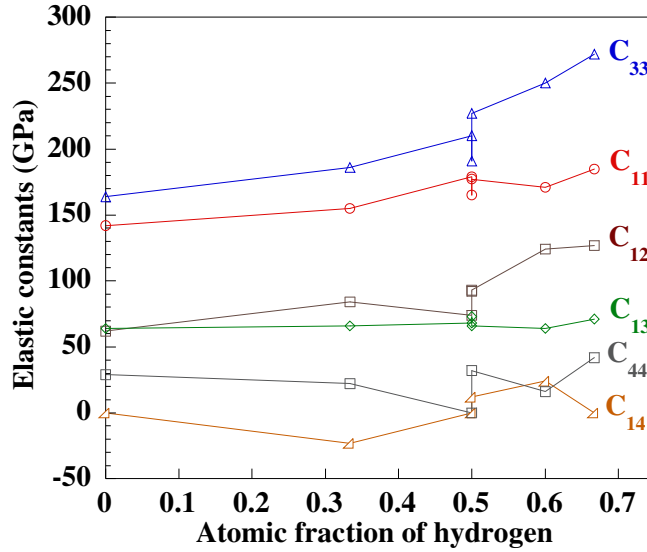


Figure 1. Elastic constants in H-Zr, as obtained from ab initio calculations.

3. Long-period multilayers in H-Zr

The previous elasticity data allow to evaluate the coherency strain energy of various multilayered structures in H-Zr. The methodology is illustrated on the case $Zr(\alpha)//Zr_2H(\zeta)$: obtaining E_{cs} for this structure is a priori of first importance, in reason of its recent experimental observation [7]. Prior to any application to cluster expansions, the validity of the calculation of E_{cs} is tested. To this end, we performed a series of « direct » ab initio assessments of $Zr(\alpha)//Zr_2H(\zeta)$ multilayer energies (noted $E(Zr//Zr_2H)$) with different periods for the basal \bar{c}^* and prismatic \bar{a}^* orientations and $x = 1/2$. The energy per cell ΔE reported on Fig.2 is defined as:

$$\Delta E = E(Zr//Zr_2H)/p - xE^{eq}(Zr) - (1-x)E^{eq}(Zr_2H) \quad (3)$$

$E^{eq}(Zr)$ and $E^{eq}(Zr_2H)$ corresponding respectively to the energies per unit cell of pure Zr and Zr_2H taken at their own unconstrained equilibrium lattice parameters. E_{cs} theoretically corresponds to the asymptotic limit of ΔE when $p \rightarrow \infty$. Fig. 2, which displays the results, reveals a behaviour sensitive to the direction of the multilayer. Whereas for prismatic orientation the agreement is reasonable (asymptotic behaviour), the situation is less clear for \bar{c}^* , with a surprisingly non-linear increase of the energy with p . This behaviour is probably due to an insufficient period for the multilayers involved in the ab initio calculations (the two-cell period of ζ along the \bar{c} axis being possibly related to long-range composition fluctuations ill-captured in supercells of limited size). The other possibilities, namely (i) a significant anharmonicity and (ii) the presence of structural instabilities, should merely be responsible for an offset of the ab initio asymptote with respect to the elastic prediction, the asymptotic profile remaining of general validity. On the whole, even though the periods considered for ab initio calculations remain quite short, the elasticity / ab initio confrontation for $\alpha//\zeta$ confirms the validity of the above scheme for the determination of coherency strain energies in H-Zr. The hypotheses underlying this model thus seem justified, in particular the harmonic approximation and zero shears perpendicular to the interface plane.

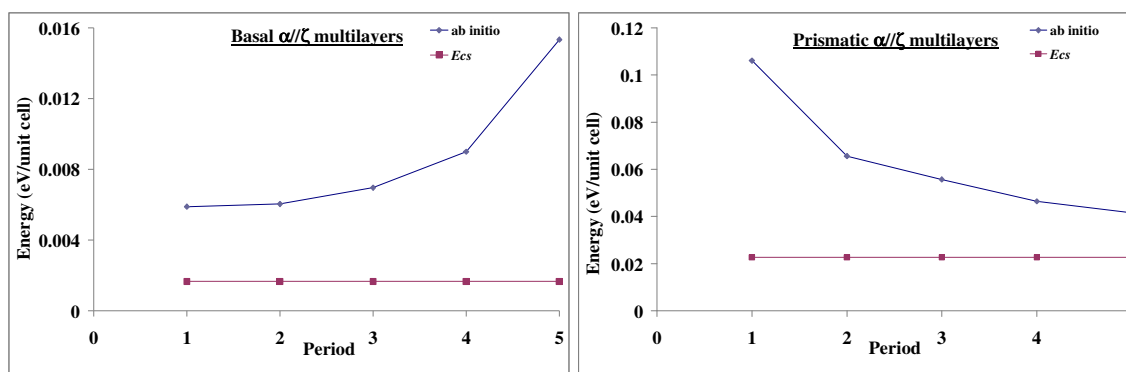


Figure 2. Energy (eV/unit cell) of basal and prismatic $Zr(\alpha)//Zr_2H(\zeta)$ multilayers: comparison between ab initio and elasticity calculations.

4. Conclusion

The present work, devoted to a « multiscale » study of multilayers built from Zr-H compounds, allowed to get better insight into the relation between the energetics (accessible to ab initio calculations) of short-period multilayers and that (determined via elasticity) for the limiting case of an infinite period. The comparison of both approaches for the $\alpha//\zeta$ multilayers seems to confirm the validity of the present extension of the « coherency strain » model to the trigonal/hexagonal case, including important generalizations of the formulation presented in the literature concerning (i) the interfacial deformation, (ii) the epitaxial condition and (iii) the handling of multisite unit cells and various site occupancies.

References

- [1] D. B. Laks, L. G. Ferreira, S. Froyen and A. Zunger, *Phys. Rev. B* **46**, 12587 (1992)
- [2] A. G. Khachaturyan, *Theory of Structural Transformations in Solids*, J. Wiley & Sons, 1983
- [3] V. Ozolins, C. Wolverton and A. Zunger, *Phys. Rev. B* **57**, 4816 (1998)
- [4] G. Kresse and J. Furthmüller, *Phys. Rev. B* **54**, 11169 (1996)
- [5] G. Kresse and J. Furthmüller, *Comput. Mater. Sci.* **6**, 15 (1996)
- [6] L. Holliger, A. Legris and R. Besson, *Phys. Rev. B* **80**, 094111 (2009)
- [7] Z. Zhao, J.-P. Morniroli, A. Legris, A. Ambard, Y. Khin, L. Legras and M. Blat-Yrieix, *J. Microscopy* **232**, 410 (2008)

Comparison of Application of a Multiphase Multiscale Approach And Continuum Formulation to Solidification Problems

O.Budenkova^{1,3}, S. Ganina², V. Ginkin², Y. Du Terrail¹, Y. Fautrelle¹

¹Grenoble Institute of Technology, SIMAP/EPM BP 75 - F-38402 Saint Martin d'Herès, France, yves.duterrail@simap.grenoble-inp.fr, yves.fautrelle@simap.grenoble-inp.fr; ²State Scientific Centre of the Russian Federation – Institute for Physics and Power Engineering, Obninsk, Bondarenko sq., 1, 249033, Russia, ginkin@ippe.ru; ³A.F.Ioffe Physico-Technical Institute of RAS, Politekhnikeskaya ul., 26, St.Petersburg, 194021 Russia

ABSTRACT

Comparison of two models for simulation of solidification of binary mixtures was performed. The first model is based on continuum formulation (CF) whereas in the second a growth kinetic of dendrites is taken into account “in average” using a multiphase multiscale Eulerian approach (MMA). For CF similar results for segregation were obtained with two numerical models, realised in software Fluent and GIGAN. In both cases formation of elongated narrow regions enriched and impoverished with the solute was revealed. Simulations performed in Fluent with application of a MMA gave a macrosegregation pattern similar to that obtained with CF whereas appearance of mesosegregation was found dependent on mass transport coefficient within a dendritic grain.

1. Introduction

Non-uniform distribution of solute is a usual phenomenon in solidification of alloys and can be observed at the scale of the whole ingot (macrosegregation) or locally as freckles or channels (mesosegregation) [1]. It is the result of action of two factors: different solubility of the components in the solid and liquid phases and relative movement of these phases during solidification. An experiment performed in chill configuration [2] demonstrated segregation which appeared due to buoyancy-induced flow in the liquid. Data obtained in [2] were used by many authors for validations of physical models and their numerical realisations, see [3], [4] and references within. Difficulties in simulation of solidification problems arise due to coupling of processes which occur at different scales: at the solid/liquid interface, between dendritic arms and in the bulk volume of liquid. To take them into account, averaging-based techniques are applied to local conservation equations for obtaining macroscopic equations. An approach which is referred here as a continuum formulation (CF) initially was formulated using the mixture theory [5] and later re-formulated using volume averaging procedure [6]. Other models which accounted for growth kinetics of dendrites are multiphase volume averaging model [7] and multiphase multiscale approach (MMA) based on statistical averaging [8]. In the present work simulations of a numerical benchmark problem stated in [9] for solidification of $Sn-10\%wt-Pb$ has been done. The first aim was comparison of results obtained within the frame of CF using two different numerical techniques realized in software Fluent and GIGAN [10]. The second objective was comparison of results obtained with different physical models, namely with CF and MMA.

2. Statement of the problem and physical models

The simulations are performed for a 2D rectangular domain $10 \times 6\text{cm}$ whose short sides are parallel to the gravity vector. Initially completely melted and stationary alloy $SnPb$ of

nominal lead concentration $C_{l,0}(Pb) = 10\%wt$ has uniform temperature T_0 corresponding to the liquidus one. The top and the bottom walls of the domain are thermally insulated, solidification occurs due to heat extract at lateral walls. Physical properties are omitted here and can be found in [9] with more detailed description of the problem.

2.1 Continuum formulation and multiscale multiphase approach

In CF evolution of two phases, solid and liquid (indices s and l , respectively), are considered. The solid phase is stationary throughout the process, density ρ , specific heat c_p and thermal conductivity k are constant and equal for both phases. Modelling of the process requires solution of mass, energy and solute conservation equations which are given below

$$\rho \frac{\partial \mathbf{V}}{\partial t} + \frac{\rho}{\varepsilon_l} (\nabla \mathbf{V}) \cdot \mathbf{V} = \nabla \cdot (\mu \nabla \mathbf{V}) - \varepsilon_l \nabla p - \frac{\mu \varepsilon_l}{K} \mathbf{V} + \varepsilon_l \tilde{\rho} \vec{g} \quad (1)$$

$$\nabla \cdot \mathbf{V} = 0 \quad (2)$$

$$\frac{\partial \rho \langle h \rangle}{\partial t} + \nabla (\rho c_p T) \cdot \mathbf{V} - \nabla \cdot (k \nabla T) = 0 \quad (3)$$

$$\frac{\partial \langle C \rangle}{\partial t} + \nabla C_l \cdot \mathbf{V} - \nabla \cdot (D \nabla C_l) = 0 \quad (4)$$

In Eqn.1-2 ε_l and ε_s - volume fractions of liquid and solid phases ($\varepsilon_l + \varepsilon_s = 1$), \mathbf{v}_l - intrinsic velocity of liquid and $\mathbf{V} = \varepsilon_l \mathbf{v}_l$, μ - viscosity, p - pressure, $\tilde{\rho}$ is defined by Boussinesq relation, K is a permeability which is defined by secondary dendritic arm spacing [9]. In Eqn.3 T is temperature, $\langle h \rangle = c_p (T - T_e) + \varepsilon_l L$ is the enthalpy in the mushy zone, L is latent heat and T_e is eutectic temperature. In Eqn.4 $\langle C \rangle = \varepsilon_l C_l + \varepsilon_s C_s$ is averaged concentration, C_l and $C_s = k_0 C_l$ - are solute concentrations in liquid and solid, respectively, k_0 is a segregation coefficient, $D = \varepsilon_l D_l$ is solute diffusion coefficient in the liquid, while no diffusion in solid phase. In the mushy zone solid and liquid phases are in chemical equilibrium, and linearized phase diagram is used, i.e. $T_{liq} = T_m + m C_l$, where T_{liq} is liquidus temperature, m is liquidus slope, and T_m is melting temperature of pure substance.

In a multiphase multiscale Eulerian approach in addition to the solid and liquid phases, the third phase for the interdendritic liquid which is enclosed within dendritic arms is introduced [7], [12]. Chemical equilibrium between solid and liquid phases is assumed only for interdendritic liquid. Concentration of solute in extradendritic liquid is defined by diffusion of solute from interdendritic liquid as well as by its convective transfer through the liquid phase. Evolution of the envelope is governed by Ivantsov equation numerically approximated in [7]. Complete set of equations for MMA is omitted here for the sake of brevity can be found in [8]. It is necessary to underline that the main difference between the two models presented here lies in different treatment of phase transition from liquid to solid.

2.2 Numerical realizations

In Fluent Eqn.1-4 for continuum formulation are discretized over the space with finite volume method and implicit time scheme is used. For calculation of mass fluxes at the boundaries of

control volumes the second order upwind scheme is used. Note that in the benchmark statement $D_l = 0$ but in both software it was taken as a small value.

In GIGAN for approximation of Eqn.1-4 an exponential method [10] in conjunction with Patankar-Spalding technique [11] and implicit time scheme are used. Obtained system of nonlinear finite-difference equations is linearized and implicit relaxation method is applied for its resolution [10]. The system of finite-difference equations is solved by the iterative method of incomplete factorization.

3. Results and discussion

3.1 Results obtained with continuum formulation

In Fig.1a and Fig.1b results obtained in Fluent and GIGAN with grid of 240x200 and 120x100 cells, respectively, are presented. In solidification of $Sn-10\%wt-Pb$ a heavier solute is rejected that causes downward flow within a mushy zone which spread from a cooled walls and, respectively, appearance of upward flow in pure liquid. This leads to impoverishment in Pb at upper part of the ingot and accumulation of the lead in form of a hill in the central part of the domain.

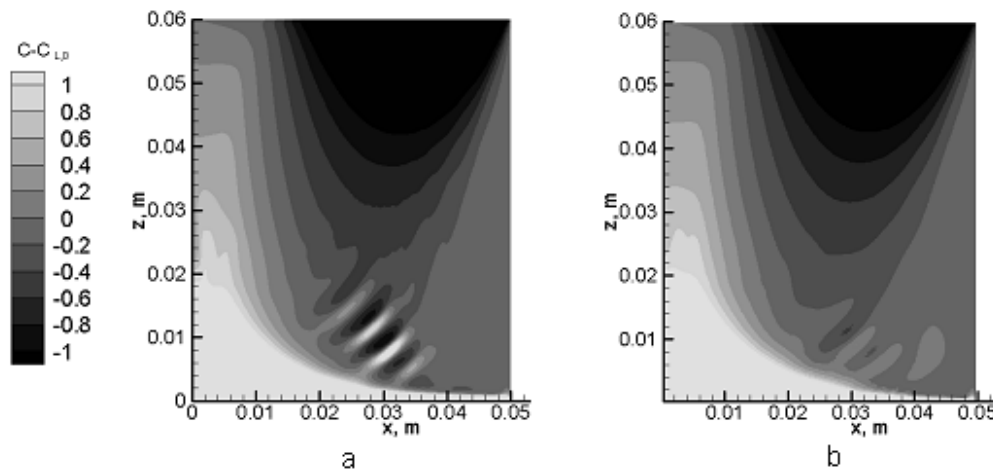


Fig.1. Distribution of average concentration of Pb relatively to nominal one $C_{L,0}$ after 120 s of solidifications obtained within CF with (a) Fluent and (b) GIGAN. Because of symmetry, a half of the domain is presented and vertical axis corresponds to the centre of the domain.

Apart from macrosegregation which was found similar in both simulations formation of alternating elongated narrow regions impoverished and enriched with Pb has been revealed. These regions originate due to local instabilities inside the mushy zone. In simulations performed with Fluent the number of these zones is larger than in GIGAN and variation of lead concentration there is significantly stronger. Similar effect of space discretization based on control volume compared to finite element was found in [5].

3.2 Results obtained with multiscale multiphase approach

Simulations were performed for several values of mass transfer coefficient $D_{l,i}$ inside a dendritic grain, whereas in pure liquid diffusion was not taken into account. A smaller diffusion coefficient corresponds to slower diffusion of solute from interdendritic liquid, to extradendritic one and, therefore, to less intensive enrichment of the bulk liquid with a solute. With $D_{l,i} = 3.0 \cdot 10^{-9} \text{ m}^2/\text{s}$ (typical value for metals) resulting macrosegregation pattern is

similar to that obtained in previous simulations, whereas local variations of concentrations of *Pb* do not exist (Fig.2a). With increasing of $D_{l,i}$ by an order, up to $D_{l,i} = 3.0 \cdot 10^{-8} \text{ m}^2/\text{s}$ one of the channels observed earlier appears. The next value taken in simulations $D_{l,i} = 3.0 \cdot 10^{-7} \text{ m}^2/\text{s}$ is hardly realistic, however, it can be interpreted as an “effective” diffusion coefficient which takes into account convective mass transfer near the dendritic tip.

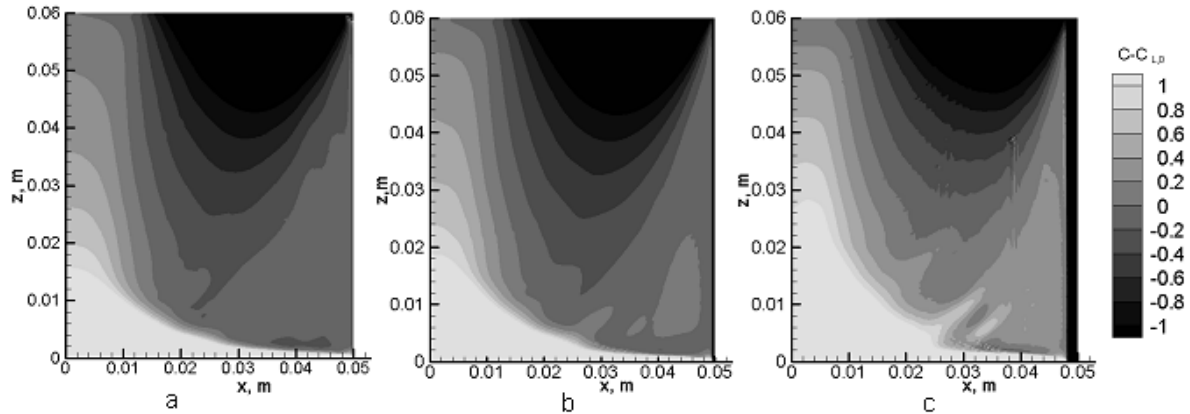


Fig.2. Distribution of average concentration of *Pb* relatively to nominal $C_{L,0}$ after 120 s of cooling obtained with MMA in Fluent for $D_{l,i} = 3.0 \cdot 10^{-9} \text{ m}^2/\text{s}$ (a), $D_{l,i} = 3.0e^{-8} \text{ m}^2/\text{s}$ (b) and $D_{l,i} = 3 \cdot 10^{-7} \text{ m}^2/\text{s}$ (c). A half of the domain is shown; vertical axis corresponds to its centre.

3. Conclusions

Simulation performed with two numerical realisations of a physical model based on continuum approach as well as simulation based on multiphase multiscale approach provided similar macrosegregation patterns in chill casting of Sn10%wtPb. The effect of molecular diffusion within a dendritic grain is put forth in MMA. Increasing diffusion promotes the channel formation along with macrosegregation.

Acknowledgements

Work of S.Ganina and V.Ginkin was supported with RFBR grants 09-08-00844 and 10-03-00338.

References

1. G.Worster, Convection in the Mushy Layer, *Annu.Rev.Mech.* 29 (1997) 91-122
2. D. J. Hebditch, J. D. Hunt, *Metall.Trans.* 5 (1974) 1557-1564
3. Th. U. Kaempfer and M. Rappaz, *Modelling Simul.Mater.Sci.Eng.* 11 (2003) 575-597
4. N. Ahmad, H. Combeau, J.-L. Desbiolles, T. Jalanti, G. Lesout, J. Rappaz, M. Rappaz and C. Stomp, *Metall. Mat. Trans.* 29A (1998) 617-630
5. W.D. Bennon and F.P. Incropera, *Int. J. Heat Mass Transfer*, 30 (1987) 2161-70
6. J. Ni and C. Beckermann, *Metall. Trans.* 22B (1991) 349-361
7. C.Y.Wang, C.Beckermann, *Metal.Mat.Trans.*, 27A (1996), 2754-2764.
8. A.Ciobanas, Y.Fautrelle, *J. Physics D: Applied Physics*, 40 (12) (2007) 3733-3762
9. M. Bellet, H. Combeau, Y. Fautrelle, et al, *Int. J. Therm. Sci.*, 48 (11) (2009) 2013-2016
10. V. Ginkin , *Proc. 2nd Int. Symp. Advances in Computational Heat Transfer*, Palm Cove, Queensland, Australia, Vol. 2 (2001) 1161-1168
11. S.V. Patankar , D. B. Spalding *J. Heat Mass Transfer*, 15 (1972), 1787-1806.
12. M. Rappaz: *Int. Mater. Rev.*, 34 (1989), pp. 93-123.

The microscopic origin of the dielectric permittivity of materials

Eric Cancès¹ and Mathieu Lewin²

¹Université Paris-Est, CERMICS Project-team Micmac, INRIA-Ecole des Ponts,
6 & 8 avenue Blaise Pascal, 77455 Marne-la-Vallée Cedex 2, France
cances@cermics.enpc.fr

²CNRS & Laboratoire de Mathématiques UMR 8088, Université de Cergy-Pontoise,
2 Avenue Adolphe Chauvin, 95302 Cergy-Pontoise Cedex, France

Several multiscale models coupling an atomistic description of matter on the one hand, and a continuum description on the other hand, have been proposed in the past decades. Such models are widely used in chemistry and molecular biology (continuum solvation models of Poisson-Boltzmann type) as well as in materials science (e.g. quasi-continuum models). However, the theoretical foundations of these models and of the coupling between atomistic and continuum regions are still largely unexplored, and are often a matter of debate.

In this talk, I will focus on the specific difficulty originating from the long-range character of the Coulomb potential. I will explain in detail the link between the slow decay of the Coulomb potential and the dielectric permittivity of crystalline materials and argue that atomistic/continuum multiscale models should properly take into account this long-range effect.

E. Cancès and M. Lewin, *The dielectric permittivity of crystals in the reduced Hartree-Fock approximation*, Arch. Ration. Mech. Anal., published online: 19 November 2009.

Dislocation core modeling of $\langle 110 \rangle$ dislocation in SrTiO_3 using Peierls-Nabarro-Galerkin method

Ph. Carrez¹, D. Ferré¹ and P. Cordier¹

¹lab. UMET, CNRS-UMR 8207, University of Lille 1, 59655 Villeneuve d'Ascq, FRANCE
philippe.carrez@univ-lille1.fr

In this study, we propose to model dislocation core in SrTiO_3 using the recently developed Peierls-Nabarro-Galerkin approach (Denoual C., PRB 70, 024106 (2004)). To that purpose, Generalised Stacking Fault (GSF) of $\{100\}$ and $\{110\}$ planes have been calculated *ab initio* using the VASP package. Inelastic Stacking Fault energy derived from GSF calculations are then introduced in the PNG method to determine stable core structure of $\langle 110 \rangle$ dislocation (both screw and edge component are calculated).

The $\langle 110 \rangle$ screw dislocation core is planar in $\{110\}$ with a core spreading larger than two lattice repeats. Such a wide core can be considered as a dissociation of a $\langle 110 \rangle$ dislocation into two collinear partials dislocations of $\frac{1}{2}\langle 110 \rangle$ Burgers vectors in agreement with experimental observations (Castillo-Rodriguez M. and Sigle W., Scripta Mat. 62, 270-273, (2010)). Besides providing a core model, PNG calculations can be used to evaluate Peierls stresses, found for $\langle 110 \rangle \{110\}$ screw dislocation between 200 and 300 MPa.

Same calculations are currently performed on the edge component. For the $\langle 110 \rangle \{110\}$ edge dislocation, calculations lead to a wider core characterized by a lower Peierls stress.

The final step of this study corresponds to a critical shear stress calculation at low temperature based on a double kink nucleation process. The nucleation energy of kink pairs have been calculated using an elastic interaction model (Koizumi et al., Acta Metall. Mater., 41, 3483-3493, (1993)). Preliminary results show that the kink pair nucleation theory is able to reproduce the main features of critical resolved shear stress in $\{110\}$ at low temperature.

Calculation of proper vacancy migration energy barriers with artificial neural networks for the modelling of vacancy clusters' migration.

N. Castin^{1,2} and L. Malerba²

¹*Université Libre de Bruxelles (ULB), Physique des Solides Irradiés et des Nanostructures (PSIN), boulevard du Triomphe CP234, Brussels 1050, Belgium*

²*Studiecentrum voor Kernenergie–Centre d'Etudes de l'énergie Nucléaire (SCK•CEN), SMA Group, NMS Institute, Boeretang 200, Mol B2400, Belgium
corresponding author: lmalerba@sckcen.be*

Neutron irradiation enhances mass transport in compounds via creation of point defects, thereby accelerating possible phase changes, which in turn result in material property changes. The development of predictive tools capable to model the kinetics of such processes is thus of great importance for the nuclear sector. This is a delicate issue, since it requires the accurate estimation of the mobility of defects redistributing atoms in a chemically complex system undergoing phase transformation.

The method we propose [1] uses a classical atomistic kinetic Monte Carlo (AKMC) paradigm. The migration energy barrier of diffusing point defects (i.e. vacancies or self-interstitials) is calculated with only a few approximations using the nudged elastic band method, as a function of the distribution of surrounding chemical species and other nearby defects. The only required physical input is a reliable inter-atomic potential for the alloy of concern. As the use of on-the-fly calculated barriers would be unfeasible in practice, an artificial neural network (ANN) is used instead, as a mathematical regression tool, trained on a set of calculated examples. The ANN input are on-site variables describing the migrating defect's neighbourhood.

This ANN-based approach has been successfully applied to the case of a single vacancy migrating in an alloy, i.e. with a changing chemical environment, for AKMC simulations of thermal annealing [1]. The generalisation of this method for the simulation of neutron irradiation damage, requires that the existence and formation of vacancy and self-interstitial atom clusters is accounted for. In this work, we take a few steps in this direction, by considering the problem of the formation of clusters of vacancies. We find that, in order to model with the proper energy barriers all diffusion events, it is necessary to include in the model the capability of dealing with spontaneous migration events that in some cases may involve more than one single migrating atom at a time and may include diffusion jumps to distances larger than first nearest neighbours.

References:

[1] N. Castin and L. Malerba, J. Chem. Phys. **132**, 074507 (2010).

Analysis of size effect induced by pile-up dislocations using Discrete Dislocation Dynamics, Strain Gradient Plasticity and Field Dislocation Mechanics

H.-J. CHANG¹, N.M. Cordero¹, M. Fivel², V. Taupin³, S. Berbenni³, and S. Forest¹

¹Centre des Matériaux Mines ParisTech CNRS UMR7633 BP87, 91000, Evry, France

²SIMaP-GMP2 BP46, Domaine Universitaire, 38402, St Martin d'Hères cedex, France

³LPMM, ENSAM, Arts et Métiers Metz, Technopole, 57078, Metz Cedex 03, France

Corresponding author: H.-J.CHANG,

Tel: +33-1-60763051 Fax: +33-1-60763150 E-mail: hjchang@mat.ensmp.fr

Understanding size effects evidenced experimentally in various situations has become one of the hottest issues of the last few years. Many models have been developed to reproduce these size effects. Some are based on generalized continuum mechanics, such as field dislocation mechanics (FDM) [1] and strain gradient plasticity (SGP) [2], and others are directly dealing with dislocations such as discrete dislocation dynamics (DDD) [3]. Generalized continuum mechanics are based on, or related to, geometrically necessary dislocations (GND) and intrinsic length scale concept. In such models, the connection to physical background remains purely phenomenological. On the other hand, DDD can make bridge from the physical origin to the continuum models since it gives access both to GND quantities and to the intrinsic lengths. As an example, Figure shows a typical dislocation microstructure obtained from DDD simulation.

In this paper, size dependent mechanical responses, such as hardening, dislocation density distributions and amount of plastic slip due to the back-stress induced by pile-up dislocations are investigated using DDD, SGP and FDM. In DDD, the distance between the nearest slip planes in a multilayer pile-up structure is set as the intrinsic length that strongly affects the size dependent mechanical responses. The continuum models are found to be able to reproduce the results obtained by DDD including size effects. In particular, a full correspondence has been obtained between SGP and DDD: the mechanical responses are affected by intrinsic length, slip system orientation and multislip activations.

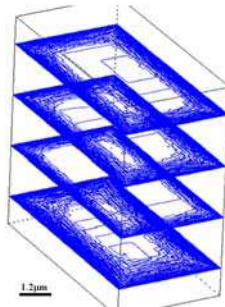


Figure Typical dislocation structure developed in confined geometry

References

- [1] A. Roy, A. Acharya, J. Mech. Phys. Solids, 53 (2005), 143.
- [2] S. Forest, Phil. Mag., 83 (2003), 245.
- [3] C.S. Shin, M. C. Fivel, M. Verdier, C. Robertson, Mater. Sci. Eng. A, 400-401 (2005), 166.

Real-Space Methods for Multiscale Modeling of Ferroelectrics

Kaushik Dayal¹, Lun Yang¹ and Jason Marshall¹

¹Carnegie Mellon University, Pittsburgh PA 15213, United States
Kaushik@cmu.edu, luny@cmu.edu, jmarshall@cmu.edu

Current ferroelectric devices, such as in thin-films, are fabricated with complex geometries and are subject to complex electromechanical loads. In these situations, spatially-varying long-range electric fields are present throughout the device as well as outside in free space. As the electric fields play a critical role in the functionality of devices, it is important to resolve them accurately.

Typical periodic boundary conditions are inadequate for the complex situations described above. We have developed accurate and efficient real-space methods to address these situations. In particular, through the application of Dirichlet-to-Neumann maps using Boundary Elements, we transform the problem from solving over all of space for the stray electric fields to a consistent local problem only over the region of interest. This enables vast savings and provides a multiscale scheme to focus the computational effort in regions of interest while being consistent with far-field conditions.

We shall present the method and related computational techniques related to Boundary Elements. We have coupled our multiscale electrostatic solver to material descriptions at two different scales, first a phase-field mode and second an atomistic multiscale (*quasicontinuum*) model. We shall describe our implementation of the coupling of the electrostatics to these descriptions, and present results of our computations to problems such as free-surface microstructure in ferroelectrics, response of ferroelectric thin-films to electrodes and piezo-force microscopy, and the electromechanics of crack tips.

Numerical Quadrature in the Quasicontinuum Method with Application to Nanoindentation Simulation

Bernhard Eidel¹, Nirav Prajapati¹

¹Interdisciplinary Centre for Advanced Materials Simulation, Ruhr-University Bochum,
Stiepeler Str. 129, 44801 Bochum, Germany,
bernhard.eidel@rub.de

Recent research in atomistic-to-continuum coupling and in particular in the Quasicontinuum (QC) method has shown a strong interest in numerical quadrature because it largely determines the methods accuracy and efficiency, [1]-[5]. Mathematical analyses of quadrature schemes often restrict to the 1-D case of atomic chain models, to simple pair potentials and to additional ad-hoc assumptions. These simplifications make the problem tractable by analytical means or alleviate numerical analysis. Doing this, mathematics has brought new insights into concurrent multiscale modelling. However, it is not clear, whether the obtained results and conclusions of such analyses can be transferred to problems without these simplifying assumptions.

The main aim of the present contribution is the numerical analysis of different quadrature rules within the QC method in a more realistic physical setting, namely in 3-D applying EAM-potentials in paradigmatic multiscale settings of computational materials science. In particular, we compare the method proposed in [4] with the cluster-based summation rule as proposed in [1] and analyzed in [2]-[5]. The quadrature schemes are assessed in representative numerical examples like nanoindentation which showcase the influence of numerical features like numerical quadrature and (adaptive) meshing on reliable predictions of key materials and process information.

References

- [1] Knap J., Ortiz M.: J. Mech. Phys. Solids 49 (2001) 1899 – 1923.
- [2] Eidel B., Stukowski A.: J. Mech. Phys. Solids 57 (2009) 87-108.
- [3] Ortner C., Luskin M.: SIAM J. Numer. Anal. 47 (2009) 3070-3086.
- [4] Gunzburger M., Zhang Y.: SIAM Multiscale Model. Simul., 8 (2010) 571-590.
- [5] Miller R.E., Tadmor E.B: Modelling Simul. Mater. Sci. Eng. 17 (2009) 053001 (51pp).

Modeling Martensitic Phase Transformations via the Self-Consistent Lattice Dynamics Approach

Ryan S. Elliott¹, Venkata Suresh Guthikonda¹

¹The University of Minnesota
Department of Aerospace Engineering and Mechanics
107 Akerman Hall
110 Union St. S.E.
Minneapolis, Minnesota 55455 USA
elliott@aem.umn.edu

The unusual properties of shape memory alloys (SMAs) are due to solid-to-solid martensitic phase transformations (MPTs) that correspond to a lattice level instability of the material's crystal structure. The high temperature phase, which is often entropically stabilized, is usually a high symmetry structure and is called the austenite phase whereas the low temperature phase has low symmetry and is called the martensite phase. Currently, there exists a shortage of material models for MPTs based on the material's atomic composition and crystal structure. The present work develops a model using a first-order self-consistent lattice dynamics approach that aims to capture the qualitative and ultimately quantitative behavior of MPTs. In this approach, a renormalization of the frequencies of atomic vibration (phonons) via a set of self-consistent equations allows the model to accurately capture how atomic vibrations affect the thermomechanical properties of the material. These renormalized phonon frequencies are dependent on both crystalline configuration and temperature.

For illustrative purposes, the model is applied to a one-dimensional bi-atomic chain. The Morse pair potential is selected to describe atomic interactions and parameters are chosen to demonstrate the model's capabilities. The model is evaluated by generating bifurcation diagrams corresponding to thermal and mechanical loading. These diagrams consist of equilibrium paths as a function of the loading parameter (temperature or stress). The paths are generated using branch-following and bifurcation techniques. A first-order MPT is predicted which involves transformation from an entropically stabilized high symmetry phase to a low symmetry phase as the temperature is decreased. It is found that the MPT can be both temperature-induced and stress-induced. Both types of MPT are required in order for a material to exhibit the full range of typical SMA behavior.

The qualitative prediction of a temperature- and stress-induced MPT indicates the likely hood that the current model can be used for the computational discovery of new SMAs. Such an undertaking would involve, first, obtaining an accurate set of interatomic potentials for the alloy system of interest and, second, using these potentials with the current self-consistent model to evaluate the shape memory behavior of the previously unstudied materials.

Smooth capping of short-range repulsive forces in hybrid atomistic/coarse-grain molecular dynamics simulation

Authors: Bernd Ensing

Affiliations: Van 't Hoff Institute for Molecular Sciences; University of Amsterdam;
Nieuwe Achtergracht 166; 1018WV Amsterdam; b.ensing@uva.nl

ABSTRACT

In adaptive multiscale simulation, particles automatically adapt their resolution when they move from the atomistic region to the coarse-grained surrounding or vice versa. The latter process entails the smooth insertion of the extra atomistic degrees of freedom onto the coarse-grain particles, which is prone to problematic atom-atom overlaps. Here we show that this so-called reverse mapping problem is significantly reduced by smoothly capping the repulsive part of the atomistic pair-interactions to a maximum absolute force. Not surprisingly, capping the interactions at too low a force affects the properties of the system, firstly seen in the pressure and the diffusion coefficient. Good results are obtained for forces capped between 10^4 and 10^8 K/Å.

1. Introduction

Hybrid atomistic/coarse-grain molecular dynamics simulation^{1,2,3}, or hybrid MD for short, is a relatively new method to model soft matter systems that exhibit an intrinsic multiscale character. Examples of such systems are polymers and bio-molecular assemblies, such as lipid membranes and proteins. These materials display interesting phenomena that take place on time and length scales that are too large to model by brute force molecular dynamics simulation in full atomistic detail. Instead, mesoscopic coarse-grain models have been developed, in which each particle typically represents a chemical group of several atoms, to model systems of micrometer and microsecond length and time scales, however at the cost of losing the atomistic details^{4,5,6}. Hybrid MD simulation aims to link the mesoscale phenomena to the underlying atomistic motions, by focusing locally in atomistic detail while treating the environment of the atomistic region at the computationally less demanding coarse-grain representation.

A key feature of a multiscale modeling method is its ability to bridge between the different molecular representations^{7,8}. A hybrid MD simulation of a fluidic system requires, in the first place, a proper coupling between the particles in the atomistic region and those in the coarse-grained environment, and secondly, a mechanism to switch between the two representations of particles that diffuse from one region to the other. Especially the on-the-fly switching from a low-resolution coarse-grain representation to the high-resolution atomistic representation is fraught with difficulty. There is not a unique solution to re-insert the atoms into a coarse-grained particle, such that the inserted degrees of freedom are in thermal equilibrium with their surrounding.

We have recently developed a hybrid MD method that combines two so-called reverse mapping techniques to smoothly map the atoms onto a coarse-grained molecule when it enters the high-resolution region⁹. In the first place, a special “healing region” is introduced in between the high and low resolution regions, in which particles gradually adapt their representation by smoothly scaling their interaction potentials². Although this approach was shown to work well

for relatively simple liquids that consist of molecules that can be represented by a single coarse-grained bead, such as liquid methane, a second reverse mapping technique is required to model molecules that consist of two or more connected coarse-grained beads. The problem with connected beads is that a proper orientation of the atomic fragments with respect to that of the molecular frame is essential to allow for a smooth insertion of the atoms when in the healing region. By preconditioning the orientations of the atomistic fragments through an auxiliary rigid body rotation dynamics in the low-resolution region, hybrid MD of interesting macromolecular soft matter systems has become possible⁹.

In the present work, we investigate an additional technique to improve the reverse mapping in hybrid MD simulation: capping of the repulsive part of the atomistic pair-potentials. Typical pair-potentials, such as the Lennard-Jones potential or the Buckingham potential describe the repulsive interaction that two closed-shell atoms feel at short distance due to the electronic Pauli exchange repulsion with a steep inverse twelfth power function or an exponential function respectively. At inter-atomic distances very close to zero the forces on the atoms become extremely large (so-called atom overlaps), which can cause havoc for the molecular dynamics integrator. Under normal, not too extreme temperature and pressure, conditions this does not happen in practice in atomistic equilibrium simulations. However, reverse mapping atomistic details into a coarse-grained molecule is not an equilibrium process and very short inter-atomic distances may occur due to the relatively soft nature of the coarse-grain beads.

Especially when the level of coarse-graining is high, that is, when a coarse-grain bead represents many atoms, and also when the underlying atomistic fragment structure is highly anisotropic, catastrophic overlaps may occur when the atomistic details are inserted into coarse-grain particles that move through the healing region toward the high-resolution region. Enlarging the healing region so that particles move on a longer transition path and thus switch resolution more gradually reduces the probability of overlaps. It is however computationally advantageous to keep the healing region as thin as possible. As an alternative, we consider here to cap the repulsive part of the pair-potential at very short distances. Anticipating our results, we find that such capping improves the reverse mapping, as indicated by better total energy conservation in hybrid MD simulation of liquid hexane, and that the capping does not affect the structural and dynamical properties of the system, unless the capping is done at too low values of the forces.

2. Methods

2.1 Pair-potential capping

The purpose of capping the atomistic pair-interactions is to avoid too large forces at atom-atom distances close to zero, which configurations can occur when atoms are gradually inserted into the coarse-grained particles during a hybrid MD simulation. The capped potentials are constructed starting from the standard 12-6 Lennard-Jones pair-potential:

$$V^{\text{LJ}}(r) = 4\epsilon \left[\left(\frac{\sigma}{r} \right)^{12} - \left(\frac{\sigma}{r} \right)^6 \right], \quad (1)$$

where r is the distance between the atoms, ϵ is the depth of the the potential well, and σ is the distance where the inter-particle potential is zero. At distances shorter than σ the first term dominates, which governs the steep r^{-12} repulsive wall.

In order to set a maximum allowed absolute force, F^{max} , at inter-particle distances shorter than

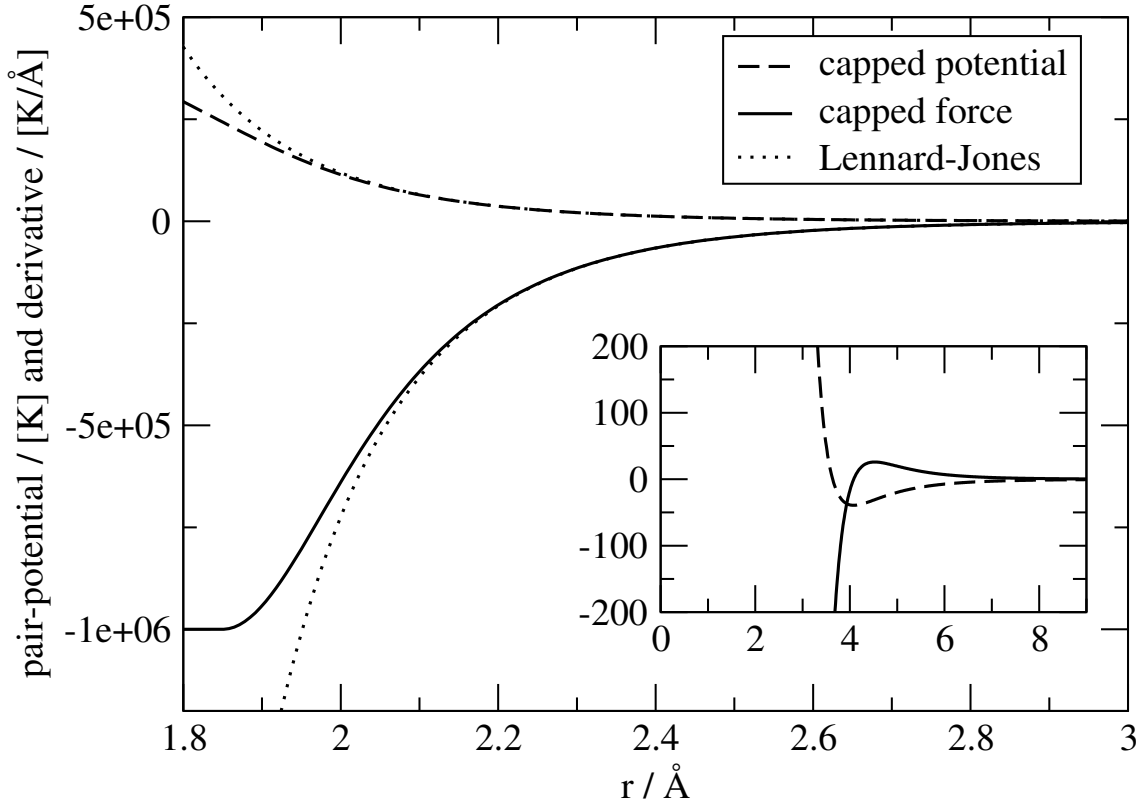


Figure 1: Comparison of the capped tabulated potential (dashed line) and force (solid line) with the original Lennard-Jones functions (dotted lines). The force is capped to -10^{-6} K/Å, which results in a linear potential at short distances. The inset zooms in on the potential well.

a cutoff r^{cut} , the force of the capped interaction is taken to be:

$$F^{\text{capped}} = \begin{cases} F^{\text{max}} & \text{if } r < r^{\text{cut}} \\ -w(r) * \frac{dV^{\text{LJ}}(r)}{dr} & \text{if } r \geq r^{\text{cut}} \end{cases} \quad (2)$$

in which $w(r)$ is,

$$w(r) = \frac{1 - \left(\frac{r^{\text{switch}}}{r}\right)^{26}}{1 - \left(\frac{r^{\text{switch}}}{r}\right)^{52}}, \quad (3)$$

a function that switches smoothly from 0 to 1 in the neighborhood of the distance r^{switch} . The cutoff distance, r^{cut} , is found by moving the position of the switch function, r^{switch} , in an iterative procedure such that the target maximum absolute force, F^{max} is set at r^{cut} . The potential belonging to this function for the force is obtained by integration. The potentials and forces are input to the MD program as tabulated functions on a grid of 4000 points between $r = 0$ and the interaction cutoff distance of 10 Å. Fig. 1 shows an example capped force and potential compared to the original Lennard-Jones potential for a carbon-carbon interaction.

2.2 Hybrid molecular dynamics

The hybrid atomistic/coarse-grain molecular dynamics simulations are performed using the algorithm presented in Refs.^{2,9}. In brief, the entire molecular system is simultaneously represented in both the atomistic and the coarse-grained detail. The system is spatially partitioned in a high-resolution region with a surrounding healing region in which the atoms are propagated

and a low-resolution region in which the coarse-grained particles are evolved. In both regions, the coordinates of the inactive representation are updated by matching the centers of mass of the particles every time step. In addition, in the low-resolution region the orientation of the inactive, frozen, atomistic fragments are evolved using an auxiliary rigid body rotation dynamics, governed by a reduced energy function of selected atomistic intra-molecular potentials¹⁰.

The coupling between atoms and coarse-grain particles, as well as the switching between representations in the healing region is governed by a hybrid potential,

$$V^{A/CG} = \sum_{\alpha\beta} \left(\lambda_{\alpha\beta} \Phi_{\alpha\beta}^{CG} + (1 - \lambda_{\alpha\beta}) \sum_{\substack{i \in \alpha \\ j \in \beta}} \Phi_{ij}^A \right), \quad (4)$$

which sums over all pairs of coarse-grain particles α and β and mixes the coarse-grain pair-interaction, Φ^{CG} , with the sum of atomistic pair-interactions, Φ^A , of atoms i grouped in α and atoms j grouped in β , using a scaling function $\lambda \in [0, 1]$ that depends on the particle positions. Further details on the hybrid MD method are found in Ref.².

3. Results

3.1 Effect of capping on structural and dynamical properties

To assess the effect of capped pair-interactions on the properties of the system, we performed a series of fully atomistic MD simulations of liquid hexane, in which the Lennard-Jones potentials were capped to maximum forces of 600, 10^3 , 10^4 , 10^6 , 10^8 , and ∞ K/Å. To this end, 250 hexane molecules were simulated in a cubic box subject to periodic boundary conditions in the NVT ensemble. A temperature of $T = 303.15$ K was maintained using the Nosé-Hoover chain thermostat. The CHARMM¹¹ force-field was used and adapted by capping the Vanderwaals interactions. The simulations were performed using our in house CM3D molecular dynamics program.

The following properties were computed: the average pressure, the carbon-carbon and carbon-hydrogen radial distribution functions, the carbon and hydrogen velocity auto-correlation functions (from which the infrared spectrum was computed), and the carbon mean-square displacement, from which the self-diffusion coefficient was obtained. In Fig. 2 is shown that the radial distribution functions (top panel) and vibration spectra (middle panel) are indistinguishable with respect to the different capped potentials. However, the capping has a noticeable effect on the mean square displacement (bottom panel), the diffusion, D , and the pressure P (see Tab. 1) for capping values lower than $F^{\max} = 10^4$ K/Å.

3.2 Effect of capping on reverse mapping in hybrid MD

To test the effect of using capped potentials on the reverse mapping in a hybrid MD simulation, we performed multiscale simulations of hexane using the previous series of capped atomistic pair-potentials. The hybrid system contained 1900 hexane molecules in a rectangular box with dimensions close to 60 x 60 x 120 Å using periodic boundary conditions. The atomistic region was chosen to be a 2D slab with a width of 24 Å flanked on both sides by a healing region with a width of 5 Å. At the coarse-grained level, hexane was modeled using the forcefield of Nielsen *et al*, in which each molecule is modeled by two beads (representing C₃H₇) bonded with

Table 1: The self-diffusion coefficient, D , obtained from the slope of the mean square displacement, and the average pressure, P , computed using interactions capped at different absolute maximum forces, F^{\max} .

F^{\max} [k/Å]	D [10^{-5} cm ² /s]	P [atm]
600	5.4	-0.38
10^3	4.7	0.27
10^4	3.9	1.7
10^6	4.0	1.7
10^8	3.7	1.6
∞	4.0	1.7

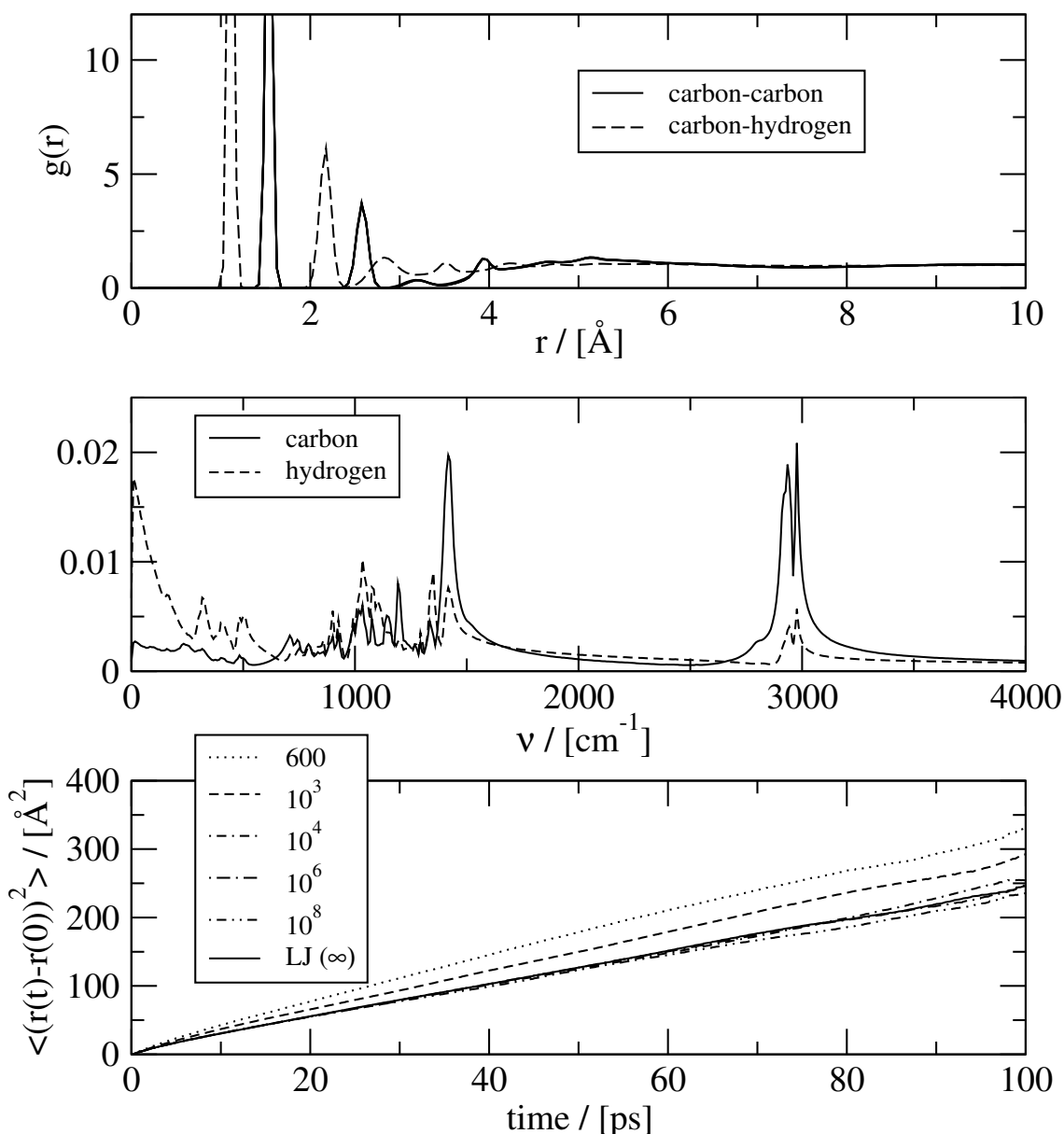


Figure 2: Structural and dynamical properties of liquid hexane modeled with Vanderwaals interactions capped at a maximum force of 600, 10^3 , 10^4 , 10^6 , 10^8 , and infinite (i.e. normal Lennard-Jones)

a harmonic spring and interacting through 9-6 Lennard-Jones pair-potentials¹². To assess the performance of the reverse-mapping, we monitor the hybrid total energy, which is very sensitive to the accuracy of the integration of the equations of motion. This hybrid total energy is not a physical property, but rather an auxiliary conserved quantity that allows for quality control.

Fig. 3 shows this total energy for 200 ps hybrid MD simulations using the potentials capped at 10^6 and 10^8 K/Å respectively, as well as the original Lennard-Jones potentials. Clearly, the total energy is not properly conserved, and shows jumps due to atom-overlaps in the healing region using the (uncapped) Lennard-Jones potentials, and a healing region width of 5 Å. The simulations using the capped potentials show very good energy conservation, indicating a smooth switching of resolution of hexane molecules. Capping at 10^6 K/Å shows slightly better performance than capping at 10^8 K/Å, and further improvement may be reached by capping at even lower absolute forces, but that may affect the dynamics of the system as was shown above.

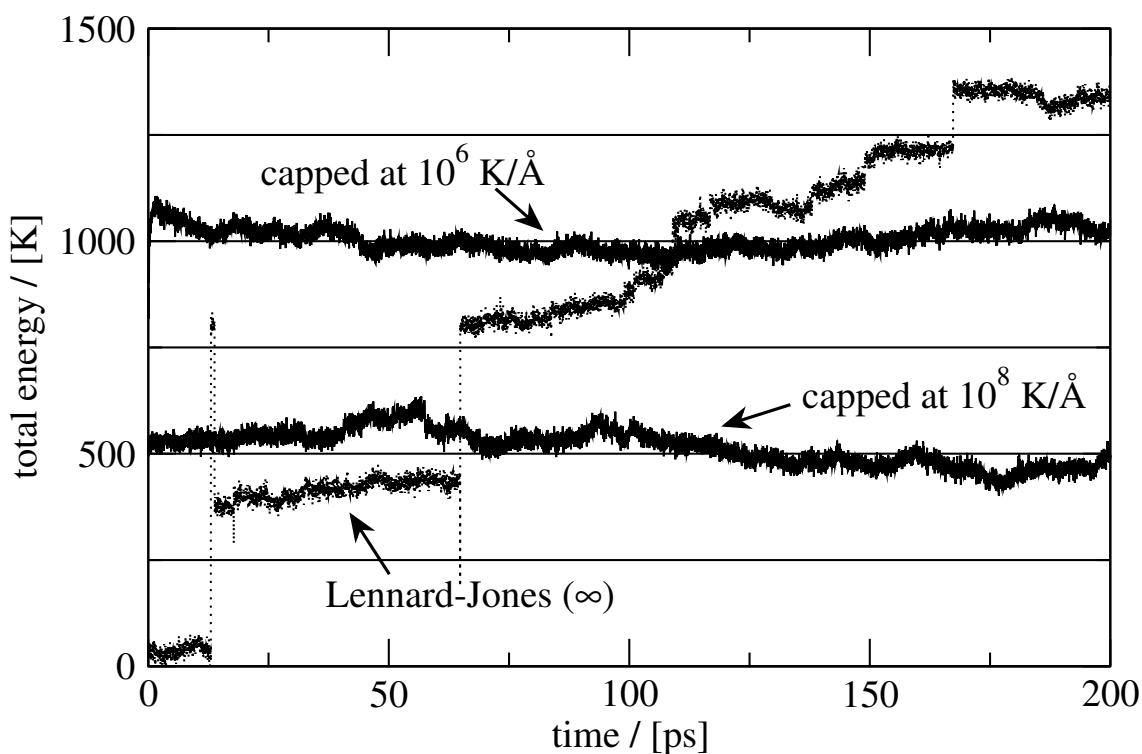


Figure 3: Hybrid total energy conservation from three different multiscale simulations of liquid hexane using pair-interaction capped at a maximum force of 10^6 , 10^8 , and infinite (i.e. normal Lennard-Jones).

Conclusion

We have investigated the effect of capping the repulsive part of the Lennard-Jones pair-potentials on structural and dynamical properties for the benefit of improving the reverse mapping of atomic fragments onto coarse-grained particles in hybrid MD simulation. Capping the interactions to a too small maximum absolute force (smaller than 10^4 K/Å in our bulk hexane calculations) is, perhaps not surprisingly, first seen to affect the pressure and the self-diffusion. Nevertheless, capping at larger values still has a positive effect on the reverse-mapping in hybrid atomistic/coarse-grain simulations, as seen from the conservation of the total energy. This is because accidental overlaps between atoms when they are inserted onto the coarse-grained particles do no longer cause extremely large repulsive forces that disrupt the MD integration.

Acknowledgments

References

- [1] M. Praprotnik, L. Delle Site, and K. Kremer. Adaptive resolution molecular-dynamics simulation: Changing the degrees of freedom on the fly. *J. Chem. Phys.*, **123**, 224106, 2005.
- [2] Bernd Ensing, Steven O. Nielsen, Preston B. Moore, Michael L. Klein, and Michele Parrinello. Energy conservation in adaptive hybrid atomistic/coarse-grain molecular dynamics. *J. Chem. Theory Comput.*, **3**, 1100–1105, 2007.
- [3] Andreas Heyden and Donald G Truhlar. Conservative algorithm for an adaptive change of resolution in mixed atomistic/coarse-grained multiscale simulations. *J. Chem. Theory Comput.*, **4**, 217–221, 2008.
- [4] F. Müller-Plathe. Coarse-graining in polymer simulation: From the atomistic to the mesoscopic scale and back. *ChemPhysChem*, **3**, 754–769, 2002.
- [5] S. O. Nielsen, C. F. Lopez, S. Srinivas, and M. L. Klein. Coarse grain models and the computer simulation of soft materials. *J. Phys. Cond. Matt.*, **16**, R481–R512, 2004.
- [6] Michael L Klein and Wataru Shinoda. Large-scale molecular dynamics simulations of self-assembling systems. *Science*, **321**, 798–800, 2008.
- [7] K. M. Mohamed and A. A. Mohamad. A review of the development of hybrid atomistic-continuum methods for dense fluids. *Microfluidics and NanoFluidics*, **8**, 283–302, 2010.
- [8] Matej Praprotnik, Luigi Delle Site, and Kurt Kremer. Multiscale simulation of soft matter: From scale bridging to adaptive resolution. *Annu. Rev. Phys. Chem.*, **59**, 545–571, 2008.
- [9] Steven O. Nielsen, Preston B. Moore, and Bernd Ensing. Adaptive multiscale molecular dynamics of macromolecular fluids. *submitted*, 2010.
- [10] B. Ensing and S. O. Nielsen. Multiscale molecular dynamics and the reverse mapping problem. In T. Dumitrica, editor, *Trends in Computational Nanomechanics*, volume 2 of *Challenges and Advances in Computational Chemistry and Physics*, pages 25–59. Springer Netherlands, 2010.
- [11] A.D. MacKerel Jr., C.L. Brooks III, L. Nilsson, B. Roux, Y. Won, and M. Karplus. Charmm: The energy function and its parameterization with an overview of the program. In P. v. R. Schleyer et al., editor, *The Encyclopedia of Computational Chemistry*, volume 1, pages 271–277. John Wiley & Sons: Chichester, 1998.
- [12] S O Nielsen, C F Lopez, G Srinivas, and M L Klein. A coarse grain model for n-alkanes parameterized from surface tension data. *J. Chem. Phys.*, **119**, 7043–7049, 2003.

**A multiscale coupling approach
based on local averaging techniques**
Konstantin Fackeldey¹, Rolf Krause² and Dorian Krause²

¹Konrad-Zuse-Zentrum für Informationstechnik Berlin (ZIB),
Takustrasse 7, 14195 Berlin, Germany
fackeldey@zib.de

²Institute of Computational Science, University of Lugano,
Via Giuseppe Buffi 13, 6900 Lugano, Switzerland

In the last three decades multiscale methods have been developed with the aim to bridge the gap between atomistic and continuum simulations.

For a seamless transition from the fine scale (atomistic) to the coarse scale (continuum) a proper handling of the transition conditions at the interface between the scales is indispensable otherwise spurious reflection will adulterate the simulation. These reflected waves are typically of high frequency and are arguably of little importance in the domain of the coarse scale.

In this talk we analyze this phenomenon and sketch the framework of the *weak coupling method*, which is capable of separating reliably the high frequency waves from the low frequency waves by employing a function space based approach. Thus we let the low frequency waves which have a proper meaning in the finite element setting pass, whereas the high frequency waves are removed by our frequency decomposition approach techniques without affecting the coupled share of the solution.

In contrast to all existing approaches in this context, the separation of the wavelength is achieved by employing a discrete L^2 – projection in a function space setting. The coupling constraints enforce matching in the range of this projection. These averaging constraints allow for the usage of standard symplectic integrators for constrained Hamiltonian systems, such as the well-known RATTLE integrator.

Identification of fundamental materials-design limits in ultra lightweight Mg-Li alloys via quantum-mechanical calculations

Martin Friák^{1*}, William Art Counts¹, Dierk Raabe¹ and Jörg Neugebauer¹

¹Max-Planck-Institut für Eisenforschung GmbH, Max-Planck-Strasse 1, D-40237, Düsseldorf, Germany (*m.friak@mpie.de)

Quantum-mechanical calculations are becoming increasingly useful to engineers interested in designing new alloys because these calculations are able to accurately predict basic material properties only knowing the atomic composition of the material. In this paper, fundamental physical properties (formation energies, elastic constants) of a dense set of bcc Mg-Li compounds are calculated using density-functional theory (DFT) and compared with experimental data. These DFT-determined properties are in turn used to calculate engineering parameters like (i) specific Young's modulus (Y/ρ) or (ii) bulk over shear modulus ratio (B/G) as an approximative indicator of either brittle or ductile behavior. The engineering parameters are then used to identify alloys that have optimal mechanical properties for light weight applications. An Ashby map containing Y/ρ vs. B/G shows that it is not possible to increase both Y/ρ and B/G by changing only the composition or local order of a binary alloy (W. A. Counts, M. Friák, D. Raabe, and J. Neugebauer, *Acta Mater* 57 (2009) 69-76). In an attempt to bypass the limitation, MgLi-X ternaries ($X=Ca, Al, Si, Cu, Zn$) are studied but none of the five solutes is able to simultaneously improve both properties (W. A. Counts, M. Friák, D. Raabe, and J. Neugebauer, *Adv. Eng. Mat.* (2010) in press).

Asymptotics-based multiconfiguration methods and the electronic structure of transition metal atoms

Gero Friesecke

Abstract: Asymptotics-based Configuration-Interaction (CI) methods are a class of CI methods which reproduce, at fixed finite subspace dimension, the exact Schrodinger eigenstates in the limit of fixed electron number and large nuclear charge. This limit has the multiscale property that the ratio of first spectral gap to ground state energy tends to zero, the experimental ratio for atoms being very close to zero, about 1 part in 1000 for Carbon and Oxygen and 1 part in 30 000 for Cr and Fe. We describe an efficient algorithm for asymptotics-based CI, with full resolution of valence electron correlations. A key ingredient is exact (symbolic) symmetry reduction of the CI space at essentially linear computational cost.

Applications to 3d transition metal atoms are in good agreement with experimental data. Unlike DFT based studies, even with the best available exchange-correlation functionals, our calculations correctly reproduce the anomalous magnetic moment and orbital filling of Chromium in the otherwise regular series Ca, Sc, Ti, V, Cr.

Joint work with Christian Mendl (TU Munich).

Generalized Mass Dynamics: An accelerated Molecular Dynamics Method based on Deterministic Equations

S. Alireza Ghasemi¹ and Stefan Goedecker¹

¹Department of Physics, Universität Basel, Klingelbergstr. 82, 4056 Basel, Switzerland;
Alireza.Ghasemi@unibas.ch

Molecular dynamics simulations all share a common problem relevant to the time scales of the natural processes being studied. This is even more challenging for ab initio molecular dynamics simulations where computationally demanding force and energy evaluations must be repeated so many times. Although there are a variety of methods to circumvent this problem but none of them can be used in a simulation for systematically calculating average thermodynamic quantities.

We have developed an accelerated molecular dynamics method which is, unlike Monte Carlo methods, based on deterministic equations and is capable of calculating average thermodynamic quantities in a systematic way. This is done without altering the potential energy landscape. In fact the atomic masses are replaced by the second derivative of the potential energy which is manipulated to avoid affecting the average thermodynamic quantities. We call this method *Generalized Mass Dynamics*. We have numerically shown that our approach samples the conformational space more efficiently than normal molecular dynamics simulations. It is particularly advantageous for ab initio molecular dynamics simulations of biomolecules.

Rate-Dependent Model of Mobility of Interfacial Microstructures in Shape Memory Alloys

Authors: Ondřej Glatz^{1,2}, Hanuš Seiner^{1,2}, Michal Landa²

Affiliations: ¹Institute of Thermomechanics, Academy of Sciences of the Czech Republic, Dolejškova 5, 18 200 Prague 8, Czech Republic; ²Faculty of Nuclear Sciences and Physical Engineering, CTU in Prague, Trojanova 13, 120 00 Prague 2, Czech Republic.

ABSTRACT

Spontaneous formation and propagation of interfacial microstructures (X and lambda) observed experimentally during the shape recovery process of single crystals of the Cu-Al-Ni shape memory alloy cannot be reliably described by the widely used, quasi-static models of SMAs. We present a simple mathematical model of mobility of the interfacial microstructure based on an assumption that the propagating microstructure dissipates energy by a viscous mechanism, whereto the viscosity parameters are empirically tuned such that the macroscopic speed of propagation of the microstructure agrees with the experimental observations. We show that such model sufficiently explains the existence of the X- and lambda-microstructures, although the morphology of these microstructures contradicts the predictions of the classical theory of martensitic microstructures.

1. Introduction

Formation of the X- and lambda-microstructures between austenite and martensite in single crystals of the shape memory alloys was firstly reported by Basinsky and Christian [1] for the In-Th alloy. In the single crystal of Cu-Al-Ni alloy (rectangular parallelepiped), formation of such microstructures was recently observed by the authors [2] during the thermally induced transition from the mechanically stabilised 2H-martensite into austenite (see this reference for detailed description of the microstructures and the experiment). Both microstructures have a shape of the letter X and consist of two mutually intersecting habit planes separating austenite from twinned regions of martensite and another pair of mutually intersecting interfaces separating these twinned regions from the single variant of martensite. The microstructures differ only in the twinning plane orientation in one of the twinned regions. As shown in [3, 4, 5] the X- and lambda- microstructures do not fulfil the geometric compatibility conditions, so according to the classical theory of Ball and James [6] they are not admissible. The aim of this paper is to develop a simple model governing the spontaneous formation and propagation of these microstructures through the specimen. Because of the incompatibility mentioned above, the elastic deformation must be taken into account. Since no external loadings are present, the quasi-static approach cannot be used, and the speed of the transition is controlled by the dissipation mechanism only.

2. Modelling

To ensure relative simplicity of implementation, we decided to base the model on a suitable variational principle. The right choice strongly depends on the way how the dissipation mechanism is understood and described. In this aspect our model differs from the most of the others (e.g. [7]).

We can consider that the energy dissipated during the process is equivalent to the work done by dissipative (or friction-like) forces, and formulate the following variational condition on total energy change rate \dot{E}

$$\dot{E} = \dot{A} + \frac{1}{2} \int_{\mathcal{V}} \sigma_{ij}^{diss.} \dot{\epsilon}_{ij} \, d\mathbf{x} \rightarrow \min , \quad (1)$$

where \dot{A} is a Helmholtz free energy change rate, $\sigma_{ij}^{diss.}$ is a *dissipative stress tensor* and ϵ is a finite strain tensor. We chose the austenite state as a reference configuration. Then, the sought strain tensor function $\epsilon_{ij}(t)$ comprises the inelastic transformation strains as well as the elastic strains. This extremal condition Eqn. (1) can be understood as a particular form of the Biot's principle (see [8]) for rate-dependent dissipative systems. Since we are dealing with the isothermal process, the Helmholtz free energy A is assumed in the form

$$A = W + E_e = c_m \mathcal{V}_m + c_a \mathcal{V}_a + E_e , \quad (2)$$

where W is the transformation part and E_e is stored elastic energy. The transformation part is assumed to be a linear function of the martensite and austenite volumes \mathcal{V}_m and \mathcal{V}_a . Notice that the time derivative of the first term of Eqn. (2)

$$\dot{W} = c_m \dot{\mathcal{V}}_m + c_a \dot{\mathcal{V}}_a \quad (3)$$

is 1-degree homogeneous in transformed volume change rate, since $\dot{\mathcal{V}}_m = -\dot{\mathcal{V}}_a$. Thus, in fact, it represents not only the change of the transformation part of the free energy, but it can also comprise the rate-dependent part of the dissipation. The dissipative tensor $\sigma_{ij}^{diss.}$ can be considered in a general form

$$\sigma_{ij}^{diss.} = \eta_{ijkl} \dot{\epsilon}_{kl} , \quad (4)$$

where η_{ijkl} is a *viscosity tensor*, see [9]. Since there are no experimental data for constants η_{ijkl} , the simple isotropic form is used. For an isotropic body this tensor has only two independent components, so the dissipative tensor can be written in the form

$$\sigma^{diss.} = \mu_V \frac{\text{tr} \dot{\epsilon}}{3} \mathbf{I} + \mu_S \left(\dot{\epsilon} - \frac{\text{tr} \dot{\epsilon}}{3} \mathbf{I} \right) , \quad (5)$$

where the *bulk viscosity* μ_V is related mostly to the thermoelasticity and the *shear viscosity* μ_S is related to the viscous motion of dislocations and twin boundaries. For simplicity, we will consider the values of μ_V and μ_S to be the same both inside all individual phases (martensite, twinned martensite, austenite) and at the interfaces. Thus, the finite jumps in ϵ_{ij} at the interface planes ensure that most of the energy is dissipated by the moving interfaces.

The model depends on four yet unspecified constants: the transformation parts of the free energy density of the martensite and austenite (c_m , c_a), and two viscosity constants (bulk viscosity μ_V , shear viscosity μ_S). Unfortunately, there are no (or poor) experimental estimates of these constants. Thus, we choose them so that the model fits observations in the main properties. The energy densities c_m and c_a are defined up to an additive constant and the model depends on their difference only, thus we set $c_a = 0 \text{ J.m}^{-3}$. The shear viscosity μ_S related to motion of dislocations is chosen to be approximately ten times smaller than the bulk viscosity. The absolute values of the constants were fitted to observed propagation velocity and expected latent heat absorption rate, which was supposed to be higher but comparable to the dissipation rate (according to infrared microscopy observations in [10] the specimen is undercooled by the microstructure motion). Here, the velocity (about 2 mm.s^{-1}) was taken from [10] and the latent heat of the transition was taken from [11]. The obtained parameters follow: $c_a = 0 \text{ J.m}^{-3}$, $c_m = 5 \times 10^7 \text{ J.m}^{-3}$, $\mu_V = 3.36 \times 10^{10} \text{ Pa.s}$, and $\mu_S = 1.2 \times 10^9 \text{ Pa.s}$.

3. Solution and Results

First of all the suitable parametrisation of the microstructure geometry must be found. Evolution of selected geometric parameters defines the finite strain tensor $\epsilon_{ij}(\mathbf{x}, t)$. Dimensions of the specimen are fixed, twinned regions are treated as homogeneous and interfaces are supposed to be exact planes. Thus, the microstructure is fully described by ten parameters defining the position of whole microstructure within the specimen (two parameters), orientations of all habit planes and martensite–twinned martensite interfaces (six parameters), and the volume fractions of the minor martensite variants in both twinned regions (two parameters). For detailed description of chosen parameters see [4, 5]. Then, the problem Eqn. (1) comprises ten-parametric optimisation. Since the underlying processes governing the orientations of the interfaces occur at faster time-scale than the movement of the whole microstructure, we split the optimisation into two nested loops. In the inner optimisation loop for the fixed microstructure position the optimal microstructure geometry is found with respect to the stored elastic energy. Then, the outer loop finds the next optimal microstructure position according to Eqn. (1). All computations were done in MATLAB in connection with Comsol Multiphysics FEM environment. For implementation details see [3, 4, 5].

Main results of the simulation of the propagating lambda-microstructure are briefly presented in Fig. 1. The results for the X-microstructure are qualitatively the same. First image illustrates evolutions paths of the microstructure positions for two distinct starting configurations. On the next graph the behaviour of the stored elastic energy along the evolution paths is presented. Notice, that the stored elastic energy increases during the motion. Last two images show the von Mises stress distribution in the cross-section of the lambda-microstructure for the starting and finishing configuration of the first path. It should be also pointed out that the behavior of computed microstructure propagation velocity is in agreement with the experimental observations reported in [10]. Within these observations the velocity drops when the microstructure is fully formed and further remains almost constant. This is because of lower dissipation during the microstructure formation.

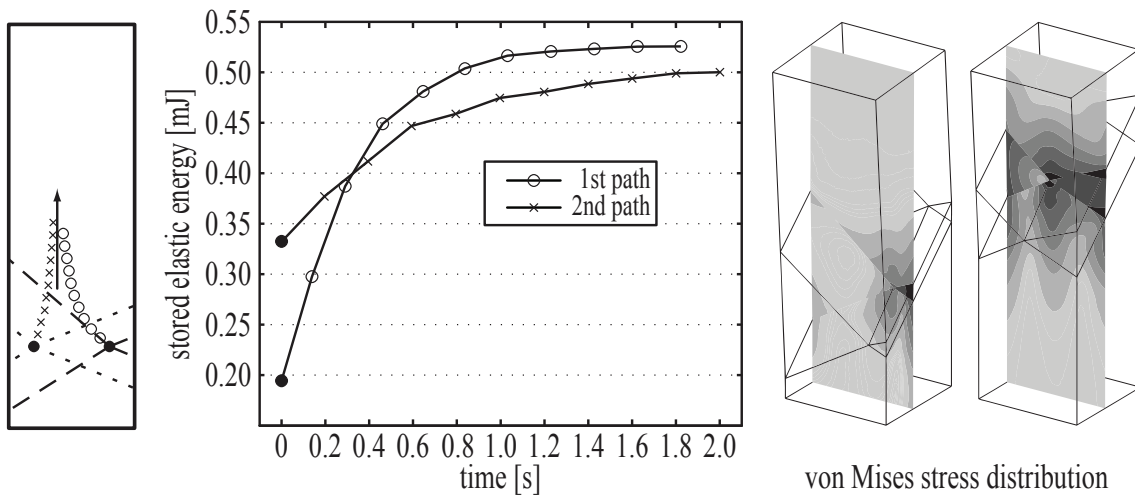


Figure 1: Lambda-microstructure evolution. Stress distribution for chosen configurations.

4. Conclusions

We have constructed a model governing the spontaneous evolution of the microstructure under the constant external conditions. The main difference from the most of the other published

models is in the incorporation of the rate-dependent dissipation mechanism, which enables us to describe fast evolution processes. We showed that our model is able to catch the main properties of the microstructure evolution. Especially, it explains observed tendency of the microstructure to evolve towards the more incompatible state (the state with the higher stored elastic energy). This behavior contradicts the classical condition on geometric compatibility, under which such microstructures are inadmissible.

Acknowledgements

Supports from the Grant Agency of ASCR (project No. IAA200100627), Czech Science Foundation (project No. 202/09/P164) and the research program of IT ASCR (CEZ:AV0Z20760514).

References

- [1] Z.S. Basinski and J.W. Christian. Experiments on the martensitic transformation in single crystals of indium–thallium alloys. *Acta Metallurgica*, **2**(1), 148–166, 1954.
- [2] Hanuš Seiner, Michal Landa and Petr Sedlák. Shape recovery mechanism observed in single crystals of Cu-Al-Ni shape memory alloy. *Phase Transitions*, **81**(6), 537–551, 2008.
- [3] Hanuš Seiner, Ondřej Glatz and Michal Landa. Interfacial Microstructures in Martensitic Transitions: From Optical Observations to Mathematical Modeling. *Int. J. for Multiscale Computational Engineering*, **7**(5), 445–456, 2009.
- [4] Ondřej Glatz, Hanuš Seiner and Michal Landa. FEM Modelling of Elastically Strained Interfacial Microstructures in Cu-Al-Ni Single Crystals. in *ESOMAT 2009 - The 8th European Symposium on Martensitic Transformations*, 2009, published by EDP Sciences (www.esomat.org), DOI: 10.1051/esomat/200903006
- [5] Ondřej Glatz. *Mathematical Modelling of Mobility of Martensitic Microstructures*. MSc thesis. Czech Technical University in Prague, Faculty of Nuclear Sciences and Physical Engineering, 2010
- [6] John M. Ball. Mathematical models of martensitic microstructure. *Material Science and Engineering*, 2003.
- [7] Martin Kružík, Alexander Mielke and Tomáš Roubíček. Modelling of Microstructure and its Evolution in Shape-Memory-Alloy Single-Crystals, in Particular in CuAlNi. *Meccanica*, **40**(4–6), 389–418, 2005.
- [8] Yuan-Cheng Fung. *Foundations of Solid Mechanics*. Prentice-Hall, 1965.
- [9] Lev Davidovich Landau and Evgeny Mikhailovich Lifshitz. *Theory of Elasticity*, volume 7 of *Course of Theoretical Physics*. Butterworth–Heinemann, 1986.
- [10] Hanuš Seiner. *Dynamic and Transient Phenomena in Single Crystals of Shape Memory Alloys*. PhD thesis. Czech Technical University in Prague, Faculty of Nuclear Sciences and Physical Engineering, 2008.
- [11] Rohan Abeyaratne and James K. Knowles. On the kinetics of an austenite \rightarrow martensite phase transformation induced by impact in a Cu–Al–Ni shape-memory alloy. *Acta Materialia*, **45**(4), 1671–1683, 1997.

Micromechanical modeling of shape memory alloys – energies and evolution

Authors: Klaus Hackl¹, Philipp Junker², Rainer Heinen³

Affiliations: ¹Institute of Mechanics, Ruhr-University of Bochum, Germany,
Klaus.Hackl@rub.de;

²Institute of Mechanics, Ruhr-University of Bochum, Germany, Philipp.Junker@rub.de;

³Research and Development, ThyssenKrupp Steel Europe AG, 47161 Duisburg,
Germany; Institute of Mechanics, Ruhr-University of Bochum, Germany,
Rainer.Fechte-Heinen@rub.de;

ABSTRACT

Shape memory alloys can be described in a uniform way relying on energetic considerations only. We present micromechanically motivated models for single and polycrystals. The approach studied here is based on energy minimization and includes hysteretic effects via a simple dissipation ansatz. It is capable of reproducing important aspects of the material behavior such as pseudoelasticity and pseudoplasticity. The influence of anisotropies in the crystalline texture as well as in the elastic constants of the austenite and the martensitic variants are also discussed. Furthermore, heat produced during phase transformations is accounted for in the model via simultaneous solution of the heat conduction equation which couples the heat production with phase transformation. The entire presentation emphasizes the usage of variational methods leading to the notion of relaxed potentials. Interrelations to various other applications of these concepts will be highlighted.

1. Introduction

Since shortly after the discovery of the special aspects in the material behavior of shape memory alloys, there have been many efforts to model its important features. The main focuses are, on the one hand, to find appropriate phenomenological descriptions for macroscopic applications and to explain microscopic properties by physical considerations, on the other hand. The literature on these topics is too extensive to be summarized here; well-known examples are, however, Ball and James¹, Stupkiewicz and Petryk²⁶, Kohn¹⁸, and Truskinovsky²⁸ for microscopic modeling.

In this paper, we connect earlier works on the energy density computation for monocrystals,^{8,7,14} with others on the modeling of polycrystals,¹¹. The connection is established based on an approach by Bruno et al.⁴ and Smyshlyaev and Willis²⁴ as described in¹².

The material behavior of shape memory alloys is characterized by transformation strains $\boldsymbol{\eta}$, chosen to be $\boldsymbol{\eta}_0 = \mathbf{0}$ for the austenite, and elastic constants collected in the fourth-order elasticity tensor \mathbb{C} . Furthermore, the chemical energy α_i is introduced to distinguish between the height of the energy wells of different crystallographic phases: $\alpha_A = \alpha_0$ for the austenite and $\alpha_M = \alpha_i$, $1 \leq i \leq n$, for the different martensitic variants.

Assuming linear elastic material behavior, the energy density for pure variants in the monocrystalline case is

$$W(\boldsymbol{\varepsilon}, \boldsymbol{i}_i) = \frac{1}{2} (\boldsymbol{\varepsilon} - \boldsymbol{\eta}_i) : \mathbb{C} : (\boldsymbol{\varepsilon} - \boldsymbol{\eta}_i) + \alpha_i,$$

where $\boldsymbol{\varepsilon}$ is the linearized strain and \boldsymbol{i}_i are the unit-vectors in $n + 1$ -dimensional variant space.

Since deformations of several percent are observed in the material behavior of shape memory alloys, it may, at first glance, seem surprising that a linear elastic model is used here. However, most of this deformation is realized by phase transformation processes while the additional elastic straining of the different phases remains clearly limited. For this reason, a linear elastic model is suitable for most technical applications which are, in general, designed to bear loads in the regime of the transformation stress where the influence of dislocation-mediated plasticity is still negligible.

The energy at every microscopic material point is determined as the one minimizing the elastic energy for a given strain $\boldsymbol{\varepsilon}$

$$W(\boldsymbol{\varepsilon}) = \min_i [W(\boldsymbol{\varepsilon}, \mathbf{i}_i)]. \quad (1)$$

Due to the non-convexity of this formulation, further energy reduction can be reached by microstructure formation on the mesoscopic level. Mathematically, this corresponds to the quasi-convexification of Eq. (1) in the sense of⁵

$$\begin{aligned} QW^{\text{mono}}(\boldsymbol{\varepsilon}) &= \min_{\mathbf{c}} QW^{\text{mono}}(\boldsymbol{\varepsilon}, \mathbf{c}) \quad \text{with} \\ QW^{\text{mono}}(\boldsymbol{\varepsilon}, \mathbf{c}) &= \inf_{\boldsymbol{\chi}, \phi} \left\{ \int_{\Omega} W(\boldsymbol{\varepsilon} + \nabla^s \phi(\mathbf{y}), \boldsymbol{\chi}(\mathbf{y})) \, d\mathbf{y} \right. \\ &\quad \left. \phi \in W_{\text{per}}^{1,2}(\Omega), \boldsymbol{\chi}(\mathbf{y}) \in \mathcal{P}_{\text{pure}}^{n+1}, \int_{\Omega} \boldsymbol{\chi}(\mathbf{y}) \, d\mathbf{y} = \mathbf{c} \right\}. \end{aligned} \quad (2)$$

Expanding Eq. (2) gives rise to the definition of the so-called *energy of mixing*

$$\begin{aligned} w_{\text{mix}}(\mathbf{c}) &= \inf_{\boldsymbol{\chi}, \phi} \left\{ \int_{\Omega} \nabla^s \phi : \mathbb{C} : \left(\frac{1}{2} \nabla^s \phi - \sum_{i=0}^n \chi_i \boldsymbol{\eta}_i \right) \, d\mathbf{y} \right. \\ &\quad \left. \phi \in W_{\text{per}}^{1,2}(\Omega), \boldsymbol{\chi}(\mathbf{y}) \in \mathcal{P}_{\text{pure}}^{n+1}, \int_{\Omega} \boldsymbol{\chi}(\mathbf{y}) \, d\mathbf{y} = \mathbf{c} \right\} \end{aligned}$$

and the alternative formulation of the quasiconvex energy density

$$QW^{\text{mono}}(\boldsymbol{\varepsilon}, \mathbf{c}) = \sum_{i=0}^n [c_i W(\boldsymbol{\varepsilon}, \mathbf{i}_i)] + w_{\text{mix}}(\mathbf{c}), \quad (3)$$

where the first addend is a Taylor-type upper bound corresponding to the assumption of a constant strain throughout the representative volume element. This formulation has also been employed in several earlier works on the energy-based modeling of shape memory alloys,^{8,9,14}. Due to the complexity of its constraints, no direct expression is known for the energy of mixing unless a maximum of two¹⁸ or three variants are considered²⁵.

2. Lamination Upper Bound

As an estimate to the energy of mixing, we introduce a lamination upper bound based on a microstructural pattern, which consists of austenite and twinned martensite. The choice of the twinned martensitic variants is constrained by the linearized lamination mixture formula

$$\boldsymbol{\eta}_i - \boldsymbol{\eta}_j = \frac{1}{2} (\mathbf{n} \otimes \mathbf{a} + \mathbf{a} \otimes \mathbf{n})$$

as developed in¹ and³. This formula determines whether variants i and j are able to form a stress free interface with each other. Only those pairs of variants that fulfill this equation are combined to twins which are then numbered pairwise (variant 1 twinned with variant 2, 3 with 4, and so on) while the austenite remains to be variant 0.

The suggested microstructure is employed to derive the second-order lamination upper bound to the energy of mixing

$$w_{\text{mix}}(\mathbf{c}) \leq w_{\text{lam}}(\mathbf{c}) = \sum_{K=1}^M d_K \theta_K (1 - \theta_K) \phi(\mathbf{i}_{2K-1} - \mathbf{i}_{2K}) \quad (4)$$

$$+ \sum_{K=1}^M \frac{(d_0 + d_1 + \dots + d_{K-1}) d_K}{d_0 + d_1 + \dots + d_K} \phi(\mathbf{d}^{(K-1)} - \boldsymbol{\theta}^{(K)})$$

with

$$\phi(\boldsymbol{\kappa}) = \inf \{ -\mathbf{G}(\boldsymbol{\omega}) : (\boldsymbol{\kappa} \otimes \boldsymbol{\kappa}) | \boldsymbol{\omega} \in \mathbb{S}^{d-1} \}$$

$$\mathbf{G}(\boldsymbol{\omega}) = \frac{1}{2} (\boldsymbol{\omega} \cdot \mathbb{C} : \boldsymbol{\eta}_k) \cdot \mathbf{T}(\boldsymbol{\omega})^{-1} \cdot (\boldsymbol{\omega} \cdot \mathbb{C} : \boldsymbol{\eta}_l) \mathbf{i}_k \mathbf{i}_l$$

$$\mathbf{u} \cdot \mathbf{T}(\boldsymbol{\omega}) \cdot \mathbf{u} = (\boldsymbol{\omega} \otimes^s \mathbf{u}) : \mathbb{C} : (\boldsymbol{\omega} \otimes^s \mathbf{u}) \in \mathbb{R}_{\text{sym}}^{d \times d},$$

where d is the spacial dimension of the problem considered, $\theta_J = \frac{c_{2J-1}}{c_{2J-1} + c_{2J}}$ is the volume fraction of the first variant within the J th twin (where $J = 1, \dots, m$ runs over the different twins), $\boldsymbol{\theta}_J = \theta_J \mathbf{e}_{2J-1} + (1 - \theta_J) \mathbf{e}_{2J}$ is the normalized phase fraction vector for the J th twin, $d_J = c_{2J-1} + c_{2J}$ is the volume fraction of the J th twin within the microstructure, and $\mathbf{d}_J = \sum_{K=0}^J d_K \boldsymbol{\theta}_K / \sum_{K=0}^J d_K$ is a vector which contains the normalized sum of the austenite and all martensitic twin phase fractions up to a certain twin J . In Eq. (4), each permutation of the ordering of the martensitic variants into twins as well as of the order of these twins gives a new value for the upper bound. A detailed derivation and proof of this bound may be found in⁷.

3. Extension to Polycrystals

Now, let us consider a polycrystalline domain consisting of a large, but finite number of crystallites N . Each crystallite j has a certain orientation given by the corresponding rotational tensor \mathbf{R}^j ; the volume fraction corresponding to this crystal orientation is denoted by ξ^j . The transformation strains have to be rotated to the local crystallographic orientation and result in $\boldsymbol{\eta}_i^j = (\mathbf{R}^j)^T \cdot \boldsymbol{\eta}_i \cdot \mathbf{R}^j$. Consequently, the elastic energy of variant i in grain j yields

$$\bar{W}(\boldsymbol{\varepsilon}, \mathbf{i}_i, \mathbf{R}^j) = \frac{1}{2} (\boldsymbol{\varepsilon} - \boldsymbol{\eta}_i^j) : \mathbb{C} : (\boldsymbol{\varepsilon} - \boldsymbol{\eta}_i^j) + \alpha_i$$

and the mesoscopic energy of the polycrystal is given by

$$Q\bar{W}(\boldsymbol{\varepsilon}) = \inf_{\tilde{\boldsymbol{\phi}}} \left\{ \int_{\Omega} QW^{\text{mono}}(\mathbf{R}(\mathbf{y}) (\boldsymbol{\varepsilon} + \nabla^s \tilde{\boldsymbol{\phi}}(\mathbf{y})) \mathbf{R}^T(\mathbf{y})) \, \text{d}\mathbf{y} \mid \tilde{\boldsymbol{\phi}} \in W_{\text{per}}^{1,p}(\Omega) \right\}.$$

Here, the monocrystalline quasiconvexification, which is not known in explicit form, would have to be computed for the crystallographic orientation present in every point of the representative volume element Ω .

In a sophisticated paper by Smyshlyaev and Willis²⁴, these authors present a strategy to employ monocrystalline upper estimates for bounding the energy of polycrystals from above:

$$Q\bar{W}(\boldsymbol{\varepsilon}) \leq Q\bar{W}_{\text{lam}}(\boldsymbol{\varepsilon}) = \inf_{\mathbf{c}} Q\bar{W}_{\text{lam}}(\boldsymbol{\varepsilon}, \mathbf{c})$$

with

$$\begin{aligned} Q\bar{W}_{\text{lam}}(\boldsymbol{\varepsilon}, \mathbf{c}) &= \frac{1}{2}(\boldsymbol{\varepsilon} - \langle \boldsymbol{\eta} \rangle) : \mathbb{C} : (\boldsymbol{\varepsilon} - \langle \boldsymbol{\eta} \rangle) - \frac{1}{2} \langle \boldsymbol{\eta} \rangle : \mathbb{Q} : \langle \boldsymbol{\eta} \rangle + \langle \alpha \rangle \\ &+ \frac{1}{2} \sum_{j=1}^N \xi^j \langle \boldsymbol{\eta} \rangle^j : \mathbb{Q} : \langle \boldsymbol{\eta} \rangle^j + \sum_{j=1}^N \xi^j QW_{\text{lam}}^{\text{mono}}(\langle \boldsymbol{\eta}^{\text{mono}} \rangle^j, \mathbf{c}^j) \end{aligned} \quad (5)$$

and

$$\langle \boldsymbol{\eta} \rangle = \sum_{i,j} \xi^j c_i^j \boldsymbol{\eta}_i^j, \quad \langle \boldsymbol{\eta} \rangle^j = \sum_i c_i^j \boldsymbol{\eta}_i^j, \quad \langle \boldsymbol{\eta}^{\text{mono}} \rangle^j = \sum_i c_i^j \boldsymbol{\eta}_i, \quad \langle \alpha \rangle = \sum_{i,j} \xi^j c_i^j \alpha_i.$$

Here, we have plugged in the second order lamination bound presented above as an estimate of the relaxation with fixed volume fractions in the monocrystalline case. The fourth order texture tensor \mathbb{Q} used in Eq. 5 is defined as follows:

$$\mathbb{Q} = \frac{1}{|\mathbb{S}^{d-1}|} \int_{\mathbb{S}^{d-1}} \tilde{\Delta}^\infty(\boldsymbol{\zeta}) d\boldsymbol{\zeta},$$

where

$$\tilde{\Delta}_{klop}^\infty(\boldsymbol{\zeta}) = \frac{2\bar{\lambda}\bar{\mu}}{\bar{\lambda} + 2\bar{\mu}} U_{kl}(\boldsymbol{\zeta}) U_{op}(\boldsymbol{\zeta}) + \bar{\mu} [U_{ko}(\boldsymbol{\zeta}) U_{lp}(\boldsymbol{\zeta}) + U_{kp}(\boldsymbol{\zeta}) U_{lo}(\boldsymbol{\zeta})],$$

$$U_{kl}(\boldsymbol{\zeta}) = \delta_{kl} - \zeta_k \zeta_l,$$

and $|\mathbb{S}^{d-1}|$ is the surface of the unit sphere.

A detailed discussion of this bound including the influence of the polycrystalline texture may be found in¹².

4. Convexification

A simple and intuitional way to obtain an estimate for the energy density of polycrystals is to assume a constant stress within each variant of each crystallite and neglecting the compatibility constraints. Since, in this case, minimization is performed over a larger set of microstructures than physically available, this so-called convexification estimate is a lower bound:

$$Q\bar{W}_{\text{conv}}(\boldsymbol{\varepsilon}, \mathbf{c}) = \inf_{\boldsymbol{\varepsilon}_i^j} \left\{ \sum_{i,j} \xi^j c_i^j W(\boldsymbol{\varepsilon}_i^j, \mathbf{i}_i, \mathbf{R}^j) \middle| \boldsymbol{\varepsilon} = \sum_{i,j} \xi^j c_i^j \boldsymbol{\varepsilon}_i^j \right\}. \quad (6)$$

The remaining constraint in Eq. (6) makes sure that the overall strain is preserved. In a finite strain formulation, further refinement of the bound could be reached by additionally incorporating minors and the determinant of the overall strain which would lead to the polyconvexification of the energy density.

The formulation given in Eq. (6) has the advantage that the minimization can be performed analytically. The solution

$$Q\bar{W}_{\text{conv}}(\boldsymbol{\varepsilon}, \mathbf{c}) = \frac{1}{2}(\boldsymbol{\varepsilon} - \langle \boldsymbol{\eta} \rangle) : \mathbb{C} : (\boldsymbol{\varepsilon} - \langle \boldsymbol{\eta} \rangle) + \langle \alpha \rangle \quad (7)$$

is discussed in¹¹ in detail for the more general case of anisotropic material properties for austenite and martensite.

In the monocrystalline case, the convexification lower bound may be used to derive an alternative estimate for the energy of mixing:

$$w_{\text{mix}}(\mathbf{c}) \geq w_{\text{conv}}(\mathbf{c}) = -\frac{1}{2} \sum_{i=0}^n c_i \boldsymbol{\eta}_i : \mathbb{C} : \boldsymbol{\eta}_i + \frac{1}{2} \sum_{i=0}^n \sum_{k=0}^n c_i c_k \boldsymbol{\eta}_i : \mathbb{C} : \boldsymbol{\eta}_k. \quad (8)$$

5. Micromechanical Model

Given the good agreement between upper and lower bounds, we choose the more straightforward convexification estimate to establish an energy-based micromechanical model for polycrystalline shape memory alloys.

In order to close the formulation, we introduce a dissipation function which is homogeneous of first order in the volume fraction change rates

$$\Delta(\dot{\mathbf{c}}) = r \sqrt{\sum_{j=1}^N \xi^j \sum_{i=0}^n (\dot{c}_i^j)^2}.$$

This kind of dissipation function has been shown to be suitable for describing rate-independent materials in^{19,20}. The general procedure of describing the dissipative aspects of the behavior of rate-independent materials by dissipation functions is discussed in¹⁰ and²¹. A more sophisticated approach to model dissipation in phase transforming materials may be found in².

The material behavior is then derived by minimizing the total power

$$\mathcal{L}(\mathbf{c}, \dot{\mathbf{c}}) = \frac{d}{dt} Q\bar{W}^{\text{rel}}(\boldsymbol{\varepsilon}, \mathbf{c}) + \Delta(\dot{\mathbf{c}}) = -\mathbf{q} \cdot \dot{\mathbf{c}} + \Delta(\dot{\mathbf{c}}) \quad (9)$$

at constant strain $\boldsymbol{\varepsilon}$, where we have introduced the thermodynamically conjugated driving force to $\dot{\mathbf{c}}$, $\mathbf{q} = -\partial Q\bar{W}^{\text{rel}}/\partial \mathbf{c}$, as an abbreviation. Furthermore, we define the *active sets* $\mathcal{A}^j = \{i \mid \dot{c}_i^j > 0 \vee (c_i^j = 0 \wedge \dot{c}_i^j > 0)\}$ as well as the *active deviator* $(\text{dev}_{\mathcal{A}^j} q)_i^j = q_i^j - \frac{1}{n_{\mathcal{A}^j}} \sum_{k \in \mathcal{A}^j} q_k^j$, $n_{\mathcal{A}^j}$ being the number of elements in \mathcal{A}^j , to finally obtain the evolution equation

$$\dot{c}_i^j = \frac{\rho}{\xi^j} [\text{dev}_{\mathcal{A}^j} q_i^j]_{\mathcal{A}^j}$$

along with the Kuhn-Tucker conditions

$$\rho \geq 0, \quad \Phi = \sum_{i,j} \frac{1}{\xi^j} (\text{dev}_{\mathcal{A}^j} q_i^j)^2 - r^2 \leq 0, \quad \rho \Phi = 0$$

and the consistency condition

$$\text{dev}_{\mathcal{A}^j} q_i^j < 0 \quad \forall \quad i \notin \mathcal{A}^j \quad (10)$$

which serves as a “switch” and determines whether a certain variant that has been inactive before has to become active in a current time step. A detailed discussion of this model may be found in¹¹.

6. Finite Element Implementation Of The Pure Model

6.1 Finite element implementation

The previously presented micromechanical model provides good results on the material point layer¹¹. Thus, we execute an implementation of this model in the scope of finite elements to predict the material behavior of whole specimens. In order to do so, we use the common total potential of a body as

$$\Pi = \int_{\Omega} Q\bar{W}^{\text{rel}} dV - \int_{\Omega} \mathbf{u} \cdot \mathbf{f} dV - \int_{\partial\Omega} \mathbf{u} \cdot \mathbf{t} dA \rightarrow \min_{\mathbf{u}} \quad (11)$$

which is going to be minimized with respect to the unknown displacements \mathbf{u} under certain constraints (supports, prescribed displacements). In Eqn. (11), Ω denotes the total volume of the body, \mathbf{f} body forces and \mathbf{t} tractions acting on the body's surface. Minimization of Eqn. (11) yields

$$\mathbf{R}_{\mathbf{u}} := \int_{\Omega} \mathbf{B}^T \cdot \tilde{\boldsymbol{\sigma}} dV - \int_{\Omega} \mathbf{N}_{\mathbf{u}} \cdot \mathbf{f} dV - \int_{\partial\Omega} \mathbf{N}_{\mathbf{u}} \cdot \mathbf{t} dA \stackrel{!}{=} \mathbf{0}, \quad (12)$$

with shape functions $\mathbf{N}_{\mathbf{u}}$, the common differential operator \mathbf{B} and the stress $\tilde{\boldsymbol{\sigma}}$ in Voigt notation.

6.2 Numerical results

We present numerical results for the model in the scope of finite elements for pseudo-elastic NiTi. In order to show convincing results we try to map the material behavior in a tension test documented by Schäfer and Wagner²². There, a stripe of pseudo-elastic NiTi was fixed on both ends and a prescribed displacement was loaded at one end whereas the other end stayed fixed. To capture the experimental factors we fix the first two rows of nodes within the discretized body. That ensures to have comparable constraints to the clamping in the experiments. The numerical results for the phase distribution of austenite are presented in Fig. 1.

We see that the transformation starts exactly where the stress peaks evolve due to boundary conditions. This behavior was observed in experiments as well. After a certain amount of austenite has transformed to a specific combination of different martensite variants, the phase transformation spreads over the body. An almost homogeneous transition follows the initiate local transformation which is in strong contrast to experiments. There, transformation fronts run through the specimen and all the phase transitions occur in those very localized zones²². However, the global material response shows the well known characteristics of poly-crystalline shape memory alloys as a plateau during phase transformation and a hysteresis due to the dissipative character of the transformations. This and further analysis of the finite element implementation of the pure model may be found in Junker and Hackl¹⁶.

7. Finite Element Implementation Of A Modified Model

7.1 Modified model

Obviously the localized, Lüders band like transformations cannot be displayed by the pure model. Therefore we modify the model in the way that we distinguish between *nucleation* and *evolution* of martensite, Hackl and Junker¹⁷. It is easy to imagine that in a pure austenitic lattice for the nucleation of martensite higher energetic bounds have to be overcome than for the propagation and evolution starting from martensite grains. We implement this fact into

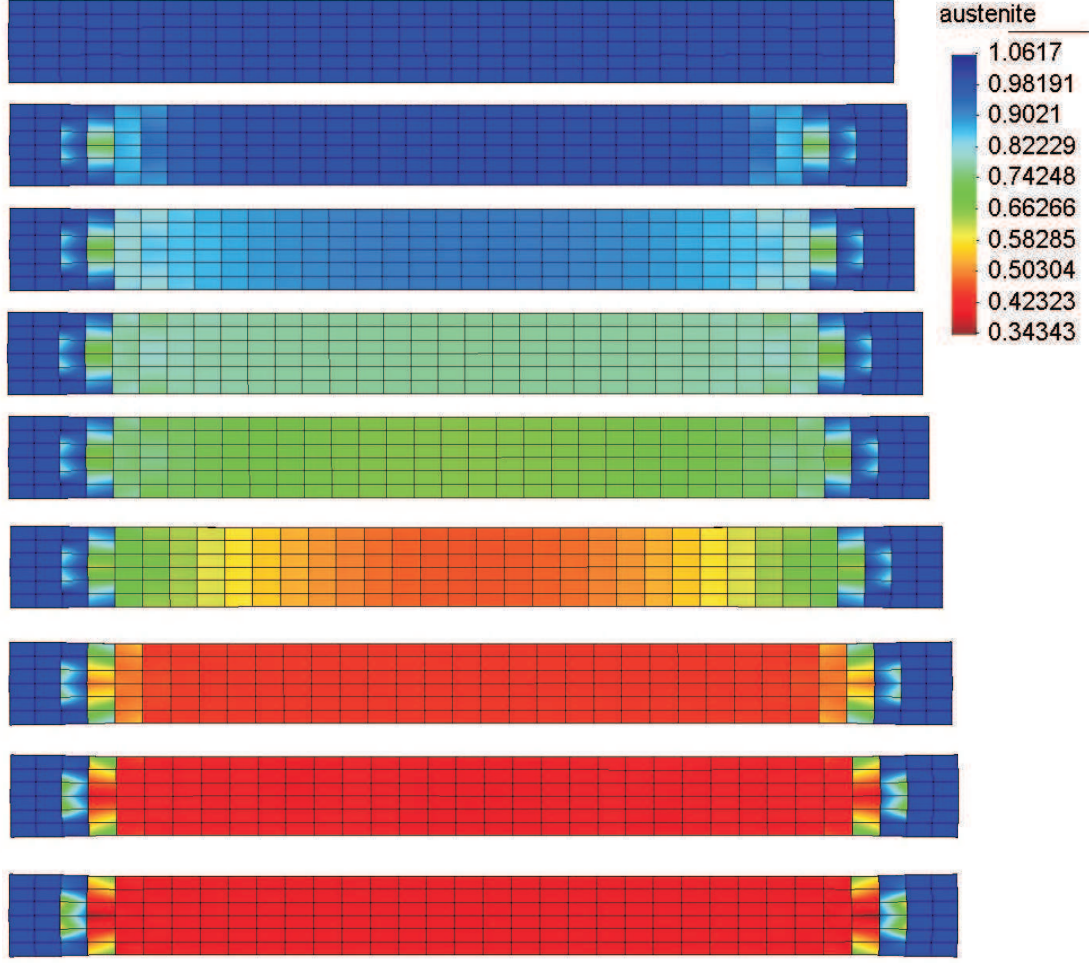


Figure 1: Distribution of the austenite phase at various load steps calculated with the pure model.

our model by a modification of our ansatz for the dissipation. Since we do not account for grain boundaries and their possibility of coherency in the entire model, we introduce a variable which serves as measure for the amount of nucleated martensite globally for the entire material point. Consequently, we use the average amount of austenite as this measure and reformulate the dissipation as

$$\Delta(|\mathbf{c}_0|) = \tilde{\mathbf{r}}(|\mathbf{c}_0|) \sqrt{\sum_{j=1}^N \xi^j \sum_{i=0}^n (\dot{\mathbf{c}}_i^j)^2}, \quad |\mathbf{c}_0| = \sum_{j=1}^N \xi^j \mathbf{c}_0^j. \quad (13)$$

with an appropriate ansatz for $\tilde{\mathbf{r}}(|\mathbf{c}_0|)$.

This new approach would yield mesh dependent results due to its softening character. To circumvent this fact, we introduce a further space dependent field variable, denoted by φ , which is coupled to the average amount of austenite. In order to do so, we expand the relaxed energy $Q\bar{W}^{\text{rel}}$ via a coupling term and additionally via the field function's gradient multiplied with some factors β and γ ,

$$Q\bar{W}^{\text{tot}} = Q\bar{W}^{\text{rel}} + \frac{\beta}{2} (\varphi + 1 - |\mathbf{c}_0|)^2 + \frac{\gamma}{2} \|\nabla\varphi\|^2. \quad (14)$$

For further details for this general approach see Dimitrijević and Hackl⁶.

Now, the extended energy $Q\bar{W}^{\text{tot}}$ is used consequently everywhere in the model instead of

$Q\bar{W}^{\text{rel}}$. Hence, the driving forces give

$$q_i^j = -\frac{\partial Q\bar{W}^{\text{tot}}}{\partial c_i^j} = -\frac{\partial Q\bar{W}^{\text{rel}}}{\partial c_i^j} + \beta(\varphi + 1 - |\mathbf{c}_0|)\delta_{0i}, \quad \delta_{0i} : \text{Kronecker-Delta} . \quad (15)$$

The changed driving forces influence the evolution of the crystallographic phases, obviously. Therefore, the evolution at each integration point is not only coupled to the other points indirectly via the displacement field but also directly via the current state of volume fractions. If we now penalize the gradient of the field variable φ we indirectly penalize the gradient of the volume fractions, too. Thus, we receive mesh independent results.

Replacing the energy $Q\bar{W}^{\text{rel}}$ by the extended energy $Q\bar{W}^{\text{tot}}$ in the potential in Eqn. (11) results in a further variational equation for φ since we have to seek for the minimum of Π with respect to all space dependent variables. Due to their independence at first glance, we receive

$$\begin{aligned} \int_{\Omega} \delta \boldsymbol{\varepsilon} : \frac{\partial Q\bar{W}^{\text{tot}}}{\partial \boldsymbol{\varepsilon}} \, dV - \int_{\Omega} \delta \mathbf{u} \cdot \mathbf{f} \, dV - \int_{\partial\Omega} \delta \mathbf{u} \cdot \mathbf{t} \, dA = 0 \, \forall \, \delta \mathbf{u} \\ \int_{\Omega} c (\nabla \varphi \cdot \nabla \delta \varphi) \, dV + \int_{\Omega} \beta (\varphi + 1 - |\mathbf{c}_0|) \delta \varphi \, dV = 0 \, \forall \, \delta \varphi . \end{aligned} \quad (16)$$

So, the factor c controls the impact of the gradient in the minimization and may be interpreted as a global parameter for surface energy. We solve the system of variational equations, Eqn. (16), in a coupled way.

7.2 Numerical results for the modified model

We show numerical results for all the same boundary value problem as presented earlier but now we make an ansatz for the dissipation coefficient being a function of the average amount of austenite as

$$\tilde{r}(|\mathbf{c}_0|) = \mathbf{r}(\mathbf{0.8} + \mathbf{0.2} \cos(2\pi|\mathbf{c}_0|)) . \quad (17)$$

This simple approach ensures that a further evolution of martensite is preferred when the nucleation has been accomplished. Since a complete vanish of martensite would again yield higher energy bounds, the energy costs increase when the average amount of austenite tends to zero. This approach is just an example. We already tried different kinds of functions which all fit in the idea for reduced energy costs and the numerical results only differed slightly if there were any differences at all.

The results which we present in Fig. 2 show at the beginning a similar material behavior as received from the pure model: At the nodes where the boundary values are prescribed stress peaks occur and force the material to transform right there. In contrast to the pure model, the transformation proceeds in these localized zones until a certain minimum value of remaining austenite has been reached. After that, the evolved transformation fronts move through the specimen until they meet. Only in the area of the Lüders like fronts all transformation occur.

8. Conclusion

We presented different aspects of energy minimization in the scope of non-convex energy functionals applied to shape-memory alloys. Based on relaxation of energies which is part of convexification, we presented a micromechanically well motivated model which depends mostly on experimentally determined material parameters.

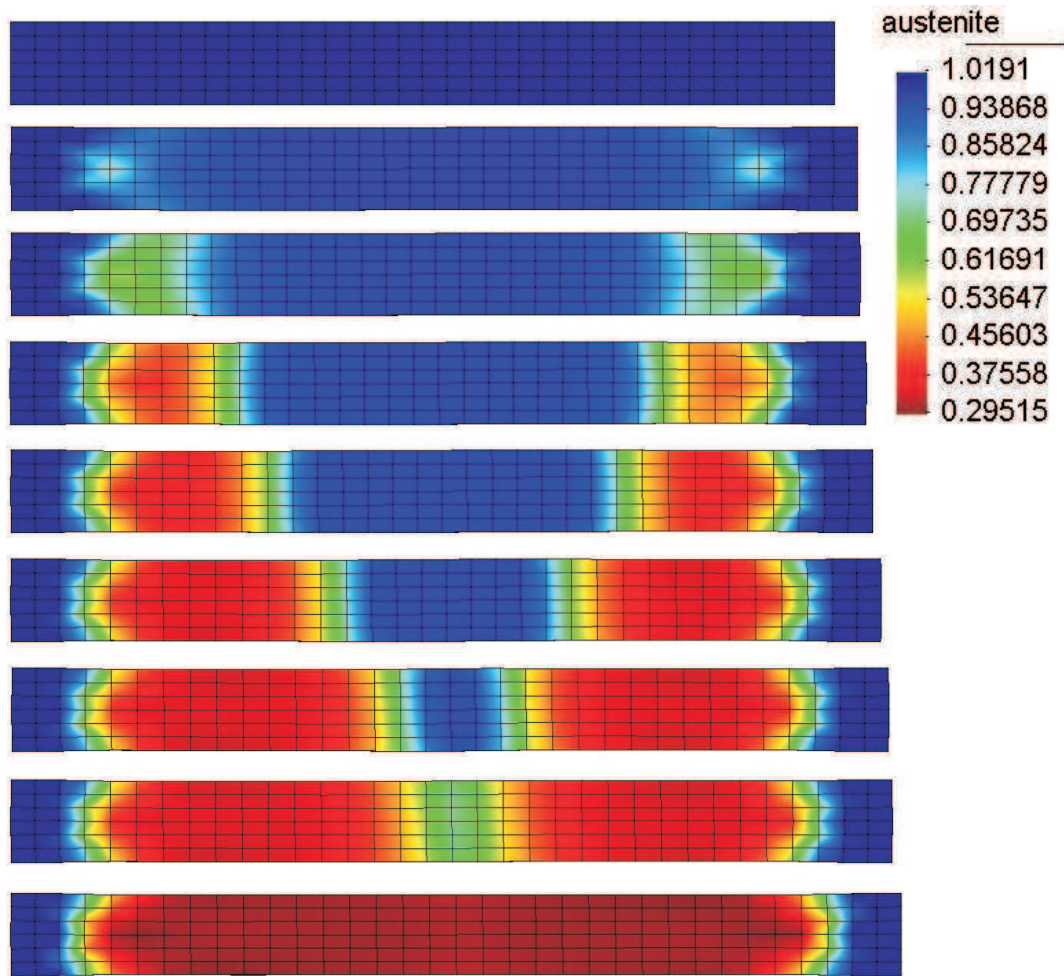


Figure 2: Distribution of the austenite phase at various load steps calculated with the modified model.

For this model we presented furthermore a finite element implementation whose results could be remarkably improved by a modified dissipation ansatz. The numerical calculation of a tension test is in nice coincidence to experimental observations.

Future work will include the simulation of cubic to monoclinic transforming, and thus thirteen-variant, materials and intermediate crystallographic phases such as the well-known R-Phase.

References

- [1] J.M. Ball, R.D. James, Arch. Rat. Mech. Anal. **100** (1987) 13–52
- [2] T. Bartel, K. Hackl, Mat. Sci. Eng. A **481** (2008) 371–375
- [3] K. Bhattacharya, *Microstructure of Martensite - Why it forms and how it gives rise to the shape-memory effect.* (Oxford University Press, New York, 2003)
- [4] O.P. Bruno, F. Reitich, P.H. Leo, J. Mech. Phys. Solids **44** (1996) 1051–1101
- [5] B. Dacorogna, J. Funct. Anal. **46** (1982) 102–118
- [6] B. J. Dimitrijević and K. Hackl, Tech. Mech. **28** (2008) 43–52

- [7] S. Govindjee, K. Hackl, R. Heinen, *Continuum Mech. Thermodyn.* **18** (2007) 443–453
- [8] S. Govindjee, A. Mielke, G.J. Hall, *J. Mech. Phys. Solids* **51** (2003) 763+
- [9] S. Govindjee, C. Miehe, *Comput. Meth. Appl. Mech. Eng.* **191** (2001) 215–238
- [10] K. Hackl, F.D. Fischer, *Proc. R. Soc. A* **464** (2008) 117–132
- [11] K. Hackl, R. Heinen, *Continuum Mech. Thermodyn.* **19** (2008) 499–510
- [12] K. Hackl, R. Heinen, *J. Mech. Phys. Solids* **56** (2008) 2832–2843
- [13] K. Hackl, R. Heinen, W.W. Schmahl, M. Hasan, *Mat. Sci. Eng. A.* **481** (2008) 347–350
- [14] R. Heinen, K. Hackl, *Comput. Meth. Appl. Mech. Eng.* **196** (2007) 2401–2412
- [15] R. Heinen, K. Hackl, W. Windl, M. Wagner *Acta Materialia* **57** (2009) 3856–3867
- [16] Philipp Junker and Klaus Hackl. *Z. Angew. Math. Mech.*, **89** (10), 2009
- [17] Philipp Junker and Klaus Hackl. In *ESOMAT 2009 - The 8th European Symposium on Martensitic Transformations*, P. Sittner, L. Heller and V. Paidar (eds.), EDP Sciences (www.esomat.org), 03007 (2009), DOI: 10.1051/esomat/200903007
- [18] R. Kohn, *Continuum Mech. Thermodyn.* **3** (1991) 193–236
- [19] A. Mielke, F. Theil, V.I. Levitas, *Arch. Rat. Mech. Anal.* **162** (2002) 137–177
- [20] A. Mielke, *Continuum Mech. Thermodyn.* **15** (2003) 351–382
- [21] M. Ortiz, L. Stainier, *Comp. Methods Appl. Mech. Eng.* **171** (1999) 419–444
- [22] Andreas Schäfer and Martin F.-X. Wagner. In *ESOMAT 2009 - The 8th European Symposium on Martensitic Transformations*, P. Sittner, L. Heller and V. Paidar (eds.), EDP Sciences (www.esomat.org), 06031 (2009), DOI: 10.1051/esomat/200906031
- [23] P. Sedlák, H. Seiner, M. Landa, V. Novák, P. Sittner, Ll. Mañosa, *Acta Materialia*, **53** (2005) 3643–3661
- [24] V. Smyshlyaev, J. Willis, *Proc. R. Soc. London A* **454** (1998) 1573–1613
- [25] V. Smyshlyaev, J. Willis, *Proc. R. Soc. London A* **455** (1998) 779–814
- [26] S. Stupkiewicz, H. Petryk, *J. Mech. Phys. Sol.* **50** (2002) 2303–2331
- [27] M.F.-X. Wagner, W. Windl, *Acta Materialia* **56** (2008) 6232–6245
- [28] L. Truskinovsky, *Continuum Mech. Thermodyn.* **6** (1994) 185–208
Int. J. Nice Research, **15**(4), 23–42, 1999.

A QM/MM Coupling Method Based on a Particle-Wise Decomposition Approach

Michael Griebel, Jan Hamaekers and Frederik Heber

Institute for Numerical Simulation, University of Bonn,
Wegelerstrasse 6, D-53115 Bonn, Germany
hamaekers@ins.uni-bonn.de

We present an approach for the coupling of the quantum mechanical (QM) scale and the molecular mechanics scale (MM). It is based on a particle-wise decomposition of the high-dimensional many-particle space the underlying Schrödinger equation lives in. This decomposition represents the energy as a finite sum of contributions which depend on the positions of single nuclei, of pairs of nuclei, of triples of nuclei, and so on. Under the assumption of locality of electronic wave functions, the higher order terms in this expansion decay rapidly and may therefore be omitted. Furthermore, additional terms are eliminated according to the bonding structure of the molecule. This way, only the calculation of the electronic structure of local parts, i.e. small subsystems of the overall system, is necessary to approximate the total ground state energy. Depending on the desired accuracy the local subproblems can be divided into subproblems which are approximately evaluated by an appropriate QM technique, e.g. DFT, CC or CI, and subproblems which are approximately evaluated with an appropriate MM force field method. In particular, the overall complexity scales linear with the number of atoms.

Moving dislocations in finite plasticity: a topological approach

Thomas Hochrainer^{1,2}

¹Fraunhofer IWM, Wöhlerstr. 11, 79108 Freiburg, Germany

²Karlsruhe Institute of Technology, izbs, Kaiserstr. 12, 76131 Karlsruhe, Germany
Thomas.Hochrainer@kit.edu

Crystal plasticity is the result of the motion and interaction of dislocations. There is, however, still a major gap between our knowledge of the behavior of individual dislocations and continuum crystal plasticity models. Important progress has recently been made in advancing averaging techniques for dislocation systems and their evolutions [1, 2]. However, these techniques mostly apply to small deformations and single slip situations. A prerequisite for averaging dislocation systems is a pseudo-continuum description of the evolution of a single dislocation [1, 3]. In the current paper we develop the pseudo-continuum description of a dislocation moving in a dislocated deforming crystal in the framework of multiplicative finite plasticity.

We argue that the understanding of dislocations as topological defects requires viewing the dislocation density tensor as a vector valued differential two-form as defined by Kondo [4]. This premise leads us to very clear geometric interpretations both of the tensor itself and of various terms appearing in its evolution equation. The key to make the geometric interpretations obvious is the differential form formalism which allows treating dislocations as functionals (so called currents), providing at the same time the required pseudo-continuum description. All extra terms resulting from considering finite deformations as compared to small deformations are related to dislocation cutting processes and the generation of kinks and jogs. We conclude that in multiple slip situations the dislocation state may in general not be fully characterized by dislocation densities solely located in the slip planes.

References

- [1] I. Groma, Link between the microscopic and mesoscopic length-scale description of the collective behavior of dislocations, *Phys. Rev. B* 56, 5807-5813 (1997)
- [2] T. Hochrainer, M. Zaiser, P. Gumbsch, A three-dimensional continuum theory of dislocations: kinematics and mean-field formulation, *Philosophical Magazine* 87, 1261-1282 (2007)
- [3] T. Hochrainer, Evolving systems of curved dislocations: Mathematical foundations of a statistical theory, Thesis, Universitaet Karlsruhe (TH), Shaker Verlag, Aachen (2007)
- [4] K. Kondo, On the geometrical and physical foundations of the theory of yielding, *Proc. 2. Japan nat. Congress of appl. Mech.* 1952 pp. 41-47 (1952)

A Multi-Scale Approach to Simulate the Forming Limit Diagrams of Aluminum Alloys

Prasad Dasappa¹, Kaan Inal¹, Raja K. Mishra², Oana Cazacu³

¹University of Waterloo, Waterloo, Ontario, N2L 3G1 Canada; ²General Motors R&D Center, Warren, Michigan, 48090, USA, ³University of Florida, REEF, Shalimar, FL 32579-1163, USA

ABSTRACT

In this paper, numerical modeling based on crystal plasticity theories at various scales are performed to incorporate the effects of microstructure and generate input for simpler and computationally efficient macroscopic (phenomenological) models. Information concerning the initial anisotropy and its evolution with accumulated deformation has been generated from measured initial texture and tensile data by employing a rate-dependent crystal plasticity model and a unit-cell finite element (FE) approach. Crystal plasticity simulations have been used for the identification of the anisotropic coefficients involved in CPB08 criterion, which is a form of the macroscopic yield criterion proposed by Plunkett *et al.* [1], which is specifically tailored for FCC metals. Numerical simulations of the forming limit diagram (FLD) are performed for the continuous cast AA-5754 aluminum sheet alloy based on the CPB08 yield function and a Taylor-type polycrystal plasticity model together with the Marciniak-Kuczynski (M-K) analysis.

1. Introduction

In industrial forming operations involving thin sheets, formability is limited by the onset of localized necking. Forming limit diagram (FLD) has proved to be a useful tool to represent conditions for the onset of necking and evaluate formability of sheet metals [2]. The Marciniak-Kuzynski (M-K) analysis [3] has been one of the most commonly used approaches for numerical determination of FLD's. FLD predictions based on the M-K analysis can be grouped into two categories based on the length scale of the simulations; macroscale (phenomenological models) and microscale (crystal plasticity models).

In this paper, numerical simulation of FLD's for aluminum sheets are performed based on the M-K analysis. The anisotropic behavior of the aluminum alloy is modeled using the yield function proposed by Plunkett *et al.* [1] and a rate sensitive crystal plasticity model together with a unit-cell approach is employed to generate input for the phenomenological yield function. Finally, a Taylor-type polycrystal plasticity model is also used to simulate FLDs and the predictions are compared to each other and experimental observations.

2. Constitutive Models

Different constitutive models (based on the length scale of the applications) are used in the numerical simulations. For micro-scale simulations, the rate-sensitive crystal plasticity theory developed by Asaro and Needleman [4] is employed in numerical models at two different length scales to obtain the response of a polycrystal aggregate (comprised of many grains). In the first model, each grain in the polycrystal aggregate is modeled with one or more finite elements. Equilibrium and compatibility is enforced throughout the polycrystal aggregate through the “weak” finite element form. In the second model, the classical Taylor assumptions are employed to obtain the response of the polycrystal aggregate. For details of the formulation we refer to Wu *et al.* [2]. Furthermore, from hereon, these models will be referred to as FE/grain and Taylor model respectively.

The yield function proposed by Plunkett *et al.* [1] is employed in the macro-scale simulations since a very recent research by Inal *et al.* [5] have shown that this yield function can be successfully applied to the description of FCC materials. For pressure-insensitive materials with no tension-compression asymmetry, the effective stress associated with Plunkett *et al.* [1] orthotropic yield criterion can be written in the form:

$$\tilde{\sigma} = \left(|\Sigma_1|^a + |\Sigma_2|^a + |\Sigma_3|^a + |\Sigma'_1|^a + |\Sigma'_2|^a + |\Sigma'_3|^a \right)^{1/a} \quad (1)$$

In Eqn. 1, $(\Sigma_1, \Sigma_2, \Sigma_3)$ and $(\Sigma'_1, \Sigma'_2, \Sigma'_3)$ are the principal values of the transformed tensors. For details of the formulation we refer to Inal *et al.* [5].

4. M-K Analysis

The M-K analysis has been performed for a continuous cast (CC) aluminum sheet alloy AA5754 to predict the FLD. The constitutive relation given below along with the above yield function has been employed in the M-K Analysis.

$$\dot{\sigma}_{ij} = \left[L_{ijkl} - \frac{\lambda_{ij}\lambda_{kl}}{\frac{\partial f}{\partial \varepsilon_p} + \mu_{ij}\lambda_{ij}} \right] D_{kl} \quad (2)$$

where, $\dot{\sigma}$ is the rate of the true stress tensor σ , L is the tensor of elastic moduli, D is the rate of deformation tensor, f is the yield function, ε_p is the plastic strain, μ_{ij} are the normals given by $\mu_{ij} = \frac{\partial f}{\partial \sigma_{ij}}$ and $\lambda_{ij} = L_{ijkl}\mu_{kl}$. The implementation is based on the method described by Wu *et al.* [2] and will not be summarized again.

5. Results and Discussion

The material considered in this study is a continuous cast AA5754 (3.1% Mg, 0.25% Mn, <0.01 % Cr, 0.24% Fe, <0.1% Si, balance Al) sheet. The initial texture for AA5754 is presented in Fig.1. The material parameters used in the crystal plasticity models were determined by curve fitting the simulated uniaxial stress-strain curve to the corresponding experimental curve (Fig.2). Tensile properties have been simulated using the FE/grain model at 7 directions between 0-90° in increment of 15°, with 0° being the rolling direction. The yield strength was selected at 0.2% offset, while the R-values were measured at 15% elongation. In the numerical simulations with the yield function, a Hollomon type power law relationship given by Eqn. 3 has been employed.

$$\sigma = E \varepsilon \text{ if } \sigma \leq \sigma_y, \sigma = K \varepsilon^N \text{ if } \sigma > \sigma_y \quad (3)$$

where, $E=69,489$ MPa, $K = 411.5$ MPa and $N = 0.2866$. The work hardening exponent, N , was calculated from the 0.2% offset until the maximum load.

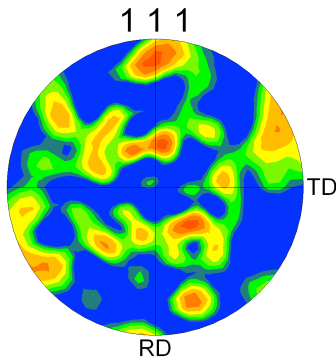


Figure 1. Initial pole figure for AA5754

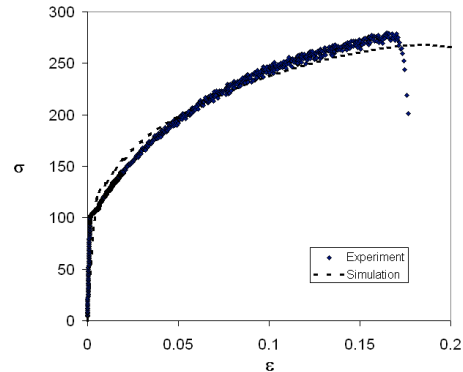


Figure 2. Experimental and simulated stress-strain curves in uniaxial tension

As mentioned in the previous section, the parameters of the yield function CPB08 can be obtained by simulations of uniaxial tension along various angles to the rolling direction with the FE/grain model. The same methodology described by Inal *et al.* [5] has been used to identify anisotropy coefficients for the yield function CPB08 by employing FE/grain crystal plasticity model. The variations of yield stresses and R-values with orientation obtained with CPB08 yield function with anisotropy coefficients obtained using the FE/Grain crystal plasticity model are presented in Figs. 3 respectively. It can be seen that CPB08 successfully captures the trends for both yield stresses and R-values. This result is a significant improvement compared to other yield functions such as Hill 1990, 1993 and Barlat 1989 (Prasad *et al.* [6]).

The predicted FLD's are shown in Figure 4. Simulations show that the FLDs predicted by both models are in very good agreement with experimental observations. For negative strain ratios, the predicted forming limits with both models are slightly higher than the experimentally measured FLD. Predictions are very close to experimental observations for positive strain ratios, where the simulation with the yield function CPB08 slightly

over predicts the experimental FLD while the simulation with the Taylor model slightly under predicts the experimental FLD. Simulations presented in this paper show that the proposed multiscale approach can successfully predict the formability of the aluminum alloy 5754. Furthermore, this methodology eliminates a large number of mechanical tests required to identify the anisotropy constants used in the phenomenological models such as the yield function CPB08.

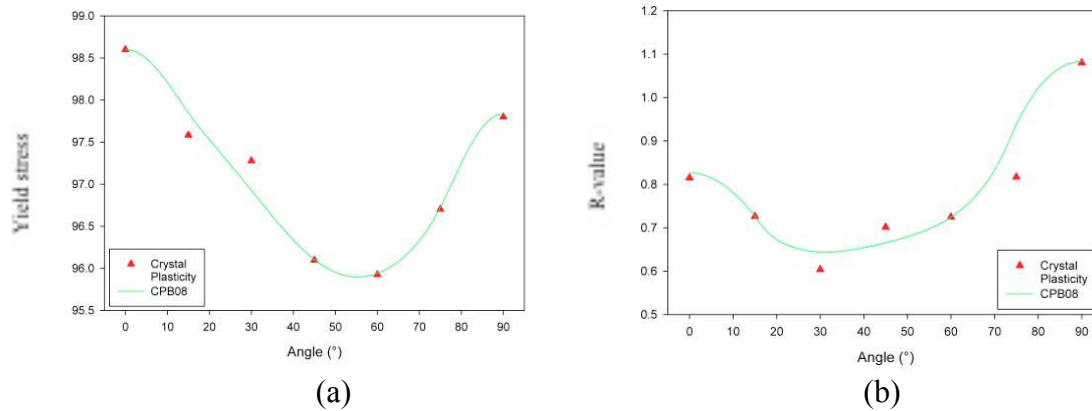


Figure 3. Comparison of (a) Yield stresses (b) R-values with orientation (w.r.t RD)

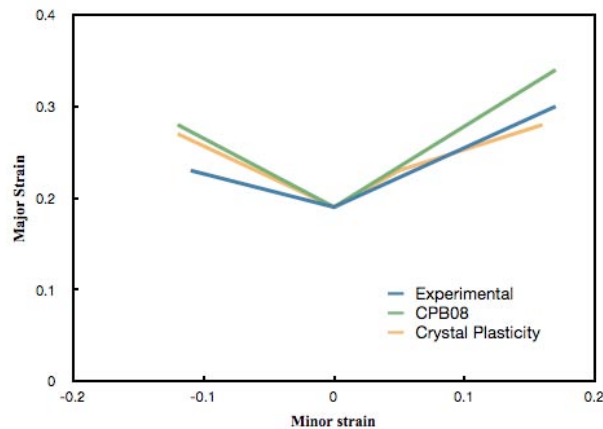


Figure 4. Experimental and predicted FLDs

References

1. B. Plunkett, O. Cazacu and F. Barlat, *Int. J. Plasticity* **24**, 847-866 (2008).
2. P.D. Wu, K. W. Neale and E. Van der Giessen, *Proc. R. Soc. London.* **453**, 1831-1848 (1997).
3. Z. Marciniak and K. Kuczynski, *Int. J. Mech. Sci.* **9**, 609-620 (1967).
4. A. Needleman and R.J. Asaro, *Acta Metall.* **33**, 923-953 (1985).
5. K. Inal, R. K. Mishra and O. Cazacu, *Int. J. Solids Structures* **47**, 2223-2233, (2010).
6. P. Dasappa, K. Inal and R. K. Mishra, *Proc. of NUMIFORM2010*, 972-980, (2010).

Novel Mechanism for Reversible Spin Transition in Prussian Blue Analogs

Mukul Kabir and Krystyn J. Van Vliet

Department of Materials Science and Engineering, Massachusetts Institute of Technology, Cambridge, MA 02139, USA

Spin transition can be induced by external perturbations such as light, heat, pressure, magnetic field and chemical substitution, and is seen in wide range of materials. This phenomenon has found wide range of promising applications as sensors, as recording media, or to tune mechanical properties of polymers. Prussian blue analogs (PBAs) (transition metal cyanides) are one of such crystalline material, exhibiting reversible spin transition under light of specific wavelengths. Illumination of visible light (500-750 nm) on $\text{KCoFe}(\text{CN})_6$ at low temperatures induces bulk magnetization, which can be eliminated by near-IR light (~ 1319 nm). Despite various experimental and theoretical attempts, the microscopic mechanism is not yet well understood. Here we perform density functional theory (corrected for the on-site coulomb repulsion, DFT+U) calculations of anhydrous $\text{KCoFe}(\text{CN})_6$. We find that the ground state has large octahedral ligand-field splitting, and consequently the ground state is low-spin ($S=0$). The spin transition to high spin ($S=2$) takes place due to the charge transfer in two steps. In the first step a $\text{Fe-}t_{2g}$ electron is transferred $\text{Co-}e_g$ through the cyanide ligand. This intermediate spin ($S=1$) state $[\text{Fe}(t_{2g}^5)\text{Co}(t_{2g}^6e_g^1)]$ is metastable, and the corresponding CoN_6 octahedra exhibits a strong Jahn-Teller distortion. This interatomic charge transfer is followed by d -electron rearrangement in the Co center as the second step. Such spin transition is strongly coupled with the PBA internal lattice. We further predict that this kind of spin transition in such materials can be induced and can be further tuned via external pressure by introducing hydrostatic strain.

Simulation of Twinning Deformation in Shape Memory Alloys

O. Kastner¹, F. Richter¹ and G. Eggeler¹

¹Institute for Materials, Ruhr University Bochum, 44780 Bochum, Germany
Oliver.Kastner@rub.de

In twinning deformation, a straight shape memory alloy (SMA) bar composed of equal amounts of martensite twins $M -$ and $M +$ is axially compressed by a load beyond the detwinning load, thus shifting all $M +$ elements into the $M -$ state. Once unloaded, the bar remains in the residual compressive strain state. Thereafter, lateral loading causes a remnant deflection due to quasiplastic $M - M -$ transitions in the stretched bar fibers. Hence, the bar is left curved upon removal of the load. Astonishingly, subsequent axial compression causes the bar to straighten [1].

We investigate this behavior by a finite-element simulation employing the material model for SMA by Müller, Achenbach and Seelecke [2]. Our investigation reveals the temporal and spatial variations of the phase fractions and correlates them to stresses and moments. The simulation results for the stress evolution at a highly stressed location are illustrated in Fig. 1, showing the spatial distribution of stress through the thickness of the bar, visualized by 27 fibers (identified as section points (SP)). Twelve SP successively achieve the transformation stress plateau. Unsymmetrical yielding imposes a shift of the neutral fiber. The initially elastic unloading causes the reversal of the stress profile. The stress state is nonuniform until the deflection is eliminated and all volume elements merge onto a unique line.

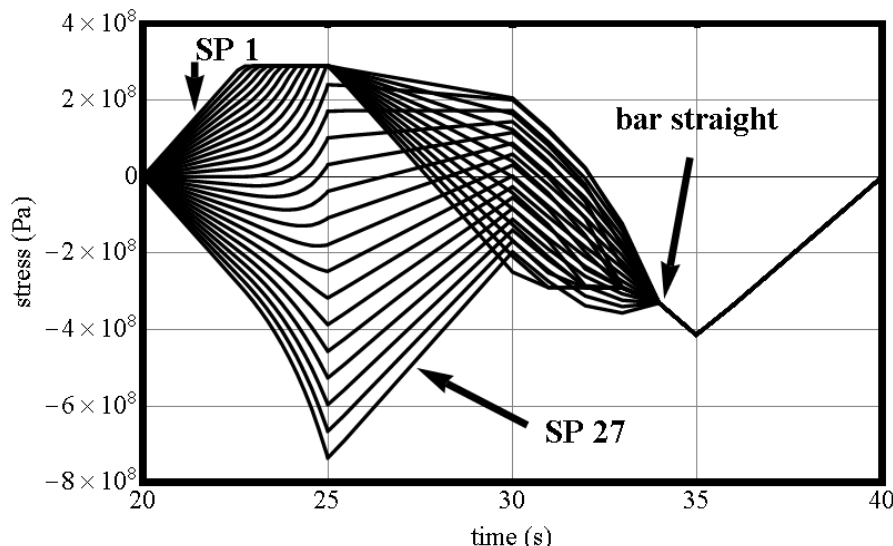


Fig. 1: Stress history for all fibers (SP) at mid-length of the bar. SP1-SP27: individual fibers across bar thickness (SP1: tension side, SP27: compression side).

Timeline (t in sec): lateral loading $20 \leq t \leq 25$, unloading $25 \leq t \leq 30$, and final axial loading $30 \leq t \leq 35$ and unloading $35 \leq t \leq 40$. Initial detwinning not shown.

[1] Y. Urushiyama, D. Lewinnek, J. Qiu, J. Tani, JSME A, 46(1), 2003, p. 60-67

[2] S. Seelecke, I. Müller, Appl. Mech. Rev., 57 (1), 2004, p. 23-46

Thermodynamic Modeling of Phase Transformations of Metals over Wide Range of Pressures and Temperatures

Konstantin V. Khishchenko

Joint Institute for High Temperatures, Russian Academy of Sciences,
Izhorskaya 13 Bldg 2, Moscow 125412, Russia, e-mail: konst@ihed.ras.ru

Description of thermodynamic properties and phase transitions of materials in a wide range of parameters is of both fundamental and practical interests. Equations of state for metals over the range from normal conditions to extremely high pressures and temperatures are required for numerical simulations of processes in continuous media under pulsed power influences (such as, for example, high velocity impingement of solids or ultrashort laser ablation of matter) at many different time scales.

In this paper, a new thermodynamic approach to modeling of equation of state for metals with taking into account the polymorphic transformations, melting and evaporation effects is proposed. Multiphase equations of state for aluminum, copper, iron, tin, lead and some other metals are obtained on the basis of the model. Phase diagrams of the substances are calculated including regions of solid, liquid and gas states. Results of calculations are given in comparison with available experimental data and quantum mechanical evaluations over a wide range of temperatures and pressures.

The proposed multiphase equations of state provide for a reliable description of thermodynamic properties of the metals in a broad region on the phase diagram. That gives an opportunity to effectively use these equations of state in numerical simulations of unsteady-state hydrodynamic processes in materials at high energy densities.

Hybrid Atomistic/Coarse-Grained-Particle Simulation of Dynamic Crack Growth in a Brittle Material

Ryo KOBAYASHI,^{1,2} Takahide NAKAMURA,^{1,2} and Shuji OGATA^{1,2}

¹Department of Scientific and Engineering Simulation, Graduate School of Engineering, Nagoya Institute of Technology, Gokiso-cho, Showa-ku, Nagoya 466-8555, Japan

²CREST, Japan Science and Technology Agency, 4-1-8 Honcho, Kawaguchi, Saitama 332-0012, Japan

E-mail address: kobayashi.ryo@nitech.ac.jp

ABSTRACT

A concurrent hybrid atomistic and coarse-grained-particle method is proposed for the simulation on fast crack propagations. The coupling method used in the method is simpler than the former approaches without loss of accuracy and efficiency. The simulation of the fast crack propagation is performed with the adaptive selection of the atomistic region for reducing the computational cost, and its result shows the present coupling method with the adaptive selection of the atomistic region is highly efficient and sufficiently accurate.

1. Introduction

The crack propagation is typical multiscale phenomenon. It is because extensive stress field controls stress concentration at the crack-tip and breakages of atomic bonds at the crack-tip are closely related to the stress concentration. For the fast brittle crack propagation, a change in stress field and energy radiation from the crack-tip have significant roles on crack speed and instability. Furthermore most materials are brittle at low temperature and become ductile at certain temperature. Therefore *multiscale*, *dynamics*, and *temperature* are important factors in the fast crack propagation.

Over the past decade a variety of multiscale simulation approaches which connect atomistic and continuum (or coarse-grained particle) methods have been proposed. Most of these approaches are limited to the simulation on static problems only, because these cannot eliminate the reflection of short-wavelength wave coming from the atomistic region to the interface of atomistic and continuum regions. Although some coupling methods, such as the bridging scale method and the bridging domain method, can reduce the reflection of short-wavelength wave, these also have drawbacks in the computational cost or flexibility on applications.

In this paper we propose a hybrid simulation method which couples atomistic and coarse-grained-particle (CGP) methods with eliminating the reflection of short-wavelength wave. Present hybrid method is applied to the simulation on the fast crack propagation with using the algorithm that adaptively changes the atomistic region to follow the moving crack-tip.

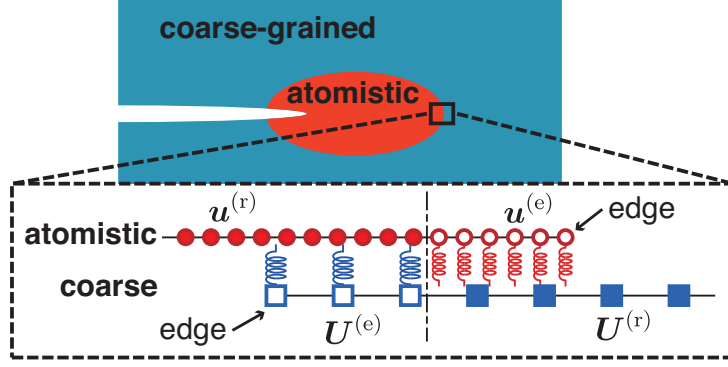


Figure 1: Schematic picture of the configuration of extra atoms/particles in the BEP coupling method. Filled circles and squares are real atoms and particles, open circles and squares are *extra* atoms and particles.

2. Coupling of Atomistic and Coarse-Grained-Particle Systems

2.1 Coarse-Grained Particle Method

In the CGP method a group of atoms is represented by a CG particle with the coarse-graining relation, $U_I = \sum_i f_{Ii} u_i$, where U_I and u_i are displacements of a CG particle- I and an atom- i , and f_{Ii} the weighting function.¹ The weighting function is obtained from the linear interpolation function N_{Ii} , which is commonly used in the finite element method or the quasicontinuum method, through $\mathbf{f} = [\mathbf{N}\mathbf{N}^t]^{-1}\mathbf{N}$. The CGP energy is defined as a statistical mechanical average concerning the atomistic Hamiltonian $\mathcal{H}_{\text{atom}}$ as

$$E_{\text{CGP}} \equiv \int d\{u\}d\{p\} \mathcal{H}_{\text{atom}} e^{-\beta \mathcal{H}_{\text{atom}}} \cdot \prod_I \delta \left(U_I - \sum_i f_{Ii} u_i \right) \cdot \delta \left(\dot{U}_I - \sum_i f_{Ii} p_i / m_i \right). \quad (1)$$

Assuming the interatomic potential in the atomistic Hamiltonian is a harmonic form, the CGP energy is obtained also in a harmonic form as

$$E_{\text{CGP}} = d(N_{\text{atom}} - N_{\text{CGP}})k_B T + \frac{1}{2} \sum_{IJ} \left(\dot{U}_I M_{IJ} \dot{U}_J + U_I K_{IJ} U_J \right), \quad (2)$$

where d , k_B , and T is the dimension, Boltzmann factor, and the temperature, M_{IJ} and K_{IJ} are the mass matrix and the stiffness matrix which are systematically calculated via the weighting function. Since M_{Ij} and K_{IJ} are constructed from a mass and a force constant in the atomistic system, elastic properties and phonon dispersions in the CGP system agree well with those in the atomistic system. Therefore the CGP method is a promising candidate to be coupled with the atomistic method.²

2.2 Bridging Extra Particles (BEP) Method

Since the shortest wavelenghtes in the atomistic and the coarse-grained systems are different, some short-wavelength components cannot exist in the coarse-grained system. This may cause the reflection of short wavelength wave coming from the atomistic region to the coarse-grained region. The reflection wave is a particular problem on coupling of the atomistic and coarse-grained systems in the simulation on dynamic problems.

To overcome the reflection at the interface, extra atoms and particles are introduced beyond the interface as shown in Fig. 1; these extra atoms and particles work as mediums to transfer

long-wavelength waves and as a sink for short-wavelength waves that cannot exist in another system.³ These extra atoms and particles feel correction (or constraining) forces as

$$f_i^{(e)} = -\frac{\partial V_{\text{atom}}}{\partial r_i^{(e)}} - \tilde{k} \left(u_i^{(e)} - \sum_I N_{Ii} U_I \right) - m_i \gamma \left(\dot{u}_i^{(e)} - \sum_I N_{Ii} \dot{U}_I \right), \quad (3)$$

$$F_I^{(e)} = -\frac{\partial V_{\text{CGP}}}{\partial R_I^{(e)}} - \sum_J \tilde{K}_{IJ} \left(U_J^{(e)} - \sum_i f_{Ji} u_i \right) - \gamma \sum_J M_{IJ} \left(\dot{U}_I^{(e)} - \sum_i f_{Ji} \dot{u}_i \right), \quad (4)$$

where \tilde{k} and \tilde{K}_{IJ} are spring constants constraining to match displacement fields of two systems, γ the damping constant concerning energy dissipation. These \tilde{k} , \tilde{K}_{IJ} , and γ are homogeneous in the extra regions except at the edge of the systems (see Fig. 1), their values at which should be larger such that displacements of two systems strictly match each other.

The γ value should be sufficiently small not to reflect incoming waves at the interface, and should not be too small to eliminate these waves inside the extra region. In a damped oscillation scheme, an oscillation frequency, ω , becomes $\sqrt{4\omega_0^2 - \gamma^2}/2$ where $\omega_0 = \sqrt{k_0/m}$ and k_0 is the characteristic force constant of the system. The damped oscillation frequency ω is required to be almost same as ω_0 not to reflect incoming waves, so here $\gamma = 0.2\omega_0$ is chosen to be $\omega = \sqrt{0.99}\omega_0$.

3. Adaptive Selection of Atomistic Region In the Crack Propagation Simulation

In order to reduce the computational cost of the simulation on the crack propagation, an algorithm that the atomistic region changes its position to pursue the crack-tip and dislocations emitted from the crack-tip is developed. An atomic strain is adopted to decide the positions of a crack-tip and dislocation cores, since the atomic strain at the crack-tip and dislocation cores take singular values. After sensing positions of the crack-tip and dislocation cores, new atomistic region is determined to have a certain width of atom layers between the crack-tip and the edge of the atomistic region.

When the atomistic region is changed, some atoms and particles are annihilated and some are created. In the case of an atom creation, which occurs when a certain position used to be in the coarse-grained region changes to be in the atomistic region, new atoms are created with displacements that are given by those of CG particles through the interpolation, $u_i = \sum_I N_{Ii} U_I$. On the other hand, new particles are created with displacements given by $U_I = \sum_i f_{Ii} u_i$.

Generally, fast moving cracks emit short-wavelength elastic waves from their crack-tips where atomic bonds snap. Since such waves cannot exist in the coarse-grained region, these waves have to be eliminated in the extra atom region. It is unknown whether the change of the atomistic region affect the reflection or elimination of such waves. Suppose that 2D system of atoms with Lennard-Jones (LJ) interatomic potential with parameters for Ar system. The system size is about $(L_x, L_y) = (1715\text{\AA}, 1386\text{\AA})$. A crack of length about 500 \AA and thickness of one atomic layer is introduced. Only the area of radius about 100 \AA around the crack-tip is chosen as the atomistic region and for the surrounding area the CGP method is applied. As an initial condition, fixed uniform tensile load is applied perpendicular to the crack by adding strain 1.0% and atomic positions are relaxed by the velocity scaling molecular dynamics. In the crack propagation simulation, the strain is increased with very low strain rate until the total strain reaches 1.5%. Figure 2 shows snapshots of atomic strain fields near the crack-tip at different time. This shows that the change of the atomistic region does not cause artificial waves and strain field around the crack-tip stays unchanged in a steady-state crack propagation. The reason why artificial waves

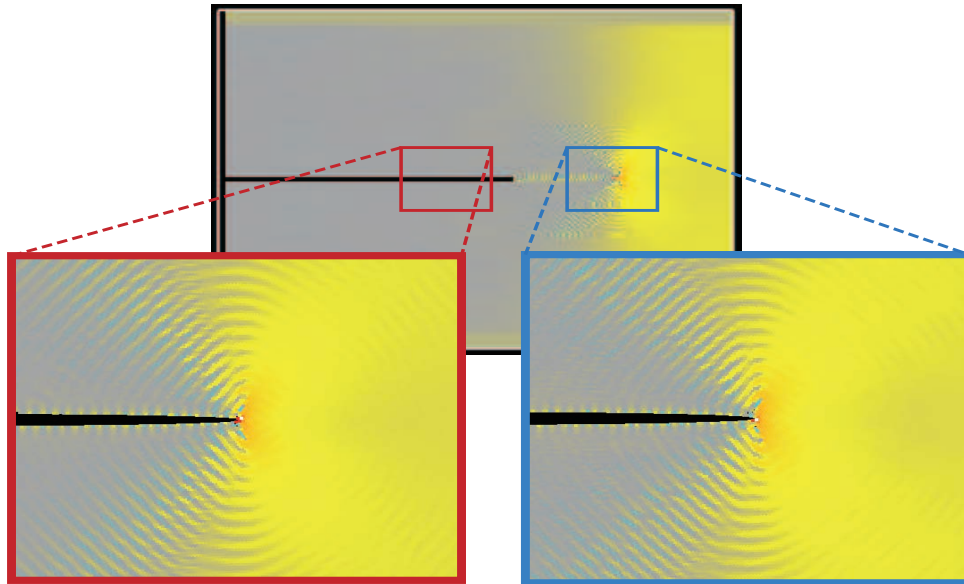


Figure 2: Snapshots of the adaptive hybrid simulation of a brittle crack propagation. Two magnified pictures show strain fields near the crack-tip at different time.

created by the change of the atomistic region are negligibly small is because the existence of the extra region. Created artificial waves at the edge of the extra region are eliminated during they pass through the extra region.

4. Conclusion

A concurrent hybrid atomistic and coarse-grained-particle method with a simple coupling scheme, called the bridging extra particles (BEP) method, is proposed. In the BEP coupling, extra atoms and particles are placed beyond the interface and they work as a sink for short-wavelength waves that cannot exist in another system. Since these extra atoms and particles move under Langevin-type equation, short-wavelength waves are eliminated such as damped oscillations. Adding the random force term with an appropriate dispersion based on the fluctuation-dissipation theorem, finite-temperature simulations should be possible.

An algorithm that the atomistic region is adaptively changed its position following the crack-tip and dislocations cores during the crack propagation simulation is developed. Since changes of the atomistic region does not cause artificial waves, the present hybrid method can provide sufficiently accurate and efficient crack propagation simulations.

References

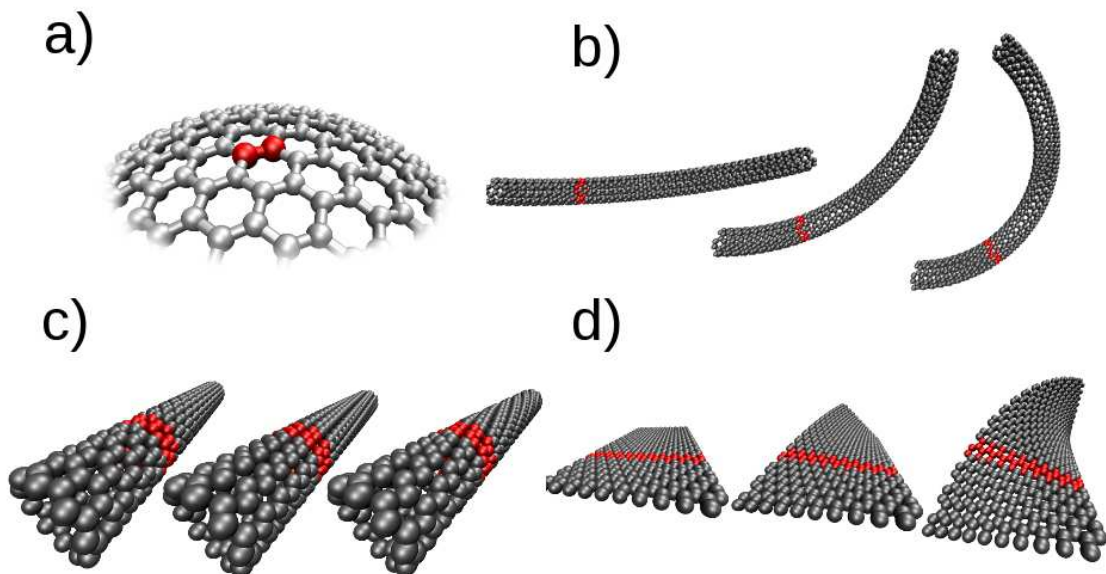
- [1] Robert E. Rudd and Jeremy Q. Broughton. Coarse-grained molecular dynamics and the atomic limit of finite elements. *Phys. Rev. B*, **58**, R5893–R5896, 1998.
- [2] Ryo Kobayashi, Takahide Nakamura, and Shuji Ogata. Development and Implementation of Recursive Coarse-Grained Particle Method for Meso-Scale Simulation. *Mater. Trans.*, **49**(11), 2541–2549, 2008.
- [3] Ryo Kobayashi, Takahide Nakamura, and Shuji Ogata. A simple dynamical scale-coupling method for concurrent simulation of hybridized atomistic/coarse-grained-particle system. *Int. J. Numer. Meth. Engng*, early view, 2009.

Simulating distorted nanomaterials: the curvature moduli of graphene

Pekka Koskinen^{1*} and Oleg O. Kit¹

¹Nanoscience Center, Department of Physics,
University of Jyväskylä, 40014 Jyväskylä, FINLAND
*email: pekka.koskinen@iki.fi

The operation principles of nanoscale devices are based on both electronic and mechanical properties of materials. Because these properties can be coupled, they need to be investigated simultaneously. At this moment, however, the electronic structure calculations with custom-made long-range mechanical distortions are impossible, or expensive at best. Here we present a unified formalism to solve exactly the electronic structures of distorted nanomaterials, and solve bending and Gaussian curvature moduli of single- and multi-layer graphene, directly. Despite being exact and fully quantum-mechanical, we show how this single method is able to grant access to multi-scale modeling of distorted nanomaterials.



Method enables simulating general distortions *continuously* with only few atoms in the unit cell: a) spherical surface (2-atom unit cell), b) bending, and c),d) twisting, for example.

Modelling of deformation behaviour of copper in Cone-Cone Method, High Pressure Torsion and Tube Twisting

V. Lemiale¹, R. Lapovok^{2,3}, A. Pougis¹, A. Molotnikov^{2,3} and Y. Estrin^{1,2,3}

¹ CSIRO Division of Process Science and Engineering, Clayton, Vic. 3169, Australia

² Department of Materials Engineering, Monash University, Clayton, Vic. 3800, Australia

³ ARC Centre of Excellence for Design in Light Metals, Clayton, Vic. 3800, Australia
Vincent.Lemiale@csiro.au

The development of an appropriate multiscale modeling framework depends on the choice of internal variables. In this study physically-based constitutive models for dislocation cell forming materials were applied to describe microstructure evolution in processes leading to extreme grain refinement. In these models the dislocation densities in the cell walls and the cell interior are used as internal variables. A particular version of the constitutive models developed was implemented in the broadly used commercial finite element software MARC via a specific user subroutine.

Our previous investigations had indicated that this modelling approach represents a versatile tool for predicting grain refinement under severe plastic deformation (SPD) processes. In the present work, we further investigated the suitability of the model for describing a range of SPD processes in which a high pressure is imposed on a specimen in combination with a shear stress. Three case studies were considered. First, a High Pressure Torsion (HPT) model was used to calibrate the material parameters based on widely available experimental data for copper. Then, two recently proposed processes, namely the Cone-Cone Method (CCM) and the High Pressure Tube Twisting (HPTT) technique, were simulated. In the talk, the predicted microstructure evolution will be discussed in relation to our recent experimental results on copper.

Simulations of Crack Propagation using Atomistic and Continuum Coupling Method

Xiantao Li¹, Zhijian Yang² and Weinan E³

¹Department of Mathematics, Penn State University, PA 16802, USA.

²Rochester Institute of Technology, NY 14623, USA

³Princeton University, Princeton, NJ 08544, USA

The problem of cracks is of central importance in the science of fracture. It is concerned with quantitative description of the mechanical properties of solid systems with cracks, aiming at characterizing the resistance of materials to crack growth. Of particular practical interest is the crack initiation under rapid loading. Due to the high strain rate associated with shock waves, the problem is usually outside the linear elasticity regime. Problems of this type involve both atomic level events and continuum scale processes, and they represent many of the challenges in multiscale material modeling. Although such problems have been studied extensively using molecular dynamics (MD) models, the results are mostly limited to the behavior of the crack tip in the presence of an existing loading environment. These atomistic-based methods are unable to treat the dynamic loading from remote boundaries, or the interaction of the stress waves with the crack tip.

We will present a computational model that integrates conventional methods for continuum models of solids, with an atomic level description – the molecular dynamics model. This new class of computational methods is able to treat areas around crack tips by explicitly modeling the atomic interactions, providing better precision than traditional experimental methods. Meanwhile, the integration with continuum models allows to simulate materials of realistic size.

The coupling method starts with a domain decomposition approach. More specifically, the entire computational domain is divided into two types of subdomains: *atomistic regions*, in which MD models are used, and a *continuum region*, in which the elastic field is smooth and the system is modeled by a continuum model. At the interface, an explicit coupling condition will be used to provide boundary conditions for both models. Both MD and the continuum models are formulated based on the same set of conservation laws, represented by a finite volume method. This offers a consistent basis for coupling the two models. Another advantage is that waves with sharp wave front, e.g. shock waves, can be treated in this setting.

We will present numerical results on the interaction of shock waves and crack tip. Additional results, which correlate crack growth with various types of loading conditions, will also be presented.

Application of Percolation Theory to Microtomography of Structured Media: Percolation Threshold, Critical Exponents and Upscaling

Jie Liu^{1,2,3} Klaus Regenauer-Lieb^{1,2,3,4}

¹Computational Geoscience, CSIRO Earth Science and Resource Engineering, Po Box 1130, Bentley, WA 6102, Australia; ²School of Earth and Geographical Sciences, University of Western Australia, 35 Stirling Hwy, WA 6009, Australia jie.liu@uwa.edu.au; ³Multi-scale Earth System Dynamics, University of Western Australia, 35 Stirling Hwy, WA 6009, Australia; ⁴Western Australian Geothermal Center of Excellence, Po Box 1130, Bentley, WA 6102, Australia

ABSTRACT

Percolation theory provides a tool for linking between microstructure and macroscopic material properties. In this paper, percolation theory is applied to the analysis of microtomographic images for the purpose of deriving scaling laws for upscaling of properties. We have tested the acquisition of quantities such as percolation threshold, crossover length, fractal dimension, critical exponent of correlation length from microtomography. By inflating or deflating the target phase and percolation analysis, we can get a critical model and the estimation of percolation threshold. Crossover length is determined from the critical model by numerical simulation. Fractal dimension can be obtained either from the critical model or from the relative size distribution of clusters. Local probabilities of percolation are used to extract critical exponent of correlation length. For near isotropic samples such as sandstone and bread the approach works very well. For strongly anisotropic samples, such as highly deformed rock (mylonite) and a tree branch, the percolation threshold and fractal dimension can be assessed with accuracy. However, the uncertainty of correlation length makes it difficult to accurately extract the critical exponents of correlation length. This aspect of percolation theory can therefore not be reliably used for upscaling properties of strongly anisotropic media. Other methods of upscaling have to be used for such media.

1. Introduction

Microtomography or micro-computed tomography (micro-CT) is becoming an important technique for research of material properties. The limitation of microtomography lies in the relationship of length scale and resolution of the images/samples: the higher the resolution, the smaller is the length scale that can be imaged in a single scan. This leads to the immediate challenge to detect the microstructure of the material in finer and finer resolution and then to connect it to the macroscale where conventional continuum mechanics applies. Scaling laws of percolation theory provide an opportunity to connect microscale to macroscale. As percolation research is mostly based on random models, albeit being recognized as a powerful tool to explore general laws of materials in nature, it has not yet gained wide acceptance in the analysis of direct observational data such as from microtomography.

We evaluate the use of percolation theory as a valuable tool for upscaling from microtomography scale to the macroscale. To achieve this evaluation, we focus on answering these two questions: 1) How to derive the percolation threshold from natural data? and 2) Can

we derive critical exponents and fractal dimension from micro-CT scans of natural samples? The first one is the most important question because percolation threshold is of great significance to material properties. For most natural samples, it is very difficult to derive the percolation threshold, because of the unavailability of a series of models with different volume fractions of the specific structure. Critical exponents and fractal dimension are recognized as universal invariance which compose scaling laws, and scaling laws enable up-scaling/down-scaling of the characteristics recognized at a certain scale. To the best of our knowledge, no critical exponents extracted from microtomographic images have yet been reported in the publicly available literature.

2. Method

Our method is based on binary microstructural models after image processing of micro-CT data. The image processing includes the segmentation of greyscale images and building up a 3-D model from a series slices. The binary microstructural model can be considered as a simple cubic lattice model, in which every cubic cell (or site) is equivalent to a voxel in image processing. In the simple cubic lattice model, the nearest-neighbours are voxels with one common plane. A cluster is a group of nearest-neighbours of the same material which are connected to each other [1]. Labeling clusters is a process of giving all cells within the same cluster the same label.

We introduce here a new technique to determine the percolation threshold of a microstructure by deflating (shrinking) and inflating (expanding) the target phase. A deflation operation is moving the boundaries of clusters one voxel inwards in all directions (positive and negative, in x-, y-, and z-directions). It reduces the volume fraction and makes the weakest bond broken. An inflation operation is moving boundaries outwards. It increases the volume fraction and might cause the nearest clusters to be connected. Both operations keep the orientation of clusters. In this way, a series of derivative models are created from the original model. These models have different volume fractions but retain a similar structure of the original sample. By analysing the percolation of these models, the critical model is identified as the percolating model which is the closest to non-percolating models. The volume fraction of the critical model is recognized as percolation threshold.

The correlation length ξ represents some average distance of any two sites belonging to the same cluster [1]. It is calculated from the statistics of all clusters of their sizes, numbers and radii. The correlation length ξ diverges when volume fraction p approaches the percolation threshold p_c , as $\xi \propto |p - p_c|^{-\nu}$. Here ν is the critical exponent of correlation length. It can be extracted by a finite-size scaling scheme [1] from the local percolation probabilities $\lambda(p, L)$ of different sub-volume-size L and different volume fraction p [2].

Fractal dimension D is the most popular measure for scale invariance currently used in the literature and can be obtained by different ways. We detect the fractal dimension from the relative size and the number of clusters defined as $D = \log N(l \geq \frac{R}{R_{\max}}) / \log l (= \frac{R}{R_{\max}})$, where the relative size of cluster l is the radius of a cluster R normalized by the largest cluster radius R_{\max} , the number of cluster N includes clusters which are equal to or larger than the normalized relative radius. One other way is based on the relationship of $\rho(L) \propto L^{D-d}$, where

the mass density $\rho(L)$ is the number of voxels belonging to the largest cluster per lattice in the measured cube with side-length L , d is lattice dimension [3]. The relationship is only satisfied in percolation threshold and for small L .

Since there are only two independent critical exponents, fractal dimension can be one of these, with any two critical exponents we can derive all other critical exponents. These critical exponents and scaling laws are used for upscaling of properties. The percolation threshold and correlation length are also basic quantities considered in upscaling.

3. Results

We tested 5 samples to verify the capability of our approach for different structured two-phase media. The samples are: a sandstone sample, a bread sample, two highly deformed rock samples, and one tree branch.

The sandstone sample is as a benchmark. It is synthetically made by compacting glass beads and cementing with calcite in-situ precipitation system (CIPS). The porosity is 24.44% and it is percolating in all 3-directions. By deflating pore structure step by step, the sixth deflated derivative model is only percolating in the z-direction. We recognize the sixth deflated model as the critical model because it is the percolating model which is the closest to the non-percolating models. The associated porosity of 3.94% is recognized as the percolation threshold. It is an order of magnitude smaller than that expected for the simple cubic lattice model obtained from random number simulations (31.16%) [1]. Bentz [4] created virtual permeable discrete microstructural models and obtained a similar percolation threshold of $3.2 \pm 0.4\%$ for porous media. This analysis is similar to our value of 3.94% and strongly supports the result of percolation threshold obtained from our sandstone sample. A series of local probabilities of percolation in 3-directions of the sandstone sample are obtained for sub-volume-size from 17 to 73 voxels. Using the finite-size scaling scheme, the critical exponent of correlation length $\nu = 0.885$ is fitted. It is very close to the theoretical analysis result of 0.88 [1].

From the derivative critical model of sandstone sample, we analysed the mass density $\rho(L)$. Our result shows $\rho(L)$ is linearly decreasing with $\log(L)$ when L is small. The fitting slope is $D-d$ and equals to -0.609, thus the fractal dimension $D=2.391$ is obtained, which is close to the theoretical result 2.5 [1]. For increasing side-length the mass density converges to a constant value. The transition from slope line to plateau should correspond to the crossover length ξ , which is a special correlation length separating the critical behaviour from the non-critical behaviour. In our model the transition occurs at $\log(L)=1.3$, thus ξ is around 20 voxels corresponding 50 μm .

As the sandstone sample has porosity higher than percolation threshold, consequently its crossover length should be smaller than 50 μm . Based upon these results, we can directly use of the transport properties obtained from the micro-scale ($\geq 50 \mu\text{m}$) for upscale modelling in the macro-scale. This deduction is verified up to laboratory scale by the comparison of numerical simulation and experimental testing.

The bread sample also gives reasonable outcomes and confirms the validity of the approach to randomly structured media.

The extrapolation of the theory to anisotropic samples gives some useful results but it fails on some aspect of the scaling relationships. For the highly deformed rock samples, percolation thresholds are 2.70% and 6.71%, respectively. The lower one represents a sample with two cracks, and the higher one represents a sample with irregularly distributed groups of pores. The fractal dimensions are 2.457 and 2.825, corresponding to lower and higher deformation, respectively. For the tree branch sample, the percolation threshold is as low as 0.31% and it is only percolating in z-direction. Multiple percolating clusters with similar sizes are encountered in the tree branch model. However, the fractal dimension is still in the range that is determined by other methods. The derivation of the critical exponents fails for all these three models. We conclude that the finite-size scaling scheme does not work for strongly heterogeneous/anisotropic samples, because of the failure of the extraction of the critical exponent of correlation length. A probable reason is that the strongly heterogeneous structure leads to additional uncertainties of correlation length and its relevant critical exponents. For heterogeneous samples, it is possible to obtain the fractal dimension from the percolation theory analysis, but is difficult to extract critical exponent of correlation length. New methods/measures need to be devised.

Acknowledgements

This project was funded through the Premier's Fellowship Program of the Western Australian Government, CSIRO OCE Postdoctoral Program, and the Geothermal Centre of Excellence of Western Australia. We are grateful to iVEC for technical support and access to the Altix supercomputer. We greatly appreciate to contributions from Florian Fuisseis, Keyu Liu, Shuo Wang, and Gerald Page for providing samples, experimental results, and constructive suggestion.

References

- [1] D. Stauffer, A. Aharony, Introduction to percolation theory, second ed., Taylor & Francis Ltd., London, 1994.
- [2] J. Liu, K. Regenauer-Lieb, C. Hines, K. Liu, O. Gaede, A. Squelch, Improved estimates of percolation and anisotropic permeability from 3-D X-ray microtomographic model using stochastic analyses and visualization, *Geochem., Geophys. Geosyst.*, 10(2009) Q05010, doi: 10.1029/2008GC002358.
- [3] A. Kapitulnik, A. Aharony, G. Deutscher, D. Stauffer, Self similarity and correlations in percolation, *J. Phys. A: Math. Gen.*, 16(1983) L269-L274.
- [4] D.P. Bentz, Virtual pervious concrete: Microstructure, percolation, and permeability, *ACI Mater. J.*, 105(2008) 297-301.

FROM ELECTRONIC STRUCTURE TO ELASTICITY

JIANFENG LU

COURANT INSTITUTE OF MATHEMATICAL SCIENCES
NEW YORK UNIVERSITY

Abstract: Ab initio electronic structure models like density functional theory have been widely used in a range of applications. The mathematical understanding of these models are still sparse. In this talk, we will discuss some recent works about the continuum limit of the electronic structure models, making connection between density functional theory and the elasticity theory. Algorithm developed based on the multiscale strategy enables electronic structure calculations for macroscopic systems. This is a joint work with Weinan E.

Phase-field Modelling of Twin Boundary Motion in Magnetic Shape Memory Alloys

Authors: Christian Mennerich¹, Frank Wendler¹, Marcus Jainta¹, Britta Nestler¹

¹ Karlsruhe University of Applied Sciences, Institute of Materials and Processes (IMP), Moltkestraße 30, 76133 Karlsruhe, Germany

ABSTRACT

Magnetic shape memory (MSM) alloys have gained major interest in the last decade because of their excellent properties as actuators and dampers that make use of the MSM effect. In single crystals strains of up to 10% could be observed, an effect that is often spoiled in polycrystalline materials. Atop an existing phase-field model for phase transitions a model for the MSM effect, i.e. for magnetically induced phase transitions, is build. This is done by extending the original model by micromagnetic energy contributions capturing magnetostatics, magnetic exchange and anisotropy as well as magnetoelastic effects. The resulting model is verified by simulating magnetic domain wall formation and twin boundary motion induced by external magnetic fields in single crystals, with the aim to go towards the analysis and prediction of twin boundary motions in polycrystalline materials in 3D.

1. Introduction

Magnetic shape memory (MSM) alloys gained major interest over the last 15 years. They offer fast response rates accompanied by giant elastic strains in moderate external fields (up to 1 Tesla), what makes them an excellent choice as components in actuators and dampers. Since the first observation of the MSM effect in 1996 (see [1]), changes in length up to ten percent have been observed in Ni₂MnGa single crystal specimens. In polycrystalline materials, the effect is often spoiled due to the different orientations of grains and the grain boundaries separating them. The MSM effect, in opposition to the thermoelastic shape memory effect, is entirely settled in the martensitic state of a material and bases on the mobility of low energetic twin boundaries. Assuming a magnetic hard material and applying an external magnetic field, it is energetically more advantageous to rearrange the microstructure than to pull local magnetic moments out of preferred directions. The phase transition from one martensitic twin variant to another is displacive and diffusionless, and the involved processes are fully reversible. Our aim is to set up a model that allows for the simulation of magnetically induced twin boundary evolution in magnetic hard materials in the martensitic state under the influence of an external applied magnetic field, tending towards covering the correct dynamics in polycrystals. The chosen approach bases on an existing phase-field model that is capable of describing phase transitions properly. The model for the MSM effect is developed atop this phase-field model by formulating the necessary micromagnetic energy contributions that drive the magnetically induced phase transformations, and extending the constituting phase-field functional appropriately. The equations of motion for concurrently evolving martensitic variants (phase fields), magnetic domain walls and elastic properties are stated. We conclude by demonstrating the applicability of our approach on selected simplified simulation scenarios.

2. The Phase-field model and magnetoelastic extensions

The adopted general phase-field model is introduced in [2]. A main advantage of the phase-field method is the avoidance of explicit front tracking by introducing a smoothly varying order parameter that separates phases by a diffuse interface of finite width ϵ . The model considers a region $\Omega \subset \mathbb{R}^3$ with $N \in \mathbb{N}$ phases, in which the order parameter $\phi(\vec{x}, t) = (\phi_1(\vec{x}, t), \dots, \phi_N(\vec{x}, t))^T : \Omega \times \mathbb{R}_{\geq 0} \rightarrow [0, 1]^N$ exists, where $\phi_\alpha = 1$ and $\phi_\alpha = 0$ characterize the bulk and the absence of pure phase $\alpha \leq N$, respectively. The general constituting integral Helmholtz free energy formulation is of Ginzburg-Landau type:

$$\mathcal{F} = \int_{\Omega} \left(\epsilon a(\phi, \nabla \phi) + \frac{1}{\epsilon} w(\phi) + f(\phi, \mathbf{c}, T, \dots) \right) d\vec{x}. \quad (1)$$

$a(\phi, \nabla \phi)$ and $w(\phi)$ are surface energy contributions. $f(\phi, \mathbf{c}, T, \dots)$ is the total bulk free energy as interpolation of bulk free energies $f^\alpha(\mathbf{c}, T, \dots)$ for every phase α , making use of a suitable smooth interpolation function $h : [0, 1] \rightarrow [0, 1]$. The bulk free energies depend on physical quantities like concentration, temperature or others, and act as driving forces for the system. Here, phases are attributed to martensitic variants. We now give the micromagnetic contributions that constitute these bulk free energies. Two fundamental simplifications are made: The restriction to isothermal settings below the Curie temperature T_{Curie} and below the martensitic start temperature T_m , and the assumption that the applied external field is constant over time. Consequently, the saturation magnetization $M_S \in \mathbb{R}$ becomes a constant, and the micromagnetic free energy is decreasing monotonically over time (cp. [3]). As additional state variables we introduce the (normalized) vector field of spontaneous magnetization $\mathbf{m} : \Omega \times \mathbb{R}_{\geq 0} \rightarrow \mathbb{S}^2$ (with \mathbb{S}^2 the unit sphere in \mathbb{R}^3) and the displacement field $\mathbf{u} : \Omega \times \mathbb{R}_{\geq 0} \rightarrow \mathbb{R}^3$. Five energy densities contribute to the magnetoelastic energy density:

$$\begin{aligned} f(\phi, \mathbf{u}, \mathbf{m}) &= e_{\text{ext}}(\mathbf{m}) + e_{\text{demag}}(\mathbf{m}) + e_{\text{exch}}(\mathbf{m}) + e_{\text{aniso}}(\phi, \mathbf{m}) + e_{\text{m-el}}(\phi, \mathbf{u}, \mathbf{m}) \quad (2) \\ &= -\mu_0 M_S (\mathbf{H}_{\text{ext}} \cdot \mathbf{m}) - \frac{1}{2} \mu_0 M_S (\mathbf{H}_{\text{demag}} \cdot \mathbf{m}) + A_{\text{exch}} |\nabla \mathbf{m}|^2 \\ &\quad - K_{\text{aniso}} \sum_{\alpha=1}^N (\mathbf{m} \cdot \mathbf{p}^\alpha)^2 h(\phi_\alpha) + \frac{1}{2} \sum_{\alpha=1}^N (\epsilon(\mathbf{u}) - \epsilon_0(\mathbf{m}))^T \mathcal{C}^\alpha (\epsilon(\mathbf{u}) - \epsilon_0(\mathbf{m})) h(\phi_\alpha). \end{aligned}$$

e_{ext} and e_{demag} are magnetostatic energy densities. The Zeeman energy density e_{ext} describes the interaction of the local magnetization \mathbf{m} with an applied external magnetic field \mathbf{H}_{ext} , where μ_0 is the micromagnetic permeability in the vacuum. The demagnetization energy (or magnetostatic self energy) density e_{demag} gives the long-range interactions between all local magnetic moments in the domain, described in terms of the demagnetization field $\mathbf{H}_{\text{demag}}$. The local variation of the magnetizations orientation is described by the exchange gradient energy density e_{exch} , where A_{exch} is the material dependent exchange stiffness constant. The micromagnetic anisotropy e_{aniso} takes into account the dependence of the local magnetization on directions of preferred magnetization, the so called easy axes. We restrict our considerations to the uniaxial case, where exactly one easy axis per variant exists. K_{aniso} is a material dependent anisotropy constant, and $\mathbf{p}^\alpha \in \mathbb{S}^2$ the unique direction of the easy axis of variant α . The coupling of micromagnetics and elasticity is realized by considering elasticity as well as eigenstrain (or stress free strain) contributions arising from the preceding martensitic transformation. Here, \mathcal{C} is the fourth order phase dependent elastic property tensor and $\epsilon(\mathbf{u})$ the second order tensor of total strain, depending on the displacement field. The total strain has to be adjusted by the eigenstrain that interacts with local magnetizations. In general, the second order eigenstrain tensor is given as $\epsilon_0(\mathbf{m}) = \frac{1}{2} \mathbf{m} \mathcal{N}(\phi) \mathbf{m}$, with \mathcal{N} the fourth order magnetostrictive property tensor. (The notation assumes the commonly used Voigt notation.) We remark, that the approach is easily generalizable to make all appearing energies dependent on martensitic variants, if adequate

variant dependent properties are known.

The equations of motion of the system are derived from variational and phenomenological principles. We are interested in the concurrent and mutually coupled evolution of the order parameter ϕ , the elastic displacement field \mathbf{u} and the spontaneous magnetization \mathbf{m} . The application of the Euler-Lagrange formalism from variational calculus gives the equations of motion for the phase fields ϕ_α ($\alpha = 1, \dots, N$) (see [2]):

$$\tau \epsilon \frac{\partial \phi_\alpha}{\partial t} = \epsilon (\nabla \cdot a_{,\nabla \phi_\alpha}(\phi, \nabla \phi) - a_{,\phi_\alpha}(\phi, \nabla \phi)) - \frac{1}{\epsilon} w_{,\phi_\alpha}(\phi) - f_{,\phi_\alpha}(\phi, \mathbf{u}, \mathbf{m}). \quad (3)$$

τ is the kinetic coefficient and λ a Lagrange multiplier to ensure the volume constraint for the order parameter. The evolution of the i -th component of the elastic displacement field ($i = 1, 2, 3$) is described via a wave equation as

$$\rho \frac{\partial^2 u_i}{\partial t^2} = \frac{1}{2} \sum_{j=1}^3 \frac{\partial}{\partial x_j} \left(\frac{\partial}{\partial x_j} (\epsilon(\mathbf{u}) - \epsilon_0(\mathbf{m}))^T \mathcal{C}(\phi) (\epsilon(\mathbf{u}) - \epsilon_0(\mathbf{m})) \right). \quad (4)$$

For the evolution of the magnetization \mathbf{m} the Landau-Lifshitz-Gilbert equation (see [3]) is adopted:

$$\frac{\partial \mathbf{m}}{\partial t} = -\frac{\gamma}{(1 + \alpha_G)^2} (\mathbf{m} \times \mathbf{H}_{\text{eff}} + \alpha_G \mathbf{m} \times (\mathbf{m} \times \mathbf{H}_{\text{eff}})). \quad (5)$$

γ is the gyromagnetic ratio and \mathbf{H}_{eff} denotes the effective magnetic field. The first term in Eq. (5) is a precessional (Larmor) term around \mathbf{H}_{eff} , the second a dissipative phenomenological damping term (with Gilbert damping constant α_G). The property $|\mathbf{m}| = 1$ has to be maintained during system evolution. The effective field is derived from the Gibbs free energy density f as $\mathbf{H}_{\text{eff}} = -\frac{1}{\mu_0 M_S} \frac{\delta f(\phi, \mathbf{m}, \mathbf{u})}{\delta \mathbf{m}}$ (cp. [4]). The contributions coming from the elastic part are small and can be neglected.

3. Numerics and Simulations

The equations introduced above are implemented using a finite differences discretization scheme basing on equisized parallelepipedic grid cells, and for the displacement field staggered grids are used, due to its wave character and for stability reasons. Eqs. (3) and (4) are integrated via explicit one-step Euler forward schemes, while for Eq. (5) a geomtric integration scheme (basing on Lie-group methods, see [5]) is implemented to respect the geometric structure of the equation. We applied the system to different simulation scenarios, focusing on the evolution due

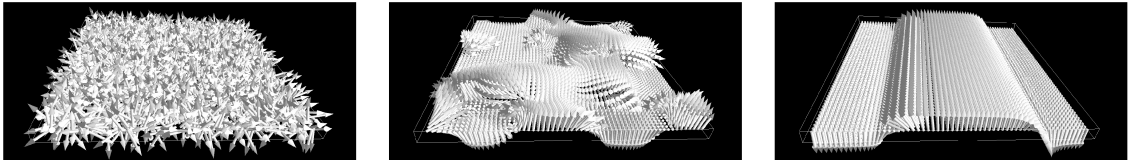


Figure 1: Magnetic domain wall formation from an initially random configuration.

to concurrent anisotropy and exchange energy. A non-dimensionalized set of parameters was set-up, leaned towards the Ni_2MnGa material system. The first setting assumes an infinitely extended crystal having an initial random oriented magnetization. The size of the simulation box is about $10\mu\text{m}$, resolved by 60×60 gridpoints (see Fig. 1). The magnetocrystalline anisotropy points in the direction orthogonal to the shown plane. Magnetic domain walls of about 83.7nm thickness form (cp. Fig. 2), what is in agreement with analytical results (cp. [6]). The second

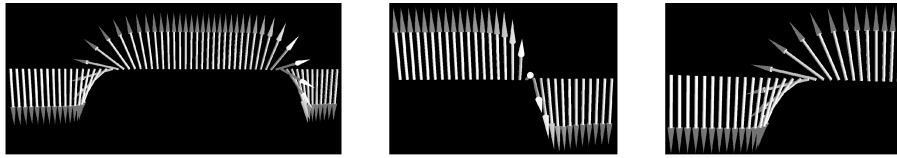


Figure 2: A 1D cross section through the plane in the final state (left), showing the developing wall types: A Bloch type wall (middle) and a Néel type wall (right).

setting (see Fig. 3) shows a periodically repeated structure of two twin variants α and β in an external applied field \mathbf{H}_{ext} pointing in direction of the positive x - y plane bisector. The simulation starts with an 180° domain wall structure. The easy axes of α and β are orthogonal, the one of β coincides with the direction of \mathbf{H}_{ext} . The variant β becomes advantageous and grows for the detriment of variant α . The growth velocity of β depends on the strength of the applied external field (see Fig. 3). Simulations taking the demagnetization and elastic contributions

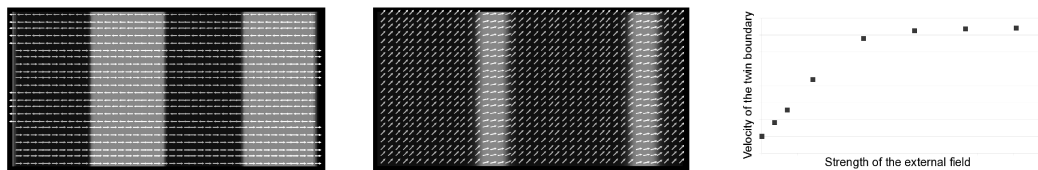


Figure 3: Magnetically induced motion of martensitic variants α and β (left and middle). Velocity of the boundary motion vs. external field strength (right).

into account, are work in progress. The implementation within the existing software framework supports the extension of the scenarios to 3D, but requires efficient algorithms to deal with the computational complexity arising from the demagnetization field. More details on the modeling approach and the simulations are given in a forthcoming paper.

Acknowledgements

The authors gratefully acknowledge the Deutsche Forschungsgemeinschaft (DFG) within the priority programme SPP 1239 for funding.

References

- [1] K. Ullakko, J. K. Huang, C. Kantner, R. C. O'Handley, V. V. Kokorin, *Large magnetic-field-induced strains in Ni_2MnGa single crystals*, Appl Phys Lett **69**, 1966 – 1968, 1996.
- [2] B. Nestler, H. Garcke, B. Stinner, *Multicomponent alloy solidification: Phase-field modelling and simulations*, J Phys Rev E **71**, 2005.
- [3] Ivan Cimrak, *A Survey on the Numerics and Computations for the Landau-Lifshitz Equation of Micromagnetism*, Arch Comput Methods E **15**, 277 - 309, 2008.
- [4] J. E. Miltat, M. J. Donahue, *Numerical Micromagnetics: Finite Difference Methods*, in: Handbook of Magnetism and Advanced Magnetic Materials (Ed. H. Kronmuller, S. Parkin), John Wiley and Sons Ltd., 2007.
- [5] D. Lewis, N. Nigam, *A geometric integration algorithm with applications to micromagnetism*, J Comput Appl Math **151**, 141-170, 2003.
- [6] A. Aharoni, *Introduction to the theory of Ferromagnetism*, Oxford Science Publication, Second Edition, 2000.

Multi-Scale Modelling Of Shell Failure For Periodic Quasi-Brittle Materials

Authors: B.C.N. Mercatoris¹, T.J. Massart²

Affiliations: ¹Université Libre de Bruxelles (U.L.B.)
Building, Architecture and Town Planning Dept.
Avenue F.D. Roosevelt 50 CP194/2, 1050 Brussels, Belgium
e-mail: {bmercato, thmassar}@batir.ulb.ac.be

ABSTRACT

A two-scale framework is presented for the failure of periodic masonry shell structures, in which membrane-flexural couplings appear. The failure behaviour of textured heterogeneous materials such as masonry is strongly influenced by their mesostructure. Their periodicity and the quasi-brittle nature of their constituents result in complex behaviours such as damage-induced anisotropy properties with localisation of damage, which are difficult to model by means of macroscopic closed-form constitutive laws. A periodic computational homogenisation procedure is used for the in-plane and the out-of-plane behaviour of such planar shells. The localisation of damage at the structural scale is represented by means of embedded strong discontinuities incorporated in the shell description. Based on the assumption of single period failure, the behaviour of these discontinuities is extracted from the mesostructure. An acoustic tensor-based criterion adapted to shell kinematics is used to detect the structural-scale failure and find its orientation. For the softening mechanical response of the macroscopic discontinuities, a new enhanced scale transition is outlined for shell failure based on an approximate energy consistency argument in order to objectively upscale the energy dissipation. The corresponding multi-scale framework results are compared to direct fine scale modelling results used as a reference for the case of masonry, showing a good agreement in terms of load bearing capacity, of failure mechanisms and of associated energy dissipation.

1. Introduction

The formulation of macroscopic constitutive laws for the behaviour of masonry is a complex task, due to its strongly heterogeneous microstructure which considerably influences its overall mechanical behaviour. Due to the quasi-brittle nature of its constituents, this results in initial and damage-induced (evolving) anisotropy properties, accompanied with localisation of damage. In its structural use, such a material may be subjected to cracking, leading to localisation of damage at both the structural and fine scales. Closed-form laws have therefore been developed for equivalent anisotropic media for elastic and cracking behaviour^{1,2}. The use of such models in the cracking regime is however impeded by their costly identification. As a complementary approach, the multi-scale computational strategies aim at solving this issue by deducing a homogenised response at the structural scale from a representative volume element (RVE), based on constituents properties and averaging theorems.

2. Multi-scale modelling of thin masonry shell

Computational homogenisation approaches allow identifying homogenised continuum properties from the constituents constitutive behaviour of a heterogeneous mesostructure. This allows the set-up of nested computational procedures in which a sample of the mesostructure is used

to determine numerically the local macroscopic material response. The definition of such a nested scheme essentially requires the definition of four ingredients: (i) a fine scale constitutive description for the constituents, (ii) the definition of a representative mesostructural sample, (iii) the choice of a coarse scale representation, and (iv) the set-up of scale transitions linking structural and fine scale quantities.

A scale transition for homogenisation towards a Kirchhoff-Love shell behaviour was recently proposed³. For the case of masonry, the microstructure may be represented by a unit cell on which a strain-periodic displacement field is imposed^{4,3}. The constituents inside the unit cell may be modelled using any closed-form formulation. As a result, the response of a coarse scale point under any loading program may be computed.

3. Upscaling framework for out-of-plane failure

In order to incorporate damage localisation effects at both the structural and fine scales, the scale transition procedure has to be adapted accordingly. For in-plane loaded structures, in which both fine and coarse scale descriptions follow similar kinematical assumptions, these adaptations have been proposed recently with different methodologies^{5,6}. This approach can be extended to shell formulations, where higher order kinematical quantities such as curvatures appear at the structural scale. This requires adaptations within the structural scale description as well as in the scale transitions.

Any localisation enhancement at the coarse scale to represent failure requires a criterion to detect localisation and to determine its orientation. However, in a computational homogenisation procedure, the macroscopic material response is not postulated a priori but rather computed from the material laws introduced at the microstructural level. This criterion should then be based on computationally homogenised results, the only information available characterising the average material behaviour. The detection of the structural scale localisation can be based on the acoustic tensor concept extended to the shell description⁷. This tensor has to be constructed based on the homogenised stiffness such that the localisation detection takes into account the coupling of flexural and membrane effects. It can be shown that such a procedure allows to extract mesostructurally motivated average localisation orientations, based on the non positive definiteness of this tensor, for various coupled flexural-membrane loading paths⁸.

The structural scale problem is solved using the finite element method and using an embedded strong discontinuity model⁹. Once structural localisation is detected, the coarse scale displacement and rotation fields are enriched by jumps along a discontinuity line, the orientation of which is deduced from the acoustic tensor-based criterion. In order to determine these additional jump fields, the weak form of equilibrium is solved together with a weak continuity condition on the stress along the discontinuity line. A material response which links the generalised stresses across the discontinuity to the jumps is therefore required to drive the discontinuity. Once the embedded discontinuity is introduced, the bulk of the element is assumed to unload elastically from the state reached at that point⁹.

Further to the recently proposed discontinuity approach where the material behaviour is defined by closed-form laws⁹, both the bulk and discontinuity material behaviours are deduced here from fine scale unit cell computations. A material secant stiffness is extracted from the unit cell in which the structural localisation has just been detected in order to compute the elastic unloading of the bulk. The material behaviour of the coarse scale discontinuity is extracted from a further damaging unit cell, denoted as Localising Volume Element (LVE), by means of

an enhanced upscaling procedure. This extraction requires the definition of average generalised strains to be applied on the LVE from the coarse scale displacement and rotation jumps. An enhanced upscaling procedure based on an approximate energy consistency has been proposed recently for the in-plane case¹⁰ and is extended to the out-of-plane case¹¹.

4. Comparison of multi-scale and fine scale results on structural examples

The proposed multi-scale scheme was implemented using parallel computation tools. Two structural wall computations are performed and the results are compared to a fine scale computation used as a reference in order to challenge the periodicity and scale separation assumptions of the computational homogenisation procedure. The results comparison is based both on the overall response of the wall and on the obtained failure mode.

The proposed approach is illustrated for the case of a masonry wall with an opening subjected to in-plane confined shearing. A good agreement is obtained between the full fine scale and multi-scale computations in terms of load bearing capacity and failure mode (see Fig. 1)¹².

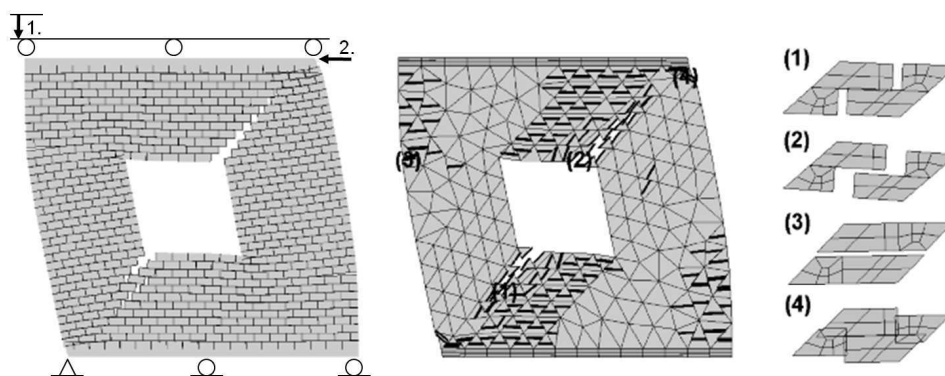


Figure 1: Deformed configuration at the peak of the in-plane confined shearing load-displacement response of the wall (the displacements of the wall are magnified by a factor of 200): (left) deformed configuration of the complete fine scale computation, (centre) deformed configuration of the multi-scale computation and (right) related deformed unit cells (the displacements of the cells are magnified by a factor of 50).

The case of stair-case out-of-plane failure mode propagation is also considered on a square masonry shell subjected to out-of-plane forces (see Fig. 2). The overall response of the wall of both the full fine scale and multi-scale computations are in good agreement. The deformed configuration at the peak of the response is shown in Fig. 2 for both models. Furthermore, this case also allows to show that the appearance of membrane-flexural couplings due to the different tensile and compressive strengths of the damaging joints is well incorporated in the homogenisation procedure and in the localisation analyses.

5. Conclusions

These results show that the multi-scale modelling yields results in good agreement with respect to complete fine scale computations for both the limit load and the failure mode. The multi-scale methodology proves to be a valuable tool for the investigation of masonry structures. In particular, it allows to account for the strong coupling between the structural response and the underlying mesostructural features of the material. Specific enhancements are however needed in order to account properly for the consequences of the quasi-brittle nature of the constituents.

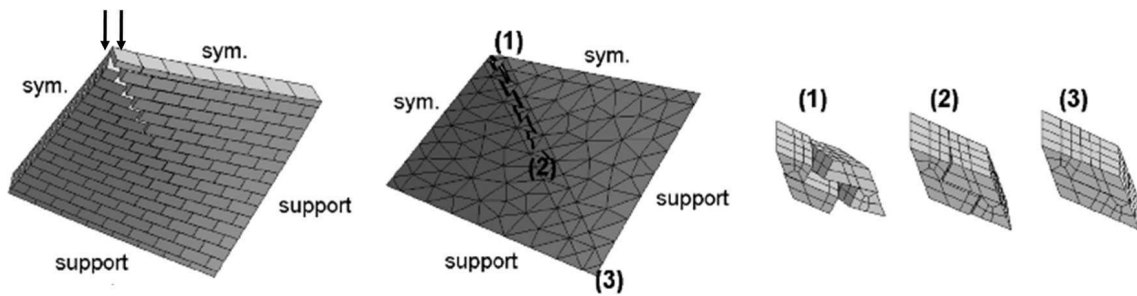


Figure 2: Deformed configuration at the peak of the response of the wall (the displacements of the deformed configuration are magnified by a factor of 500): (left) deformed configuration of the complete fine scale computation, (centre) deformed configuration of the multi-scale computation and (right) related deformed unit cells.

References

- [1] P.B. Lourenço, R. de Borst and J.G. Rots. A plane stress softening plasticity model for orthotropic materials, *Int. J. Num. Meth. Engng.*, **40**(21), 4033–4057, 1997.
- [2] P.B. Lourenço. Anisotropic softening model for masonry plates and shells, *J. Struct. Engng. ASCE*, **126**(9), 1008–1016, 2000.
- [3] M. Mistler, A. Anthoine and C. Butenweg. In-plane and out-of-plane homogenisation of masonry, *Comput. Struct.*, **85**, 1321–1330, 2007.
- [4] A. Anthoine. Derivation of the in-plane elastic characteristics of masonry through homogenization theory, *Int. J. Solids Struct.*, **32**(2), 137–163, 1995.
- [5] T.J. Massart, R.H.J. Peerlings and M.G.D. Geers. An enhanced multi-scale approach for masonry wall computations with localization of damage, *Int. J. Num. Meth. Engng.*, **69**, 1022–1059, 2007.
- [6] T. Belytschko, S. Loehnert and J.H. Song. Multiscale aggregating discontinuities: A method for circumventing loss of material stability, *Int. J. Num. Meth. Engng.*, **73**, 869–894, 2008.
- [7] J. Makowski and H. Stumpf. Strain localization in stress-resultant theory of shells, *Mech. Research Comm.*, **25**(4), 455–465, 1998.
- [8] B.C.N. Mercatoris, P. Bouillard and T.J. Massart. Multi-scale detection of failure in planar masonry thin shells using computational homogenisation, *Engng. Fract. Mech.*, **76**(4), 479–499, 2009.
- [9] F. Armero and D. Ehrlich. Finite element methods for the multi-scale modeling of softening hinge lines in plates at failure, *Comput. Meth. Appl. Mech. Engng.*, **195**, 1283–1324, 2006.
- [10] B.C.N. Mercatoris and T.J. Massart. Assessment of periodic homogenisation-based multi-scale computational schemes for quasi-brittle structural failure, *Int. J. Multiscale Comput. Engng.*, **7**(2), 153–170, 2009.
- [11] B.C.N. Mercatoris and T.J. Massart. A coupled two-scale computational scheme for the failure of periodic quasi-brittle thin planar shells and its application to masonry, *Int. J. Num. Meth. Engng.*, accepted for publication.
- [12] B.C.N. Mercatoris. Multi-scale modelling of shell failure for periodic quasi-brittle materials, *PhD thesis*, Université Libre de Bruxelles, 2010.

A mathematical model for the evolution of microstructures in elastoplasticity

Alexander Mielke¹

¹Weierstrass Institute for Applied Analysis and Stochastics, Berlin, Germany

Finite-strain elastoplasticity leads to three types of geometric nonlinearities. The first is due to the geometric nonlinearity of finite strain elasticity induced by frame indifference. The second is due to the multiplicative decomposition of the strain tensor in an elastic and a plastic part. Moreover, plastic invariance makes the dissipation potential geometrical nonlinear.

As a consequence these tensors should be treated as elements of the multiplicative matrix groups.

As a consequence the statics of incremental problems for such model develop microstructure unless gradient terms are used to regularize the model. To describe experimentally observed microstructures, Hackl and Kochmann [2009] have proposed a model where certain classes of simple or sequential laminates are treated as "internal variables" in the sense general dissipative materials, also called generalized standard materials. We provide a mathematical framework to treat this model rigorously. To avoid formation of further microstructure we introduce a weak regularization forbidding these microstructures to develop further oscillations.

We explain how the functional analysis for an existence theory can be adapted using ideas from metric spaces to be able to handle the underlying geometric nonlinearities rigorously.

UNDERSTANDING COUPLED MULTISCALE METHODS: QUASICONTINUUM METHOD AS AN EXAMPLE

PINGBING MING

Abstract

We shall discuss the general strategy for the understanding of the coupled multiscale method in solids, particularly, quasicontinuum method will be used as an demonstrative example.

1. INTRODUCTION

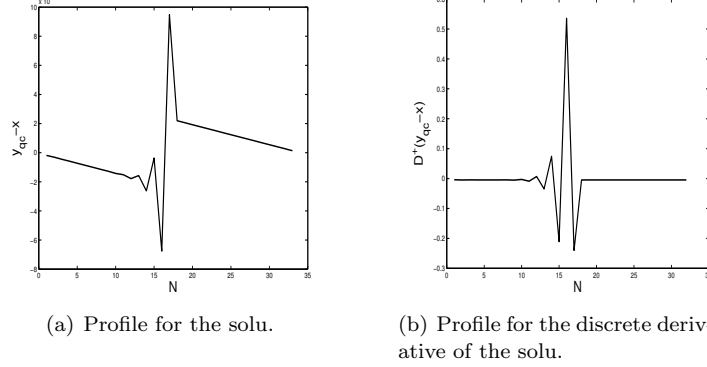
A coupled macro-micro modeling approach is preferred in order to capture both the macroscale behavior of the system and the important details of such local events. There are many different strategies for coupling [1] and we will focus on the domain-decomposition type coupling in this short note. Particularly we shall consider the quasicontinuum (QC) method [17].

Quasicontinuum method is among the most successful multiscale methods for modeling the mechanical deformation of solids. So far its main success is in modeling the static properties of crystalline solids at zero temperature, even though various attempts have been made to extend QC to modeling dynamics at finite temperature. At the same time, QC has attracted a great deal of attention from the numerical analysis community, since it provides the simplest example for understanding the algorithmic issues in coupled atomistic-continuum methods. Indeed one main challenge in multiscale, multi-physics modeling is to understand the stability and accuracy of multi-physics algorithms. This is of particular interest for coupled atomistic-continuum algorithms, since the nature of the continuum models and atomistic models are quite different. Specifically, we would like to understand:

- (1) whether new numerical instabilities can arise as a result of atomistic continuum coupling;
- (2) whether the matching between the continuum and atomistic models causes large error.

The second issue is particularly important: It is inevitable to introduce some error at the interface where the atomistic and continuum models are coupled together. The question is how large this error is and whether this error also affects the accuracy of the numerical solution away from the interface. We also note that Weiqing Ren [13] has demonstrated, using examples from fluid mechanics, that new numerical instabilities can arise as a result of coupling atomistic and continuum models.

QC provides the simplest example for analyzing the issues outlined above for the following reason: at zero temperature, the atomistic model can be regarded as a consistent discretization of the Cauchy-Born continuum model [2]. We note that the Cauchy-Born continuum model is the right continuum limit of the atomistic model whenever the system is in the elastic regime [6, 7]. Since QC uses the Cauchy-Born rule in the continuum region (or the local region, in the QC terminology), the

FIGURE 1. Error profile for the original QC solution with $N = 16$ 

models used in the continuum and atomistic regions (or local and nonlocal regions) are consistent. The only remaining issue is what happens at the interface when the two models couple.

2. EXPLICIT EXAMPLES FOR GHOST-FORCE ERROR

Indeed errors are introduced by QC at the interface. The simplest and most well-known example is the “ghost force”, i.e., forces that act on the atoms when they are in equilibrium positions. When atoms are in equilibrium positions, the forces acting on them should vanish. So whatever forces present is numerical error.

For the one-dimensional chain, we have studied the error caused by the ghost force in the case when there is an external force in [10, 12]. For the case when there is no external force and the interaction potential is harmonic and the next nearest neighbor interaction is taken into account, the error takes an *explicit* form, which allows us to see exactly how the error caused by the ghost force looks like; see Fig. 1. Such explicit error form was firstly derived in [12], see also [4] for a similar discussion.

For the high-dimensional case, we [3] recently obtained the explicit form of the error caused by the ghost-force. They consider a square lattice and the interaction potential is harmonic. In this case, it is not enough to taken into account the first and the second neighborhood interaction, since there is no ghost-force in this set-up. Instead they consider the first and the third interaction. Their results are summarized in the following theorem, and we refer to [3] for more details.

Theorem 2.1. *The error in the local region (continuum model) is*

$$y(m, n) = -\frac{2\varepsilon}{N} \sum_{\substack{k=1 \\ k \text{ is odd}}}^{2N-1} \frac{\mathcal{Q}_k}{P_k r_k - R_k p_k} \frac{\sinh[(M+m)\alpha_k]}{\sinh[(M-1)\alpha_k]} \rho_k \cot \frac{k\pi}{4N} \sin \frac{k\pi}{2N} (n+N),$$

where

$$\mathcal{Q}_k = (r_k + 6p_k)(5F_0 - F_1) - (R_k + 6P_k)(5f_0 + f_1).$$

The error in the nonlocal region (atomistic model) is

$$y(m, n) = -\frac{2\varepsilon}{N} \sum_{k=1, k \text{ odd}}^{2N-1} \frac{\mathcal{Q}_{m,k}}{P_k r_k - R_k p_k} \cot \frac{k\pi}{4N} \sin \frac{k\pi}{2N} (n + N),$$

where

$$\mathcal{Q}_{m,k} = (-1)^m F_m(r_k + 6p_k) - f_m(R_k + 6P_k),$$

and

$$\begin{cases} P_k = [-2F_{\bar{1}} + F_1 - \rho_k(-F_{\bar{1}} + 5F_0)](\gamma_k, \delta_k), R_k = (3F_0 + 9F_{\bar{1}} + F_2 - 5F_1)(\gamma_k, \delta_k), \\ p_k = [2f_{\bar{1}} - f_1 - \rho_k(f_{\bar{1}} + 5f_0)](\gamma_k, \delta_k), r_k = (3f_0 - 9f_{\bar{1}} + f_2 + 5f_1)(\gamma_k, \delta_k), \\ \rho_k = \frac{\sinh[(M-1)\alpha_k]}{5 \sinh[M\alpha_k] + \sinh[(M-1)\alpha_k]} \end{cases}$$

with

$$\begin{cases} F_m(\gamma, \delta) = \frac{\sinh[(M+1-m)\gamma] + \sinh[(M-m)\gamma] \cosh \delta - (-1)^m \cosh[(M-m)\delta] \sinh \gamma}{\cosh \gamma + \cosh \delta}, \\ f_m(\gamma, \delta) = F_m(\delta, \gamma), \end{cases}$$

and

$$\begin{cases} \cosh \gamma_k = \frac{1 + \sqrt{25 + 8\lambda_k}}{4}, & \cosh \delta_k = \frac{-1 + \sqrt{25 + 8\lambda_k}}{4}, \\ \cosh \alpha_k = 1 + \frac{\lambda_k}{5}, & \lambda_k = 2 \sin^2 \frac{k\pi}{4N}. \end{cases}$$

Based on the above equations, we estimate the error of the solution and its discrete derivative in [3]. In particular, we prove that the width of the interfacial layer is $\mathcal{O}(\varepsilon |\ln \varepsilon|)$ in the sense that the error for the discrete derivative of the solution is $\mathcal{O}(\varepsilon)$ outside the interfacial layer.

It is demonstrated that the ghost-force may lead to large errors, in particular for the deformation gradient. Such error may push the system to the basin of attraction of another nearby minimum. Physically, this suggests that it may cause unphysical dislocation nucleation around the tip of a propagating crack [19], see also [14, 15] for the related discussion.

3. ERROR ANALYSIS

For one-dimensional problem, the accuracy of the quasicontinuum method is analyzed using a series of models with increasing complexity [12], we refer to [4] for the progress of other groups. We view the interface as an internal numerical boundary where two different numerical schemes meet, both are consistent with the underlying PDE, in this case the Cauchy-Born elasticity model. We have shown in [12] and a follow-up paper [11] that the accuracy and stability issues in QC can be understood following standard practices in classical numerical analysis: we calculate the local truncation error (LTE) of the different variants of QC. We will see that even though the LTEs for the ghost-force removal procedures are all $\mathcal{O}(1)$, they are of divergence form and are actually $\mathcal{O}(\varepsilon)$ in a weak norm, which is actually the so-called *Spijker norm* appeared in the homogeneous difference schemes [18, 16, 9]. We also study the stability issues and give an example of a geometrically consistent scheme that is unstable. We then show, following the strategies presented in [6], that the stability condition and the LTE analysis implies that ghost-force removal procedures recover uniform first order accuracy. The ghost-force removal strategy

includes the force-based QC [14], the quasinonlocal QC [15] and the geometrically consistent scheme proposed by E, Lu and Yang [5]. The details may be found in [10, 8, 12].

So far almost all works are confined to one-dimensional problem. The extension to higher-dimensional problem is possible by following the above strategy. For example, we have proved in [11] that the quasinonlocal QC converges with first order accuracy in two-dimensional problem with a planar interface. Actually, the main technical points for the extension to high dimensional problem with planar interface have been sketched in [12]. However, this leaves out the situations when the interface has corners. At this point, very little is known in that case.

REFERENCES

1. F.F. Abraham, J.Q. Broughton, N. Bernstein and E. Kaxiras, *Concurrent coupling of length scales: methodology and applications*, Phys. Rev. **B60**(1999), 2391–2402.
2. M. Born and K. Huang, *Dynamical Theory of Crystal Lattices*, Oxford University Press, 1954.
3. J.R. Chen and P.B. Ming, *Explicit solution for quasicontinuum methods in 2D*, preprint, 2010.
4. M. DOBSON AND M. LUSKIN, *An analysis of the effect of ghost force oscillation on quasicontinuum error*, ESAIM: M2AN. **43**(2009), 591-604.
5. W. E, J. Lu and Jerry Z. Yang, *Uniform accuracy of the quasicontinuum method*, Phys. Rev. B **74**(2006), 214115.
6. W. E and P.B. Ming, *Cauchy-Born rule and the stability of the crystalline solids: static problems*, Arch. Rational Mech. Anal. **183**(2007), 241–297.
7. W. E and P.B. Ming, *Cauchy-Born rule and the stability of the crystalline solids: dynamic problems*, Acta Math. Appl. Sin. Engl. Ser. **23**(2007), 529–550.
8. W. E and P.B. Ming, *Analysis of the nonlocal quasicontinuum method*, preprint, 2008.
9. H.-O. Kreiss, T.A. Manteuffel, B. Swarts, B. Wendroff and A.B. White, Jr., *Supra-convergent schemes on irregular grids*, Math. Comp. **47**(1986), 537–554.
10. P.B. Ming, *Error estimate of force-based quasicontinuum method*, Comm. Math. Sci., **5**(2008), 1089–1095.
11. P.B. Ming, *Analysis of quasinonlocal quasicontinuum method in two-dimension*, in preparation.
12. P.B. Ming and Jerry Z.J. Yang, *Analysis of a one-dimensional nonlocal quasicontinuum method*, Multiscale Model. Simul., **7**(2009), 1838–1875.
13. W.Q. Ren, preprint.
14. V.B. Shenoy, R. Miller, E.B. Tadmor, R. Phillips and M. Ortiz, *An adaptive finite element approach to atomic scale mechanics-the quasicontinuum method*, J. Mech. Phys. Solids **47**(1999), 611–642.
15. T. Shimokawa, J.J. Mortensen, J. Schiøz and K.W. Jacobsen, *Matching conditions in the quasicontinuum method: removal of the error introduced in the interface between the coarse-grained and fully atomistic region*, Phys. Rev. **B 69** (2004), 214104.
16. M.N. Spijker, *Stability and convergence of finite difference schemes*, Thesis, University of Leiden, 1968.
17. E.B. Tadmor, M. Ortiz and R. Phillips, *Quasicontinuum analysis of defects in solids*, Phil. Mag. **A73**(1996), 1529–1563.
18. A.N. Tikhonov and A.A. Samarskiĭ, *Homogeneous difference schemes on nonuniform nets*, Zh. Vychisl. Mat. i Mat. Fiz., **2**(1962), 812–832; English transl. in U.S.S.R. Comput. Math. and Math. Phys. **2**(1962), 927–953.
19. JERRY Z. YANG AND X. LI, *Comparative study of boundary conditions for molecular dynamics simulations of solids at low temperature*, Phys. Rev. B, **73** (2006), 224111.

LSEC, INSTITUTE OF COMPUTATIONAL MATHEMATICS AND SCIENTIFIC/ENGINEERING COMPUTING, AMSS, CHINESE ACADEMY OF SCIENCES, NO. 55 ZHONG-GUAN-CUN EAST ROAD, BEIJING, 100190, PEOPLE'S REPUBLIC OF CHINA

E-mail address: mpb@lsec.cc.ac.cn

Advancement of the coarse-grained particle method for finite temperature solids

Takahide Nakamura,^{1,2} Ryo Kobayashi,^{1,2} and Shuji Ogata^{1,2}

¹Department of Scientific and Engineering Simulation, Graduate School of Engineering,
Nagoya Institute of Technology, Gokiso-cho, Showa-ku, Nagoya 466-8555, Japan

²CREST, Japan Science and Technology Agency, 4-1-8 Honcho, Kawaguchi, Saitama
332-0012, Japan

ABSTRACT

The coarse-grained particle (CGP) method [1,2] has been proposed for crystalline solids. In the CGP method, the total energy of the CGP system is defined as the statistical ensemble average of the atomic energy with the weighting function in the phonon approximation. Though the method well reproduces the phonon spectrum, it substantially underestimates the deformation energy. In this paper, we optimize the weighting function from both points of the phonon spectrum and deformation energy. We then incorporate the atomic anharmonicity at finite temperatures that is ignored in the original formulation of the CGP method.

1. Introduction

We might state that there exists almost no limitation in size for the classical simulation of atoms using $O(N)$ algorithms on modern parallel machines. However the time step cannot be changed and hence the total simulation time still remains small. It is useful to reduce computational costs and to increase the time step by coarse-graining the atomic system. The coarse-grained particle (CGP) method [1] has been proposed for crystalline solids and we have developed it for more accuracy [2].

2. The coarse-grained particle method

A CGP represents a group of atoms under constraint $\mathbf{U} = \mathbf{w}\mathbf{u}$ with the displacements \mathbf{u} and \mathbf{U} for the atoms and CGP's, respectively. A similar constraint is applied also to their velocities. Here \mathbf{w} is a $N_{\text{CGP}} \times N_{\text{atom}}$ matrix and is called the weighting function. Under those constraints, the total energy of the CGP system is calculated as the ensemble average of the atomic energy. That is,

$$E_{\text{CGP}} = \frac{1}{Z_{\text{CGP}}} \int d\mathbf{u} d\dot{\mathbf{u}} E_{\text{atom}} \exp\left(-\frac{E_{\text{atom}}}{k_{\text{B}}T}\right) \delta(\mathbf{U} - \mathbf{w}\mathbf{u}) \delta(\dot{\mathbf{U}} - \mathbf{w}\dot{\mathbf{u}}) \quad (1)$$

with the delta function $\delta(x)$.

Taking the harmonic approximation for the inter-atomic interaction energy (i.e.

$$E_{\text{atom}} = \frac{1}{2} \dot{\mathbf{u}}^T \mathbf{m} \dot{\mathbf{u}} + \frac{1}{2} \mathbf{u}^T \mathbf{D} \mathbf{u}, \text{ Eqn. (1) can be rewritten as}$$

$$E_{\text{CGP}} = \frac{1}{2} \dot{\mathbf{U}}^T \mathbf{M} \dot{\mathbf{U}} + \frac{1}{2} \mathbf{U}^T \mathbf{K} \mathbf{U} + 3k_{\text{B}}T(N_{\text{atom}} - N_{\text{CGP}}) \quad (2)$$

Here $\mathbf{K} = (\mathbf{w}\mathbf{D}^{-1}\mathbf{w}^T)^{-1}$, $\mathbf{M} = (\mathbf{w}\mathbf{m}^{-1}\mathbf{w}^T)^{-1}$, $\mathbf{D}_{ij} = \frac{\partial^2 V_{\text{atom}}}{\partial r_i \partial r_j}$, and $\mathbf{m}_{ij} = m_{\text{atom}} \delta_{ij}$. We may simulate

coarse-grained dynamics by taking Eqn. (2) as the Hamiltonian.

Merits of the CGP method are: First, the CGP interaction can be determined from the first principles. It is possible to coarse-grain any atomic system if its inter-atomic potential is available. Second, all the atomic phonons are included in the total energy of the CGP system through the ensemble average. That makes the CGP method more suitable to a situation in which the coarse-graining level is not high than other continuum-based methods. There are, however, some demerits: The shape of weighting function is not optimized. The atomic anharmonicity and finite temperature effects are neglected because of the harmonic approximation of the inter-atomic interaction. Besides, since the matrix-inverse calculation requires high computational cost, the periodic boundary condition must be applied; it means that the CGP method cannot be used for inhomogeneous systems.

3. The optimization of the weighting function

In the well-known finite-element method, the constraint is $\mathbf{u} = \mathbf{N}\mathbf{U}$ with the interpolation function \mathbf{N} . On the other hand, the constraint of the CGP method is $\mathbf{U} = \mathbf{w}\mathbf{u}$. When we set $\mathbf{w} = [\mathbf{N}\mathbf{N}^T]^{-1}\mathbf{N}$ as the matrix-inverse of \mathbf{N} , we call it ‘‘original \mathbf{w} ’’. Using the original \mathbf{w} , the phonon dispersion relation of the CGP system corresponds well to that of the atomic one. We dare state that it is the only reason to use the original \mathbf{w} . Is it safe to use the original \mathbf{w} ? Another important measure of judgment is the correctness of the deformation energy. We therefore compare the deformation energy between the atomic and CGP systems by applying the same displacements

$$U_l^{(\alpha)} \propto \exp\left[-\frac{(R^0 - R_l)^2}{\alpha^2}\right] \quad \text{and} \quad u_i^{(\alpha)} \propto \exp\left[-\frac{(r^0 - r_i)^2}{\alpha^2}\right]. \quad (3)$$

Here $R^0 = r^0$ is the same peak-position of the displacements.

As a test, we consider the system of 55 CGP’s that is obtained by coarse-graining a spring-beads system composed of 550 atoms (the spring constant $k_{\text{atom}} = 1$; mass $m_{\text{atom}} = 1$; atomic interval $a_{\text{atom}} = 1$) under the periodic boundary condition in 1-dimension. The CGP interval $a_{\text{CGP}} = 10$. We call the situation ‘‘CG10’’ since a single CGP represents 10 atoms. As Fig. 2 (right) shows, the CGP deformation-energy with the original \mathbf{w} deviates substantially from the atomic one at small α (i.e., the spiky displacement). We now optimize the weighting function so that the deviation is minimized. We note that the range of α shown in Fig. 2 (right) is so determined that the calculated deformation energies for various $R^0 (= r^0)$ take on the same value in the range. In the optimization we assume that the weighting function is linear with respect to the distance from a CGP between the two neighboring CGP’s. The original and optimized \mathbf{w} are shown in Fig. 1. Correspondingly, both the phonon dispersion relation and the deformation energy are shown in Fig. 2. By making the absolute value of original \mathbf{w} smaller, we find that the deformation energy of the CGP system gets closer to that of the atomic one. On the other hand, the phonon dispersion relation is almost the same between the original and optimized \mathbf{w} . It may be because the dependence of \mathbf{M} on the shape of the weighting function is similar to that of \mathbf{K} .

To summarize, it is enough to use the original \mathbf{w} if one is interested in the correctness of the phonon-dispersion relation only. The optimized \mathbf{w} should be used if one is interested in the correctness of the (spiky) deformation energy also.

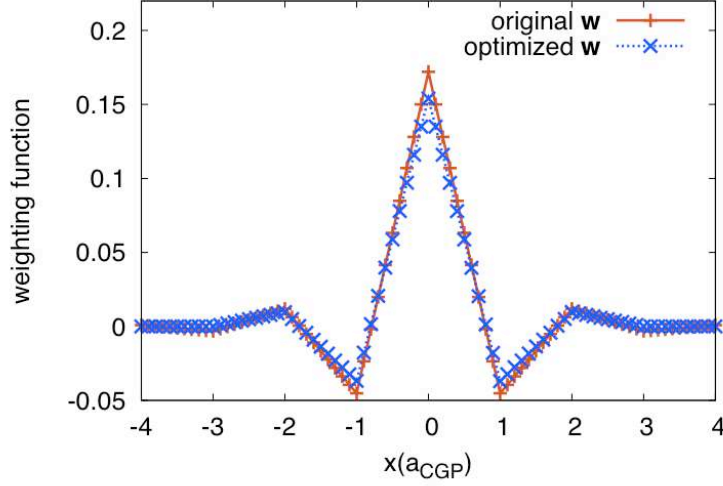


Figure 1. The original weighting function and the optimized weighting function for CG10.

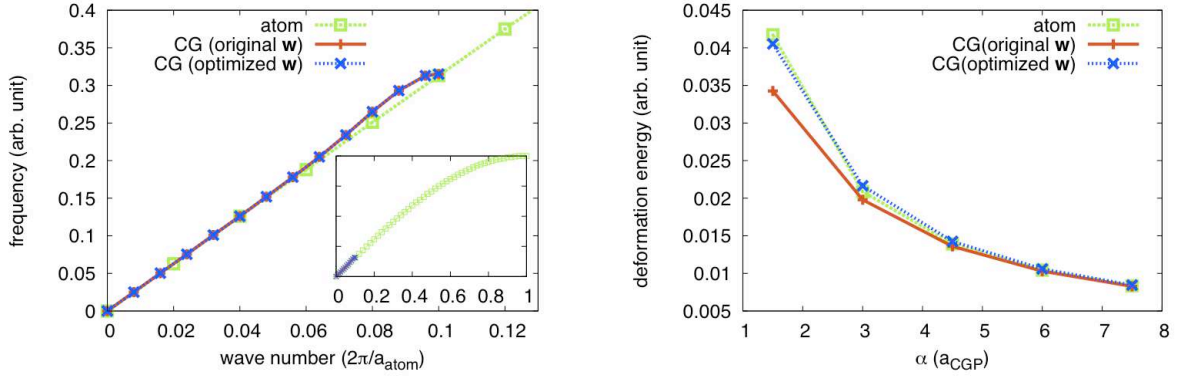


Figure 2. The dispersion relation (left) and the deformation energy (right) of CG10. The displacement is Eqn. (3) for the deformation energy.

4. The finite temperature effects

In the CGP method, the partition function Z_{CGP} is defined. Therefore the forces on the CGP's at finite temperatures can be calculated as the derivative of the free energy. The I -th CGP force is then expressed as

$$F_{\text{CGP}, I} = \frac{1}{\Delta U_I} \left\{ \sum_j^{\text{atom}} \left\langle \left(u_j - \langle u_j \rangle \right) f_{\text{atom}, j} \right\rangle_{T, V, U+\Delta U} - \sum_j^{\text{atom}} \left\langle \left(u_j - \langle u_j \rangle \right) f_{\text{atom}, j} \right\rangle_{T, V, U} \right\}. \quad (4)$$

The CGP forces can be determined by calculating Eqn. (4) with the Monte Carlo method. The force calculation can be performed locally since the averaging is done for the forces and displacements of those atoms relating to the I -th CGP only. Such a locality helps to realize efficient parallel-calculations of the forces; hence, the application to an inhomogeneous system is possible.

As a test, we consider the system of 25 CGP's that is obtained by coarse-graining 1250 Ar atoms (Lennard-Jones pot.) under the periodic boundary condition in 2-dimension. We calculate the force on the 1st CGP through Eqn. (2) and Eqn. (4) when it is displaced by U_{1x} at $T=1\text{K}$ or 30K (Fig. 3). Note that the weighting function is not optimized and the thermal expansion is not considered for simplicity. At $T=1\text{K}$ and small displacement, the two results are almost the same. The effect of anharmonicity is substantial when U_{1x} is larger than $0.2a_{\text{CGP}}$ at $T=1\text{K}$. At $T=30\text{K}$ both anharmonicity and finite temperature effect are observed.

At $T=30\text{K}$ with small displacement, since our Monte Carlo sampling is not enough, thermal fluctuation makes the significant difference between the two results.

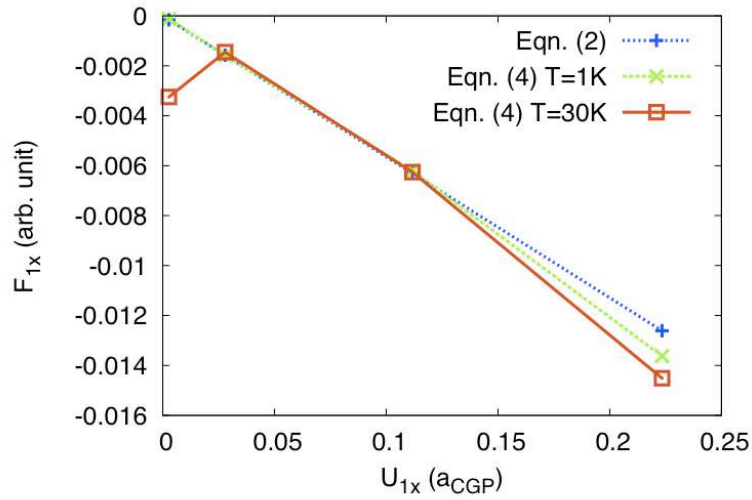


Figure 3. The force of the 1st CGP calculated with various methods.

As explained above, it is now possible to calculate the CGP forces including atomic anharmonicity and finite temperature effects. Making a table of the CGP force at several displacements and temperatures in advance can simulate the coarse-grained dynamics. The simulation runs in this direction are in progress.

References

- [1] R.E. Rudd and J.Q. Broughton, *Phys. Rev. B* **58**, R5893 (1998).
- [2] R. Kobayashi, T. Nakamura, and S. Ogata, *Mat. Trans.* **49**, 2541 (2008).

Hybrid quantum-classical simulation on the Li-graphite intercalation compound

Nobuko Ohba^{1,2,3,*}, Shuji Ogata^{2,3}, Ryo Kobayashi^{2,3},
Shunsuke Yamakawa¹, and Shi-aki Hyodo^{1,3}

¹Toyota Central Research & Development Laboratories, Inc., 41-1 Aza Yokomichi,
Oaza Nagakute, Nagakute-cho, Aichi-gun, Aichi 480-1192, Japan

²Department of Scientific and Engineering Simulation, Graduate School of Engineering,
Nagoya Institute of Technology, Gokiso-Cho, Showa-ku, Nagoya 466-8555, Japan

³CREST, Japan Science and Technology Agency, 4-1-8 Honcho, Kawaguchi, Saitama
332-0012, Japan

*Electronic address: e4606@mosk.tytlabs.co.jp

ABSTRACT

The lithium (Li)-graphite intercalation compounds are put to practical use as a negative electrode of the Li-ion battery. In this material, it is important to understand not only the static electronic structure but also the dynamics of Li simultaneously. We apply originally developed hybrid quantum (QM)-classical (CL) simulation code to analyze diffusion processes of the Li-graphite intercalation compound. The region including the inserted Li and neighboring C atoms is treated with electronic state by the real space density-functional theory (DFT), and this region is embedded in a CL system of the C atoms of graphite based on an empirical interaction model. For inter-layer interaction of graphite, an atomic potential model based on Lennard-Jones potential is originally constructed and added in a CL molecular dynamics calculation of the whole system. Buffered cluster method is adopted to couple the QM and CL boundary. The valence electron density of Li obtained by DFT calculation is almost zero and the Li in graphite layers is considered as Li cation (Li^+). The QM region is adjusted to the movement of Li. The diffusion coefficient calculated by the mean-square-displacement of Li atom in the present hybrid dynamics is in good agreement with experimental one.

1. Introduction

Graphite forms intercalation compounds with some metals or small molecules inserted between its layers. The lithium (Li)-graphite intercalation compound is put to practical use as a negative electrode of a Li-ion battery. In this type of battery, the Li ions can be shuttled between the positive and negative electrode through the non-aqueous electrolyte and separator diaphragm. Basically, the charge-discharge reactions of Li-ion batteries involve the migration of Li ions in the electrode or electrolyte materials, the charge transfer at their insertion into (or extraction from) the host electrodes, and the structural changes of electrodes. The transport properties of Li in the graphite layers especially affect the power performance of Li-ion batteries, and the knowledge of diffusion process is required for the design and optimization of Li-ion batteries. In order to understand the mechanism of Li diffusion in more detail, it is essential to clarify the overall relation between the bonding nature of Li and C atoms of the graphite and its structural change. From the theoretical point of view, the coupled calculation should be progressed in focusing on not only the static properties such as the electronic structure on the Li-graphite intercalation compounds but also the dynamics of Li simultaneously.

Generally, the classical molecular dynamics (MD) simulation based on an empirical atomic interaction potential model for large systems are enabled by using an abundance of computer resources, but cannot handle the chemical reaction such as the formation or scission of chemical bonds. On the other hand, computational efficiency of the first-principles MD technique which treats not only electronic states but also time evolution for atoms is greatly promoted, but a calculation scale is still limited. Further enhancement of the performance of computer is desirable to apply this method to the system of real scale. Following such a situation, hybrid quantum (QM)-classical (CL) simulation schemes attract great interest as one of the calculation method aiming at both large-scale and high accuracy. In this scheme, the reaction region where the electronic structure should be defined is treated by a highly accurate calculation technique such as the density functional theory (DFT), and this region is embedded in a CL system of atoms based on an empirical interaction model. It is expected that we can simulate the realistic large-scale system reproduced the physical phenomenon with our interests by using hybrid scheme.

In this study, we apply originally developed hybrid QM-CL simulation code to analyze diffusion process of the Li-graphite intercalation compounds. The region including the inserted Li and neighboring C atoms is treated with electronic state by the real space DFT. On the other hand, the classical MD method using empirical interatomic potential is provided to the movement of the rest C atoms of graphite. Buffered cluster method [1] is applied for coupling of the QM and CL region.

In Sec. 2, we describe the details of the calculation method using in this study. The results of the electronic state and the diffusion process of the Li in graphite by hybrid QM-CL simulation on Li-graphite intercalation compound are shown in Sec. 3.

2. Calculation Method

2.1 Buffered Cluster Method

In the hybrid QM-CL simulation, the atomic bond is cut at the QM-CL boundary and dangling bond forms. As for this dangling bond, its influence on electronic state or bonding distance of the atoms in QM region should be removed. The link-atom method that uses hydrogen atoms for termination of the QM atoms is usually applied to couple the QM-CL boundary. By using link-atom method, however, there is the case that influence of the surface reconstruction with the relaxation of the boundary atom extends to the atoms of whole system and a large distortion from the original stable structure is produced. In this study, we adopt the buffered cluster method (BCM) [1], which requires no link-atoms and is more precise and a general-purpose model. In the BCM, additional atoms called buffer atoms are put to terminate the dangling bond of QM atoms at QM-CL boundaries. The positions of the buffer atoms are adjusted so as to minimize the potential energy under the constraint of fixing the position of QM atoms for CL calculation of the QM region. In the QM calculation, the positions of the buffer atoms are not relaxed. Therefore various surface reconstructions of the QM cluster region are suppressed in the BCM.

2.2 Quantum mechanical calculation

For the QM calculation, we apply the real space DFT which is easy to accomplish the parallel computation and can set boundary condition arbitrarily. The details of the algorithm are described in Refs.[2,3, and 4]. Troullier-Martins type normconserving pseudopotentials [5] are used for interaction with electrons and the nucleus (ions) and only valence electrons are considered. The generalized gradient approximation (GGA) formula introduced by Perdew, Burke, and Ernzerhof [6] is applied to the exchange-correlation energy term. The Kohn-Sham

orbitals and Hartree potential are represented with a value on the Cartesian mesh points in real space coordinates. The second order derivatives of orbitals are approximated by the fourth-order finite-difference method [7]. Data on the mesh points are divided in the small domain and stored every computation node in order to calculate on a parallel computation fast. The multi-grid method [8] is employed for acceleration of convergence of the long-wavelength components of the wave function on the mesh points. The grid spacing, h , is set to be 0.55 a.u. This is converted into the cutoff energy for plane waves to expand the wave functions of $(\pi/h)^2 \sim 33\text{Ry}$. In addition, the dense grid spacing ($h/3$) around atoms is used for the rapidly varying pseudopotentials.

To avoid increasing of the computational cost in the case of a large QM region, the order- N computational technique adopted the approach of the divide and conquer method is developed. Here we introduce the Kohn-Sham Hamiltonian added the interaction between the regions as corrections for a high degree of accuracy, which is provided by performing a derivative of total energy of all system with respect to the charge density of each region.

2.3 Classical molecular dynamics

The classical MD calculation is performed under the periodic boundary condition for whole system and with the Velocity Verlet algorithm to integrate Newton's equations of motion. Brenner type [9] of interatomic potential for C atoms of graphite is provided. In the Brenner type potential, the cut-off distance of the interaction is set to be 2.0\AA . Although only the interaction between the nearest neighbors of atom within basal planes is considered, the inter-layer interaction is not taken in. Therefore following atomic potential model V_{vdw} is originally constructed and added in a classical MD calculation of the whole system;

$$V_{\text{vdw}}(r) = 4\epsilon \left\{ \left(\frac{\sigma}{r} \right)^{12} - g(Z) \left(\frac{\sigma}{r} \right)^6 \right\} f(r) \quad . \quad (1)$$

The basic form of this model is Lennard-Jones potential, and r shows a distance between two atoms in different layers. $f(r)$ is a cut-off function of the suitable form so that a value at a long distance smoothly becomes zero. We introduce parameter Z which expresses a difference of AA- and AB- stacking structure, and $g(Z)$ of AA-stacking is smaller than that of AB-type.

3. Results

Firstly, we set QM regions of various shapes and sizes which are considerably important in calculation for the Li-graphite intercalation compound. We confirm that the crystal structure is sufficiently stable and there is no unreasonable distortion in the QM-CL boundary. Furthermore, we check that the hybrid QM-CL simulation adopted in this study gives good convergence of total energy of the QM-CL hybrid system during time evolution.

Next, we show the charge density distribution of a valence electron provided by the QM calculation in Fig.1. The bonding nature between Li-C which is not considered in the classical MD calculation is able to be known by setting QM region including Li atom. In addition, since the valence electron density around the Li atom becomes almost zero, the Li has positive charge and the C atoms of graphite have negative charge as the result of charge transfer form Li to C atoms.

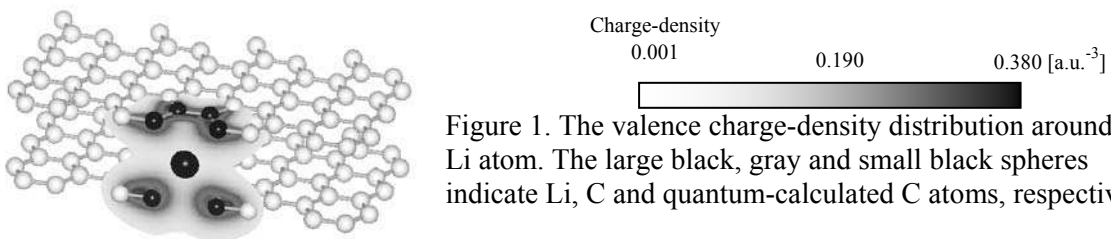


Figure 1. The valence charge-density distribution around the Li atom. The large black, gray and small black spheres indicate Li, C and quantum-calculated C atoms, respectively.

It is necessary to adapt a QM region following the movement of the Li so that the diffusion process of Li in graphite is investigated by the hybrid calculation. Therefore, we examine desirable size of QM region in which so that the forces on the C atoms are smoothly connected at the time of the renewal of the QM region. As a result, about 24 C atoms in each top and bottom of the Li atom should be set as the QM region in order to get rid of influence with the renewal of the QM region.

A snapshot of Li diffusion process provided from a hybrid calculation is depicted in Fig. 2. The layer where Li is inserted in is set to be AA-stacking structure, and other layers are set to be AB-stacking. The motion of Li atom is tempted by that of the graphite C atoms, and tends to become slow when the movement of the C atoms calms down. The diffusion coefficient calculated by the mean-square-displacement of Li atom in the present hybrid dynamics is $7 \times 10^{-5} \text{ cm}^2/\text{sec}$, which is in good agreement with experimental one reported the values of order of $10^{-5} \text{ cm}^2/\text{sec}$ [10] for the dilute stage 1 phase. In the case that we do not consider the inter-layer interaction of graphite, the calculated diffusion coefficient is ten times larger than that with the inter-layer interaction, so it is confirmed that the effect of the inter-layer interaction is important for the diffusion process in the Li-graphite intercalation compound.

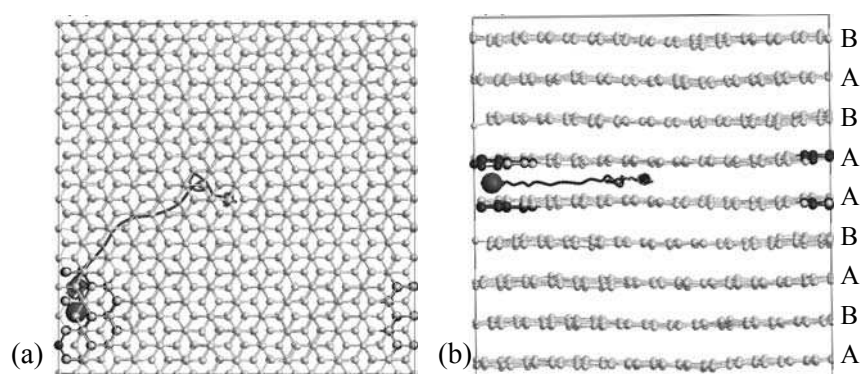


Figure 2. The snapshot in the Li diffusion process by the hybrid calculation. The large black, gray and small black spheres indicate Li, C and QM-calculated C atoms, respectively. The line expresses the trajectory of the Li atom. (a) Top view. (b) Side view. The letters of 'A' or 'B' denote the stacking structure of graphite.

Acknowledgements

We wish to thank Dr. T. Tamura for helpful discussions.

References

- [1] S. Ogata, Phys. Rev. B **72**, 045348 (2005).
- [2] S. Ogata, E. Lidorikis, F. Shimojo, A. Nakano, P. Vashishta, and R. K. Kalia, Comput. Phys. Commun. **138**, 143 (2001).
- [3] S. Ogata, F. Shimojo, R. K. Kalia, A. Nakano, and P. Vashishta, Comput. Phys. Commun. **149**, 30 (2002).
- [4] F. Shimojo, T. J. Campbell, R. K. Kalia, A. Nakano, S. Ogata, P. Vashishta, and K. Tsuruta, Future Gen. Comp. Sys. **17**, 279 (2000).
- [5] N. Troullier and J. L. Martins, Phy. Rev. B **43**, 1993 (1991).
- [6] J. P. Perdew, K. Burke, and M. Ernzerhof, Phy. Rev. Lett. **77**, 3865 (1996).
- [7] J. R. Chelikowsky, N. Troullier, and Y. Saad, Phys. Rev. Lett. **72**, 1240 (1994).
- [8] A. Brandt, Math. Comput. **31**, 333 (1977).
- [9] D.W. Brenner, Phys. Rev. B **42**, 9458 (1990); **46**, 1948(E) (1992).
- [10] A. Funabiki, M. Inaba, Z. Ogumi, S. Yuasa, J. Otsuli, and A. Tasaka, J. Electrochem. Soc., **145**, 172 (1998).

Atomistic/Continuum Hybrid Models: Ghost Forces and Consistency

C. Ortner¹, A. Shapeev², H. Wang¹, and L. Zhang¹

¹ Mathematical Institute, University of Oxford, 24—29 St. Giles', Oxford OX1 3LB, UK
ortner@maths.ox.ac.uk

² EPFL, SB-IACS-ANMC, Station 8, CH-1015, Lausanne, Switzerland

Low energy equilibria of crystalline materials are typically characterised by localized defects that interact with their environment through long-range elastic fields. By coupling atomistic models of the defects with continuum models for the elastic far field one can, in principle, obtain models with near-atomistic accuracy at significantly reduced computational cost. However, several pitfalls need to be overcome to find a reliable coupling mechanism.

Possibly the most widely discussed among these pitfalls are the so-called “ghost forces” that typically arise in energy-based atomistic/continuum coupling mechanisms. In this talk I will discuss the construction and analysis of energy-based atomistic/continuum coupling methods with and without ghost forces, and particularly focus on understanding the resulting model errors. To this end I will first review some results on one-dimensional model problems and then describe some recent developments in higher dimensions. Using a new notion of “atomistic stress” I will show that, in 1D, absence of ghost forces does imply “high accuracy” of the coupling scheme but that in 2D/3D this is less clear.

A novel multiscale method for atomic–continuum coupling with continuity of both field function and corresponding 1st-order differential

Venkataraman P¹, Hua Li and T Y Ng

¹ School of Mechanical and Aerospace Engineering,
Nanyang Technological University,
50 Nanyang Avenue, Singapore 639798, Republic of Singapore
E-mail: venk0013@ntu.edu.sg

ABSTRACT

A novel multiscale numerical method is presented for the concurrent coupling of microscopic and macroscopic dimensions. The proposed multiscale method employs the molecular dynamics method for atomic level simulation and the meshless Hermite-cloud method for continuum level simulation. One of the advantages of the Hermite-cloud method is its capability of analyzing both the field function and corresponding first-order differential simultaneously. The method is a strong-form technique based on the reproducing kernel particle approach, and is truly meshless in nature as it does not require any kind of background mesh for integration. The seamless coupling algorithm, based on the Schwarz alternating scheme, provides the accurate interface between the continuum and atomic domains, by ensuring the compatibility conditions. The developed multiscale numerical method is validated through numerical examples, and the results show that the present method is accurate, efficient, robust and simple to implement, with a wide application potential.

Keywords: multiscale model, concurrent coupling, molecular dynamics, meshless method, transition region, Hermite scheme.

1. Introduction

Most engineering problems are governed by processes occurring across multiple time and length scales. The inherent limitations associated with mono scale approaches such as molecular dynamics or ab-initio methods for solving such problems, have led to an increased focus on the development of multiscale simulation methods [1]. In Multiscale problems such as crack propagation or nano-indentation, the computational domain of the problem is divided into atomic and continuum sub-domains and the transition domain bridges them together. The atomic domain is restricted to the localized region where atomic physics dominates. This make it computationally feasible to study problems over larger length scales and also results in better computational efficiency, as the computational power is mainly deployed to the region where it is most needed. The main objective of this paper is to propose a novel multiscale model to couple atomic and continuum domain. The Hermite-Cloud method used in the continuum domain is a strong-form technique that uses the point collocation approach for the discretization of the governing PDE, thus eliminating the need for any background mesh. The coupling algorithm uses the alternating Schwarz method [2] to ensure the compatibility of both the field variable and the corresponding first-order derivative across the overlapping transition region. The classical wave propagation problem in one space dimension is used to demonstrate the capability of the handshaking algorithm, in coupling both length and time scales.

2. Discretization of Atomic and Continuum Domains

In the proposed multiscale model, molecular dynamics (MD) method is used in the atomistic domain. MD method is a deterministic approach to solve a many-body problem comprising of interacting atoms. In this work, the atomic domain is modeled as a spring mass system governed by the harmonic potential $U(r_{ij}) = \frac{1}{2}k(r_{ij} - r_0)^2$, where k is the spring stiffness, r_{ij} the inter-atomic distance between the atoms r_i and r_j , and r_0 is the equilibrium bond distance. The force between the atoms is obtained as the negative derivative of this potential function with respect to the inter-atomic distance r_{ij} . The dynamic trajectories of the atoms, defined by the atomic position and momentum, are obtained by integrating the Newton's equation of motion using an appropriate integration scheme.

The continuum domain is discretized using the meshless Hermite-Cloud method, which is the is discussed in detail in [3]. This method uses the classical reproducing kernel particle method, the point collocation technique and the Hermite interpolation theorem to obtain an approximate solution for both the field variable and its corresponding first-order derivative. In the Hermite cloud method, the approximate solution $f^h(x)$ of a one-dimensional function

$f(x)$ is constructed as $f^h(x) = \sum_{n=1}^{NT} N_n(x) f_n + \sum_{m=1}^{NP} \left(x - \sum_{n=1}^{NT} N_n(x) x_n \right) M_m(x) f_{xm}$, Where NP and

NT are the total number of scattered points in the domain, and $N_n(x)$ and $M_m(x)$ are the shape function for the function $f(x)$ and its first-order derivative $f_x(x)$ respectively, defined at the n^{th} node. The first-order derivatives of the unknown function $f_x(x)$ are approximated

in a similar fashion as $f_x^h(x) = \sum_{m=1}^{NP} M_m(x) f_{xm}$. Auxiliary conditions are introduced to handle

the additional unknown $f_x(x)$, which are obtained by taking partial derivatives of the approximate solution. The governing PDE system is discretized using the point collocation method. The approximate solutions are substituted into the discretized form of the PDE and combined with the auxiliary conditions resulting in a set of algebraic equations corresponding to the unknown variables f_i and f_{xi} , which are then assembled into a matrix form and solved using any of the direct or iterative solvers..

3. Coupling Algorithm

The main objective of the handshaking/coupling algorithm is to ensure compatibility between the atomic and continuum domains. The multiscale algorithm in this paper uses the well known Schwarz method for overlapping sub-domains, ensuring compatibility of both the field variable and its first-order derivative, between the atomic and continuum domains. To solve the partial differential boundary value problem defined over the domain Ω , the problem domain is divided into atomic and continuum sub-domains Ω^a and Ω^c such that $\Omega = \Omega^a \cup \Omega^c$, with subscripts a and c referring to the atomic and continuum domains respectively. The atomic domain is restricted to the zone where a detailed description is required and the continuum description is used elsewhere. The transition region, where the atomic and continuum domains overlap, contains both atoms and meshless nodes. The boundary value problem is now solved using the Schwarz method as follows. The continuum sub-domain is solved first with the boundary conditions enforced along the transition and continuum boundaries. The results of the continuum simulation containing the field variable and the first-order derivative information is then used to generate the necessary boundary

conditions for the solving the problem over the atomic sub-domain, through interpolation. Next, the atomic sub-domain is solved separately by enforcing the necessary boundary conditions along transition and atomic domain boundaries. The field variable values at the atomic locations in the transition region are obtained from the continuum simulation through interpolation. From the results of the atomistic simulation, the field variable values at all the nodal locations in the transition domain are updated and the continuum simulation is repeated. The procedure is repeated iteratively until the solution converges. Convergence check is done ensured by checking if the norm of the field variable values in the transition region over two successive iterations is below a certain acceptable error tolerance or $\|f_{k+1} - f_k\|_2 \leq \delta$, where f_{k+1} and f_k are the field variable values in the transition domain Ω' , and δ is the error tolerance. The subscripts k and $k+1$ refer to the iterations at the previous and current steps respectively.

An interpolation function is required to facilitate information exchange between nodes and atoms in the transition domain, during the transfer of boundary conditions. With both the field variable and the first-order derivative information available, we construct a Hermite interpolation polynomial to transfer information between nodes and atoms. For the transfer of information from the atoms to nodes, following an atomistic simulation, we make use of the Lagrange interpolation polynomials as the derivative information is not available in this case. The interpolation polynomial are used to evaluate the field variable value at any atomic or nodal location in the transition region. The major advantage of using interpolation polynomials, for transferring information between the nodes and atoms and vice versa is that the atoms and nodes need not be coincident in the transition domain. In other words, the continuum points need not be graded down to coincide with their corresponding atomic points in the transition domain permitting more freedom in the distributions.

4. Numerical Example

The multiscale model is validated by solving a benchmark test problem. In the numerical example presented, the atomic and continuum domains are respectively modeled using the harmonic potential and the Hermite-Cloud method, discussed in Section 2. The numerical accuracy of the multiscale model is measured using the global and relative error measures defined in [3] and [4]. The classical one-dimensional wave propagation problem over an infinite domain [5] is considered for validating the multiscale model.

The computational model for this problem is shown in Fig. 1, with the atomic domain positioned at the center, the continuum domain at either side and the transition domain at the overlapping regions. The problem is solved with 82 nodes and 301 atoms with an average nodal and atomic spacing of 0.1 and 0.02 units, respectively. The problem is solved using the coupling algorithm discussed in section 3. To account for the different time scales in the continuum and atomic simulation, the time step in the continuum domain is chosen as a multiple of the atomic time step. In the current problem a time step of $\Delta t = 0.01$ is used in the continuum domain with a multiplication factor of 5. Time integration in the atomic and continuum domains is carried out using the Leap frog and Newmark integration schemes, respectively.

The simulation is run for 360 time steps corresponding to $t = 3.6$ units in the continuum domain. Fig. 2 shows four snap shots of the analytical and numerical solution of the normalized displacements at the beginning of the simulation and after every 120 time steps. As the wave is symmetrical about the origin, the results are plotted only for half of the computational domain. The results of the multiscale simulation are compared with the analytical solution using the global errors measure within every time step. It is observed from

Fig. 2 that the results of the multiscale simulation correspond well with the analytical solution. The maximum global error observed during the entire simulation is 3.28%. It is also observed that the wave is able to propagate through the transition domain into the continuum region, except for a few perturbations observed in the numerical solution, which are due to the reflection of the wave as it passes from the atomic domain into the continuum region.

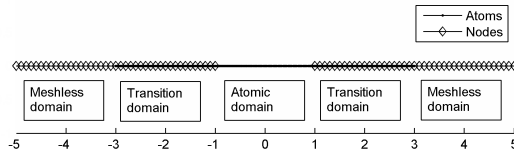


Figure 1. Computational model for 1-D dynamic problem

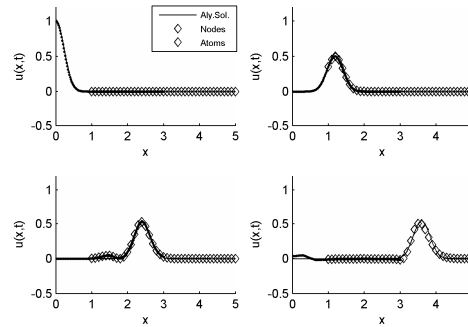


Figure 2. Snapshots of the analytical and multiscale simulation results at different time instances for 1-D wave propagation problem

5. Conclusion

A novel multiscale numerical scheme is developed in this paper to couple the atomic and continuum domains based on the alternating Schwarz scheme. The highlight of the current method is its simplicity, which eliminates the need for complex mesh generation activity in the continuum domain. The use of interpolation functions in the transition region also permits independent control over the distributions of atoms and nodes in the atomic and continuum domains, respectively. The capability of the method in coupling both time and lengths scales is further validated through transient wave propagation problems one space dimension. In conclusion, the present multiscale method fulfills its objective of providing accurate results at a reduced computational expense by employing multiple time/length scales, while ensuring a seamless interface between the two domains.

References

1. Ronald EM and Tadmor EB (2009) A unified framework and performance benchmark of fourteen multiscale atomistic/continuum coupling methods. *Modelling and Simulation in Materials Science and Engineering* 17: 053001
2. Alfio Quarteroni AV (2005) *Domain Decomposition Methods for Partial Differential Equations* Oxford Science Publications
3. Li H, Ng TY, Cheng JQ and Lam KY (2003) Hermite–Cloud: a novel true meshless method. *Computational Mechanics* 33: 30-41
4. Gu YT and Zhang LC (2006) A Concurrent Multiscale Method Based on the Meshfree Method and Molecular Dynamics Analysis. *Multiscale Modeling & Simulation* 5: 1128-1155
5. Gockenbach MS (2002) *Partial Differential Equations: Analytical and Numerical methods* Society for Industrial and Applied Mathematics

Title: Model of Topological Changes in Discrete Dislocation Dynamics

Authors: Petr Pauš¹, Michal Beneš¹, Jan Kratochvíl²

Affiliations: ¹Department of Mathematics, Faculty of Nuclear Sciences and Physical Engineering, Czech Technical University in Prague, Trojanova 13, Prague, Czech Republic, petr.paus, michal.benes@fjfi.cvut.cz; ²Department of Physics, Faculty of Civil Engineering, Czech Technical University in Prague, Thákurova 7, Prague, Czech Republic, kratochvil@fsv.cvut.cz

ABSTRACT

This contribution deals with the numerical simulation of dislocation dynamics, their interaction, merging and other changes in the dislocation topology. The glide dislocations are represented by parametrically described curves moving in gliding planes. The simulation model is based on the numerical solution of the dislocation motion law belonging to the class of curvature driven curve dynamics. Mutual forces between dislocations are incorporated in the model. We focus on the simulation of the cross-slip of two dislocation curves where each curve evolves in a different gliding plane and after applying certain stress, the curves may merge. The simulation of the Frank-Read source of dislocations which describes how new dislocations are created is also presented. Merging and splitting of multiple (more than two) dislocation curves in persistent slip bands and their interactions in channels of the bands are also simulated.

1. Introduction

The dislocations are defined as irregularities or errors in crystal structure of the material. The presence of dislocations strongly influences many of material properties. Plastic deformation in crystalline solids is carried by dislocations. Theoretical description of dislocations is widely provided in literature such as^{5,6,11}. Dislocation is a line defect of the crystalline lattice. Along the dislocation curve the regularity of the crystallographic arrangement of atoms is disturbed. The dislocation can be represented by a curve closed inside the crystal or by a curve ending on the surface of the crystal. At low homologous temperatures the dislocations can move only along crystallographic planes (gliding planes) with the highest density of atoms. The motion results in mutual slipping of neighboring parts of the crystal along the gliding planes.

This justifies the importance of developing suitable mathematical models^{10,13,2,7}. From the mathematical point of view, the dislocations can be represented by smooth closed or open plane curves which evolve in time. Their motion is two-dimensional as they move in glide planes. The evolving curves can be mathematically described in several ways. One possibility is to use the *level-set method*^{12,15,4}, where the curve is defined by the zero level of some surface function. One can also use the *phase-field method*¹.

2. Dislocations and mean curvature flow

The interaction of dislocations and bulk elastic field can be approximately described using the curvature flow as follows (see¹⁴). We consider perfect dislocation curves with the Burgers vector $\vec{b} = (b, 0, 0)$ oriented in the x -direction of the x, y, z coordinate system. The dislocation curve motion Γ is located in a glide plane, in our case in the xz -plane. The glide of dislocation is

governed by the relaxation law in the form of the mean curvature flow equation in the direction of the normal vector

$$Bv = L\kappa + b\tau_{app}, \quad (1)$$

where B is a drag coefficient, and $v(x, t)$ is the normal velocity of a dislocation at $x \in \Gamma$ and time t . The term $L\kappa$ represents self-force expressed in the line tension approximation as the product of the line tension L and local curvature $\kappa(x, t)$. The term τ_{app} represents the local shear stress acting on the dislocation segment produced by the bulk elastic field. In our simulations, we consider “stress controlled regime” where the applied stress in the channel is kept uniform. This is an upper bound limit case. The other limiting case is “strain controlled regime” as described in⁷. The applied stress τ_{app} is the same in every point of the line and for numerical computations we use $\tau_{app} = const.$

3. Parametric description

The motion law (1) in the case of dislocation dynamics is treated by parametrization where the planar curve $\Gamma(t)$ is described by a smooth time-dependent vector function $X : S \times I \rightarrow \mathbb{R}^2$, where $S = [0, 1]$ is a fixed interval for the curve parameter and $I = [0, T]$ is the time interval. The curve $\Gamma(t)$ is then given as the set $\Gamma(t) = \{X(u, t) = (X^1(u, t), X^2(u, t)), u \in S\}$.

The evolution law (1) is transformed into the parametric form as follows. The unit tangential vector \vec{T} is defined as $\vec{T} = \partial_u X / |\partial_u X|$. The unit normal vector \vec{N} is perpendicular to the tangential vector and $\vec{N} \cdot \vec{T} = 0$ holds. The curvature κ is defined as

$$\kappa = \frac{\partial_u X^\perp}{|\partial_u X|} \cdot \frac{\partial_{uu} X}{|\partial_u X|^2} = \vec{N} \cdot \frac{\partial_{uu} X}{|\partial_u X|^2},$$

where X^\perp is a vector perpendicular to X . The normal velocity v is defined as the time derivative of X projected into the normal direction, $v = \partial_t X \cdot \partial_u X^\perp / |\partial_u X|$. The equation (1) can now be written as

$$B\partial_t X \cdot \frac{\partial_u X^\perp}{|\partial_u X|} = L \frac{\partial_{uu} X}{|\partial_u X|^2} \cdot \frac{\partial_u X^\perp}{|\partial_u X|} + b\tau_{app},$$

which holds provided the vectorial evolution law is satisfied

$$B\partial_t X = L \frac{\partial_{uu} X}{|\partial_u X|^2} + b\tau_{app} \frac{\partial_u X^\perp}{|\partial_u X|}. \quad (2)$$

This equation is accompanied by the periodic boundary conditions for closed curves, or by fixed-end boundary condition for open curves, and by the initial condition. These conditions are considered similarly as in³. For long time computations with time and space variable force, the algorithm for curvature adjusted tangential velocity is used. Details are described in¹⁶. To incorporate a tangential redistribution, a tangential term α has to be added to the equation (2).

$$B\partial_t X = L \frac{\partial_{uu} X}{|\partial_u X|^2} + L\alpha \frac{\partial_u X}{|\partial_u X|} + b\tau_{app} \frac{\partial_u X^\perp}{|\partial_u X|}. \quad (3)$$

For numerical approximation we consider a regularized form of (3). The equation is then solved by means of matrix factorization. Since there are two components of X , two linear systems are solved in each timestep.

4. Application in dislocation dynamics

Dislocation curves as defects in material evolve in time. The dislocation evolution history contains shape changes of open curves, closing of open dislocation curves up to collision of dipolar loops (see¹¹). Interaction of dislocation curves and dipolar loops has been studied, e.g., in^{10,7}. Our numerical simulations were performed under the following set of parameters:

Burgers vector magnitude	$b = 0.25 \text{ nm}$
Line tension	$L = 2 \text{ nN}$
Drag coefficient	$B = 1.0 \cdot 10^{-5} \text{ Pa} \cdot \text{s}$
Applied stress	$\tau_{app} = 40 \text{ MPa}$

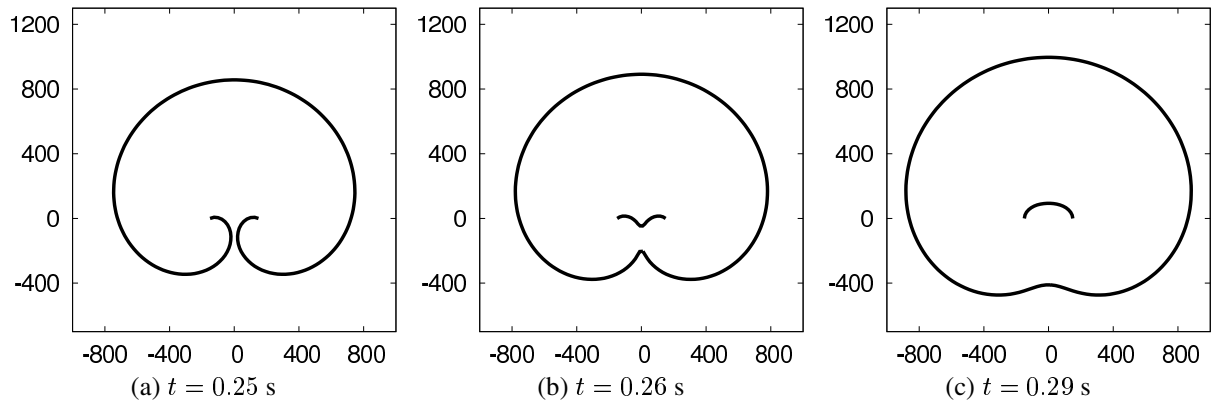


Figure 1: Frank-Read source, $\tau_{app} = 40 \text{ MPa}$, $t \in (0, 0.29)$, curve discretized by $M = 400$ nodes.

The example in Fig. 1 shows the simulation of the Frank-Read mechanism (see^{5,11}) which describes how new dislocation loops are created. The open dislocation curve is fixed at $[-150 \text{ nm}, 0 \text{ nm}]$ and $[150 \text{ nm}, 0 \text{ nm}]$, and is forced to evolve under the applied stress $\tau_{app} = 40 \text{ MPa}$. The evolution continues until it touches itself. At this moment, the curve splits into two parts, i.e., the dipolar loop and the dislocation line. The loop continues in expansion. The dislocation line will again undergo the same process. The Frank-Read source cannot generate unlimited number of dislocation loops because new loops interact with each other and slow down the source. The source can usually generate about 300 or 400 of dipolar loops. Parameters of the simulation are $t \in (0, 0.29)$, $M = 400$.

5. Conclusion

The simulation of dislocation dynamics is important in practice as dislocations affect many material properties. Dislocation dynamics can be mathematically modelled by the mean curvature flow. We presented a method based on a parametric approach. We applied the model to situations similar to the real context including a mechanism of creating new dislocations (i.e., Frank-Read source, cross-slip, etc.). The scheme had to be improved by an algorithm for tangential redistribution of points and by an algorithm for topological changes for parametric model.

References

- [1] Beneš, M.: Phase field model of microstructure growth in solidification of pure substances. *Acta Math. Univ. Comenianae* 70, 123–151 (2001)
- [2] Beneš, M., Kratochvíl, J., Křišťan, J., Minárik, V., Pauš, P.: A Parametric Simulation Method for Discrete Dislocation Dynamics. *European Journal of Physics* (submitted)
- [3] Deckelnick, K., Dziuk, G.: Mean curvature flow and related topics. *Frontiers in numerical analysis*, 63–108 (2002)
- [4] Dziuk, G., Schmidt, A., Brillard, A., Bandle, C.: Course on mean curvature flow. Manuscript 75p., Freiburg (1994)
- [5] Hirth, J.P., Lothe, J.: *Theory of Dislocations*. John Willey, New York (1982)
- [6] Kroupa F.: Long-range elastic field of semi-infinite dislocation dipole and of dislocation jog. *Phys. Status Solidi* 9, 27–32 (1965)
- [7] Křišťan, J., Kratochvíl, J., Minárik V., Beneš M.: Simulation of interacting dislocations glide in a channel of a persistent slip band. In: *Modeling and Simulation in Materials Science and Engineering* 17 (2009)
- [8] Mikula, K., Ševčovič, D.: Evolution of plane curves driven by a nonlinear function of curvature and anisotropy. *SIAM J. Appl. Math.* Vol. 61 No. 5, 1473–1501 (2001)
- [9] Mikula, K., Ševčovič, D.: Computational and qualitative aspects of evolution of curves driven by curvature and external force. *Computing and Visualization in Science* Vol. 6 No. 4, 211–225 (2004)
- [10] Minárik, V., Beneš, M., Kratochvíl, J.: Simulation of Dynamical Interaction between Dislocations and Dipolar Loops. *J. Appl. Physics* (accepted)
- [11] Mura, T.: *Micromechanics of Defects in Solids*. Springer (1987)
- [12] Osher, S., Fedkiw, R.P.: *Level set methods and dynamic implicit surfaces*. Springer, New York (2003)
- [13] Pauš, P., Beneš, M.: Direct approach to mean-curvature flow with topological changes, to appear in *Kybernetika* (2009)
- [14] Sedláček, R.: Viscous glide of a curved dislocation. In: *Philosophical Magazine Letters*, 76(4): pp. 275–280 (1997)
- [15] Sethian, J.A. : *Level set methods and fast marching methods*. Cambridge University Press, Cambridge (1999)
- [16] Ševčovič, D., Yazaki, S.: On a motion of plane curves with a curvature adjusted tangential velocity. In: <http://www.iam.fmph.uniba.sk/institute/sevcovic/papers/cl39.pdf>, arXiv:0711.2568, 2007.

Acknowledgements

This work was partly supported by the project MSM No. 6840770100 “Applied Mathematics in Technical and Physical Sciences” and by the project No. LC06052 “Nečas Center for Mathematical Modelling” of the Ministry of Education, Youth and Sport of the Czech Republic.

Non-stationary moving dislocations: from core equations to an equation of motion

Yves-Patrick Pellegrini¹

¹CEA, DAM, DIF, F-91297 Arpajon, France.
Email: yves-patrick.pellegrini@cea.fr

This talk revisits some of the concepts put forward by Eshelby in a landmark paper [1] to address dynamic dislocation problems. I will first present the derivation by means of Mura's eigenstrain method, of dynamic generalizations of the Peierls-Nabarro equation for dislocations cores of screw or edge dislocations. The resulting equations are of integrodifferential nature, with a nonlocal kernel in space and time. That for the edge involves in addition a convolution with the second spatial derivative of the displacement jump function. These equations correctly reduce, in the stationary limit, to Weertman's equations that extend the static Peierls-Nabarro model to finite constant velocities [2].

Next, building on another idea in Ref. [1], these dynamic core equations are used to derive a dynamic equation of motion for screw and edges, that constitutes the rigorous counterpart of an approximate equation of motion recently proposed for moderate velocities by Pillon et al. [3] on a phenomenological basis. The new equation, of simple structure, is non-local in time and has a relatively transparent structure, solely determined by known energy functions computed *at constant velocity*. It encompasses subsonic and transonic velocity regimes, accelerated or not. In special limits, known results are retrieved, including Rosakis' Model 1 for the equation of motion of a stationary dislocation with viscous drag [4]. Among new results, the frequency-dependent mass of an *edge* dislocation oscillating at moderate velocity is obtained while that of the screw dislocation, known already, is retrieved [5].

References:

- [1] J.D. Eshelby, Phys. Rev. 90, 248-255 (1953). *The equation of motion of a dislocation.*
- [2] Y.-P. Pellegrini, Phys. Rev. B 81, 024101 (2010). *Dynamic Peierls-Nabarro equations for elastically isotropic crystals.*
- [3] L. Pillon, C. Denoual, Y.P. Pellegrini, Phys. Rev. B 76, 224105 (2007). *Equation of motion for dislocations with inertial effects.*
- [4] P. Rosakis, Phys. Rev. Lett. 86, 95-98 (2001). *Supersonic dislocation kinetics from an augmented Peierls model.*
- [5] Y.-P. Pellegrini, preprint arXiv :1003.5198. *Screw and Edge dislocations with time-dependent core width: from core equations to an equation of motion (submitted).*

Keywords : Dislocation dynamics, Equation of motion, Peierls-Nabarro model, Plasticity.

Theory and Molecular Dynamics Modeling of Spall Fracture in Liquids

**Vasily V. Pisarev, Alexey Yu. Kuksin, Genri E. Norman, Vladimir V. Stegailov
and Alexey V. Yanilkin**

Joint Institute for High Temperatures of RAS, 13 bldg. 2 Izhorskaya str., Moscow, 125412,
Russia
Moscow Institute for Physics and Technology, 9 Institutskiy per., Dolgoprudnyy, Moscow
region, 141700, Russia.

The model of fracture of liquid under tension is developed from the results of molecular dynamics (MD) calculations of void nucleation and growth rates. The model is based on the "nucleation-and-growth" (NAG) approach introduced initially by D. Curran, L. Seaman and D. Shockey. The fracture under dynamic loading is considered, when homogeneous void nucleation is relevant. The model derives the kinetics of fracture at mesoscale from the kinetics of elementary processes of void nucleation and growth in metastable liquid. The properties of highly metastable liquid are studied in MD simulations with Lennard-Jones interatomic potential.

Surface tension and viscosity of Lennard-Jones liquid are calculated to estimate the void nucleation rate using the classical nucleation theory and to obtain the void growth kinetic using hydrodynamics. The dependencies of nucleation rate and growth kinetics on pressure and temperature are also obtained from MD simulations.

The correspondence between our results on nucleation rate and predictions of the classical nucleation theory are discussed. The growth of nanometer-size voids is shown to be well described by the Rayleigh-Plesset equation.

The fracture model is applied to the estimation of spall strength of liquid. The calculations of void size distribution by the proposed kinetic model are in agreement with the distributions obtained in direct large scale MD simulations (64 million atoms). The spall strength evaluated by the model is in good agreement with the experimental data (shock wave tests on hexane) and direct MD simulations.

Reweighting the path ensemble in transition path sampling

Jutta Rogal¹, Wolfgang Lechner², Jarek Juraszek³, Bernd Ensing² and Peter G. Bolhuis²

¹Interdisciplinary Centre for Advanced Materials Simulation
Ruhr-Universität Bochum, 44780 Bochum, Germany
email: jutta.rogal@rub.de

²van't Hoff Institute for Molecular Sciences, University of Amsterdam
Nieuwe Achtergracht 166, 1018WV Amsterdam, The Netherlands

³Computational Biophysics, Spanish National Research Centre
Melchor Fernandez Almagro 3, 28029 Madrid, Spain

Sampling rare events in complex, high dimensional systems, such as crystal nucleation, protein folding and chemical reactions, remains a challenge for computational studies. Employing regular all-atom molecular dynamics (MD) simulations with a time step of a few femtoseconds becomes quickly unfeasible as the system tends to spend most of the time in a stable state hardly sampling the transition barrier regions of the phase space. Yet, these rare events dominate the dynamical behaviour over an extended time scale.

Among other approaches, transition path sampling (TPS) provides a possibility to explore transitions between stable states in rare event systems. One of the key advantages in TPS is that an a priori definition of a reaction coordinate is not required. In addition, since the dynamics used in TPS correspond to the actual underlying physical dynamics, the true kinetic mechanism is sampled. Transition interface sampling (TIS), a variant of TPS, has been developed to improve the calculation of rate constants by introducing a number of interfaces along a certain order parameter, through which the positive effective flux can be measured.

Here we introduce a reweighting scheme for the path ensembles within the TIS framework. Once the sampling has been performed in the biased TIS ensemble, the reweighting allows for the analysis of free energy landscapes and committor projections in an arbitrary order parameter space. In addition we suggest that the reweighted path ensemble can be used to optimize possible non-linear reaction coordinates.

Multiscale Methods with Application to Wave Propagation in Heterogeneous Materials

Olof Runborg

KTH
Lindstedsv 3, 10044 Stockholm, Sweden
olofr@nada.kth.se

We discuss the heterogeneous multiscale method framework for multiscale problems. As an application we consider the wave equation in a medium with a rapidly varying speed of propagation. We construct a multiscale scheme which can compute the correct coarse behavior of wave pulses traveling in the medium, at a computational cost essentially independent of the size of the small scale variations. This is verified by theoretical results and numerical examples. We also consider the long time case where macroscopic dispersive effects originating from the microstructure appear.

The Hall-Petch effect in nanocrystalline materials – a phase-field-crystal approach

Axel Voigt¹, Rainer Backofen¹, Francisco Bernal¹ and Roland Gärtner¹

¹Department of Mathematics, TU Dresden, 01062 Dresden, Germany,
axel.voigt@tu-dresden.de, rainer.backofen@tu-dresden.de,
francisco.bernal@tu-dresden.de, roland.gaertner@tu-dresden.de

The successful application of nanocrystalline materials in industrial applications requires a detailed knowledge of mechanical properties and understanding of deformation behaviour. On a microcrystalline level the hardness and yield strength of the material typically increases with the decreasing grain size, a phenomenon known as the Hall-Petch-effect. The underlying theory is rationalized through the pileup of dislocations at grain boundaries created in the process of plastic deformation. In [3] molecular dynamic simulations are used to show a reverse Hall-Petch-effect for nanocrystalline copper which shows a softening with grain size. Our goal is to simulate this effect using a phase-field-crystal approach, which can be viewed as a local approximation to a classic dynamic density functional theory for solid state phenomena. By definition it operates on diffusive time scales and thus in contrast to classical molecular dynamics allows to reach time scales of industrial applications. After describing the approach and quantitatively comparing results for different materials, we use the phase-field-crystal model for various experiments.

- structure and motion of Lomer dislocation dipole in fcc metals, as used as a benchmark problem for other multiscale atomistic/continuum coupling methods [4]
- dislocation pile up at grain boundaries
- grain growth with grain rotation

All simulations are based on a finite element discretization of the phase-field-crystal model, which are implemented in AMDiS [1,2].

[1] Backofen, Bernal, Voigt: Int. J. Materials Research (to appear)

[2] Backofen, Rätz, Voigt: Phil. Mag. Lett. 87 (2007) 813

[3] Schiotz, Di Tolla, Jacobsen: Nature, 391 (1998) 561

[4] Miller, Tadmor: Modelling Simul. Mater. Sci. Eng. 17 (2009) 053001

